FABRICATION AND CHARACTERIZATION OF SHARKSKIN MIMICKED CHITOSAN-GRAPHENE OXIDE NANOCOMPOSITE MEMBRANES

by

Sabra Rostami

B.S., Chemical Engineering, Sahand University of Technology, Tabriz, Iran, 2012

Submitted to the Institute of Biomedical Engineering
in partial fulfillment of the requirements
for the degree of
Master of Science
in
Biomedical Engineering

Boğaziçi University
2016

FABRICATION AND CHARACTERIZATION OF SHARKSKIN MIMICKED CHITOSAN-GRAPHENE OXIDE NANOCOMPOSITE MEMBRANES

APPROVED BY:

Assoc. Prof. Dr. Bora Garipcan .....
(Thesis Advisor)

Assist. Prof. Dr. Duygu Ege .....

Assist. Prof. Dr. Özgur Gül .....

DATE OF APPROVAL: 19 August 2016

ACKNOWLEDGEMENTS

First and foremost, I would like to express my utmost thanks and sincere gratitude and respect to my supervisor, Assoc. Prof. Dr. Bora Garipcan, whose continuous support and patience inspired me all the way both in this project and in my academic life. Your trust and belief in me and constitutive criticism to this research were instrumental and encouraging which made this project possible. Your optimism have pushed me in ways I could never have imagined. No words could ever express my gratitude and honor to have been your student.

I extend my thanks and gratitude to Assist. Prof. Dr. Duygu Ege and Assist. Prof. Dr. Ozgur Gül, for their contributions and guidance. I would also like to express my utmost thanks and respects to Assist. Prof. Dr. Ayse Ak and Assoc. Prof. Dr. Esin Ozturk Isik for their prized contribution in professional and personal life.

Much gratitude goes to my team mate, Fatih Puza, my beloved colleagues, Fatma Zehra Erkoc, Sezin Eren, Hilay Şencan, Ozgen Ozturk, Bengu Aktas, Alp Ozgun, Berkay Erenay, Ecem Sahin, Muge Turkaydin, Gamze Bolukbasi Ates and my dearest friends, Hayriye Oztatli, Hatice Kaya, Oznur Demir, Elif Donmez, Roya Nouri Rikabad, Altay Burusan and Morteza Abbaszadeh for their unwavering support, constant encouragement, and for their long lasting friendship. Along the way, I have received support from too many people to count. Even though their names are not written here, I would like to express my appreciation and gratefulness.

Last but most important of all, I have to thank my parents for their endless love, support and encouragement throughout my life. Thank you both for believing in me, giving me strength to reach for the stars, pursue my dreams and thrive in every aspect of my life. You are the reasons for who I am today and I dedicate this thesis to you both with all my heart.

ACADEMIC ETHICS AND INTEGRITY STATEMENT

I, Sabra Rostami, hereby certify that I am aware of the Academic Ethics and Integrity Policy issued by the Council of Higher Education (YÖK) and I fully acknowledge all the consequences due to its violation by plagiarism or any other way.

Name :

Signature:

Date:

ABSTRACT

FABRICATION AND CHARACTERIZATION OF SHARKSKIN MIMICKED CHITOSAN-GRAPHENE OXIDE NANOCOMPOSITE MEMBRANES

In the presented thesis, fabrication and characterization of sharkskin mimicked polymeric membranes were investigated with the aim of achieving membranes with enhanced biological, physicochemical and mechanical properties namely biodegradability using Chitosan as the main polymer and Graphene Oxide(GO) as the additive. Sharkskin micro-patterns are known to have antibacterial effects therefore possibility of replicating its surface topography with chitosan, was hypothesized and proved to be achievable. In order to replicate sharkskin surface structure, soft lithography method was chosen by using Polydimethylsiloxane (PDMS). Chitosan solution was prepared by dissolving purified pristine Chitosan in dilute acetic acid solution (2%v/v). For Chitosan/GO nanocomposites membranes, solutions of chitosan containing various amounts of GO (0.1%w/w, 0.2%w/w and 0.3%w/w) were prapared using solvent-casting method, Chitosan/GO solutions were cast upon sharkskin negative PDMS molds. Mechanical characterizations including Elongation at Break and Tensile Strength were done using Chitosan based plain membranes. Scanning Electron Microscopy(SEM) was conducted as morphological characterization along with Raman Spectroscopy, X-ray Photoelectron Spectroscopy (XPS), Water Contact Angle and Swelling Ratio as chemical characterizations. According to the results, the hypothesis of possibility of mimicking the surface micro-pattern of sharkskin using biodegradable natural polymer was verified. Additionally, preparation of sharkskin mimicked chitosan/GO nanocomposite membranes proved to be possible with acceptable quality of replication. Furthermore, adding GO to chitosan, resulted in considerable improvements of chemical and mechanical properties of polymer.

Keywords: Chitosan, Graphene Oxide, Biomimic Structures, Soft Lithography, Solvent Casting, Composite

ÖZET

KÖPEKBALIĞI DERİSİ TAKLİT EDEN KİTOSAN/GRAFEN OKSİT NANOKOMPOZİT MEMBRANLARIN ÜRETİMİ ve KARAKTERİZASYONU

Bu tezde,temel polimer kitosan ve katkı maddesi grafen oksit(GO) olan köpekbalığı derisi taklit edilmiş polimerik membranların üretimleri ve karakterizasyonları gerçekleştirilerek biyobozunurluk, biyouyumluluk ve arttırılmış esneklik gibi biyolojik, kimyasal ve mekanik özellikleri geliştirilmiş membranların elde edilmesi amaçlanmıştır. Antibakteriyel özellik gösterdiği bilinen köpekbalığı derisi mikro desen yüzeyinin, yine aynı özelliğe sahip olan kitosan ile taklit edilebileceği hipotezi öne sürülmüş ve doğrulanmıştır. Köpekbalığı yüzey yapısını taklit edebilmek için yumuşak litografi yöntemi seçilmiştir. Polidimetilsiloksan(PDMS), negatif kalıpların üretimi için kullanılmıştır. Devamında, saflaştırılmış kitosan seyreltik asetik asit (% 2 v/v) solüsyonu ile çözünerek kitosan çözeltisi hazırlanmıştır. Kitosan/GO nanokompozitleri hazırlamak için farklı miktarlarda GO(%0.1 w/w, %0.2 w/w, %0.3 w/w) içeren kitosan çözeltileleri, grafen oksitin ultra-homojenize edilmesinden sonra kitosan solüsyonuna eklenmesiyle elde edilmiştir. Bu kitosan/GO çözeltileri köpekbalığı derisi negatif kalıpları üzerine dökülmüştür. Kopma uzaması ve çekme dayanımını içeren mekanik karakterizasyonlar düz kitosan membranlar ile gerçekleştirilmiştir. Taramalı elektron mikroskobu (SEM) morfolojik karakterizasyon için kullanılırken, Raman Spektroskopisi, X-Ray Fotoelektron Spektroskopisi(XPS), Su temas açısı ve şişme testi ile kimyasal karakterizasyon düz ve köpekbalığı taklidi olan membranlarda gerçekleştirilmiştir. Sonuçlar, biyobozunur doğal polimer kullanılarak köpekbalığı derisinin mikro desenlerinin taklit edilebileceği hipotezini doğrulanmıştır. Ek olarak, köpek balığı derisini taklit eden kitosan/GO nanokompozit membranların uygun taklit kalitesine sahip olduğu gözlemlenmiştir. Ayrıca, kitosana GO eklenmesi polimerin kimyasal ve mekanik özelliklerinde kayda değer iyileşmeler sağlamıştır.

Anahtar Sözcükler: Köpekbalığı derisi, Kitosan, Grafen Oksit, Biyobenzer Yapılar, Yumuşak Litografi, Solvent Döküm, Kompozit

TABLE OF CONTENTS

LIST OF FIGURES

LIST OF TABLES

LIST OF SYMBOLS

W	Weight
C	Carbon
N	Nitrogen
O	Oxygen
Si	Silicon

LIST OF ABBREVIATIONS

SEM	Scanning Electron Microscopy
XPS	X-Ray Photoelectron Spectroscopy
SSM	Sharkskin Mimicked
CH	Chitosan
GO	Graphene Oxide
DI	Central nervous system
PDMS	Polydimethylsiloxane
RT	Room Temperature
CH/GO	Chitosan/Graphene Oxide nanocomposite
DMSO	Dimethyl Sulfoxide
RPMI	Roswell Park Memorial Institute medium
TCP	Tissue culture plate
FBS	Fetal bovine serum
MW	Molecular Weight
LMW	Low Molecular Weight
UHMW	Ultra High Molecular Weight
DDA	Degree of Deacethylation

1. INTRODUCTION

1.1 Motivation

Nature has evolved the objects with desired functionality using commonly found materials. These naturally fabricated ordered structures aim to achieve optimum functionality. The knowledge of various functions provided by objects and processes found in nature can give us guidelines to produce nanomaterials, nanodevices, and processes with desired functionality. Some of these remarkable naturally fabricated designs are lotus leaf, rose petal, gecko feet, and sharkskin [1]. Each of these, have extraordinary capabilities due to design of their natural superficial surfaces. Hence, tendency towards studying natural structures and surfaces along with their potential applications in medicine and engineering has attracted considerable attention over the past decades. These studies mostly have focused on surface structure, its characteristics and effects [1, 2].

On the other hand, several studies have shown the effects of surface topography on activities of cells and microorganisms. For instance it has been proved that by culturing stem cells on smooth surfaces, the probability of differentiation to neural cells is more likely than other types of cells such as osteoblast and fibroblast. Also, recent studies on effect of surface morphology on proliferation and migration of bacterial colonies have shown that specific surface micro-patterns such as sharkskin, limit bacterial growth which would result in decrease in speed of spread of bacterial contaminations [3, 4].

Over the years, many engineered systems and products have been designed to help in different aspects of medical science namely drug delivery, infection control, wound healing, etc. In this path many natural structures, organic and synthesized chemicals were discovered such as Chitosan(CH) which is obtained from deacetylation of Chitin which is obtained from shell of marine animals like shrimp [5]. Also, very

recently Graphene Oxide(GO) which is a carbon based nanomaterial synthesized from graphite was discovered. Both GO and CH possess exceptional properties. GO has enhanced mechanical properties as well as biological and chemical properties. On the other hand, CH is nontoxic, biodegradable and biocompatible. Combination of these two powerful materials could provide new nanocomposites, engineered for any desired purposes [6, 7]

In the light of these discoveries over the past couple of decades, science has developed various methods to fabricate structures most similar to natural structures such as biomimetic and bioinspiration [2]. Biomimetics is noteworthy since it involves an equal trade between human beings and the environment. It is a gateway for scientists to design many things that nature has spent billions of years perfecting [8]. Biomimetic techniques enable researchers to replicate natural structure with highest precision and quality [9]. Therefore biomimetic provides a proper means to pursue researches concerning natural structures, in particular surface morphology [2].

Among all noticeable natural structures, sharkskin is being extensively investigated for its drag-reduction and antibacterial effects. Bioinspired by the shape and design of sharkskin denticles, numerous studies has been going on concerning the claims of antibacterial property of sharkskin being due to its surface topography. Based on the results obtained by several groups, bioinspired sharkskin templates showed significant decrease in the amount of bacterial colonies on the surface, verifying the proposed hypothesis [10, 11].

The possibility of fabrication of a polymeric substrate with specific surface topography in combination with chemicals with exceptional characteristics could lead to achievement of a unique structure for several purposes such as wound healing, surface-coverings, protecting layers for implants, etc.

With the inspirations of recent studies along with hopes of designing and producing biomimicked surfaces with potentials of serving in diverse aspects of biomedical field, combining chemical properties with morphological properties hold great promises

in achieving our goals.

1.2 Objectives

In this thesis, surface micro-topography of sharkskin was replicated using chitosan as the primary polymer, which is natural in origin and has exceptional biological and chemical properties along with GO as the additive. GO was blended with chitosan solution so as to prepare CH/GO nanocomposites. Main objectives of this study were:

1. Biomimicking surface micro-topography of sharkskin,
2. Fabrication and characterization of sharkskin mimicked CH membranes,
3. Preparation and characterization of CH/GO nanocomposites membranes,
4. Investigation of effect of GO concentration on cellular attachment and proliferation.

1.3 Outline

This thesis is presented as follows: In chapter 2, background information regarding sharkskin, sharkskin effect, biomimicking techniques, chitosan, GO and CH/GO composite were explained. In chapter 3, experimental procedures were described in detail. In chapter 4, the results were presented and in chapter 5, the discussion of obtained results was given.

2. BACKGROUND

2.1 Novel Applications of Biomimetic Techniques in Biomedical Engineering

It has been almost 3.8 billion years since life is estimated to have appeared on earth [1]. During this time, some species have extinct such as dinosaurs, some have lived on without any changes like microorganisms. But majority of animal species have gone through extensive alterations with the aim of survival by adaptation to new and mostly harsh environmental conditions. These adaptations occurred spontaneously and to the most possible extent. As a result, many animals have developed extraordinary mechanisms and characteristic features; whether these capabilities served for defense and protection or simply emerged as a result of evolution.

Some of these remarkable features are Lotus leaf, rose petal, gecko feet, and sharkskin structure. The one thing that all these have in common is that they all are topographical characteristics and any benefit or outcome of either one of these, emerges solely from geometric features and morphological structure of the surfaces in micron and nano-scales [1, 2].

Lotus leaf effect was investigated and resulted in introduction of superhydrophobic surfaces with a high static water contact angle above 150° and contact angle hysteresis of less than 10° which help lotus leaf to exhibit extreme water repellence and self-cleaning properties. At a low value of contact angle hysteresis, water droplets may roll in addition to sliding, which facilitates the removal of contaminant particles [11].

Unlike the Lotus leaf, some rose petals, such as scallions, and garlic exhibit superhydrophobicity with high contact angle hysteresis. In these structures, a water droplet stays pinned to the surface of these leaves, completely opposite to what happens in lotus leaf. The different behavior of wetting between the Lotus leaf and the rose

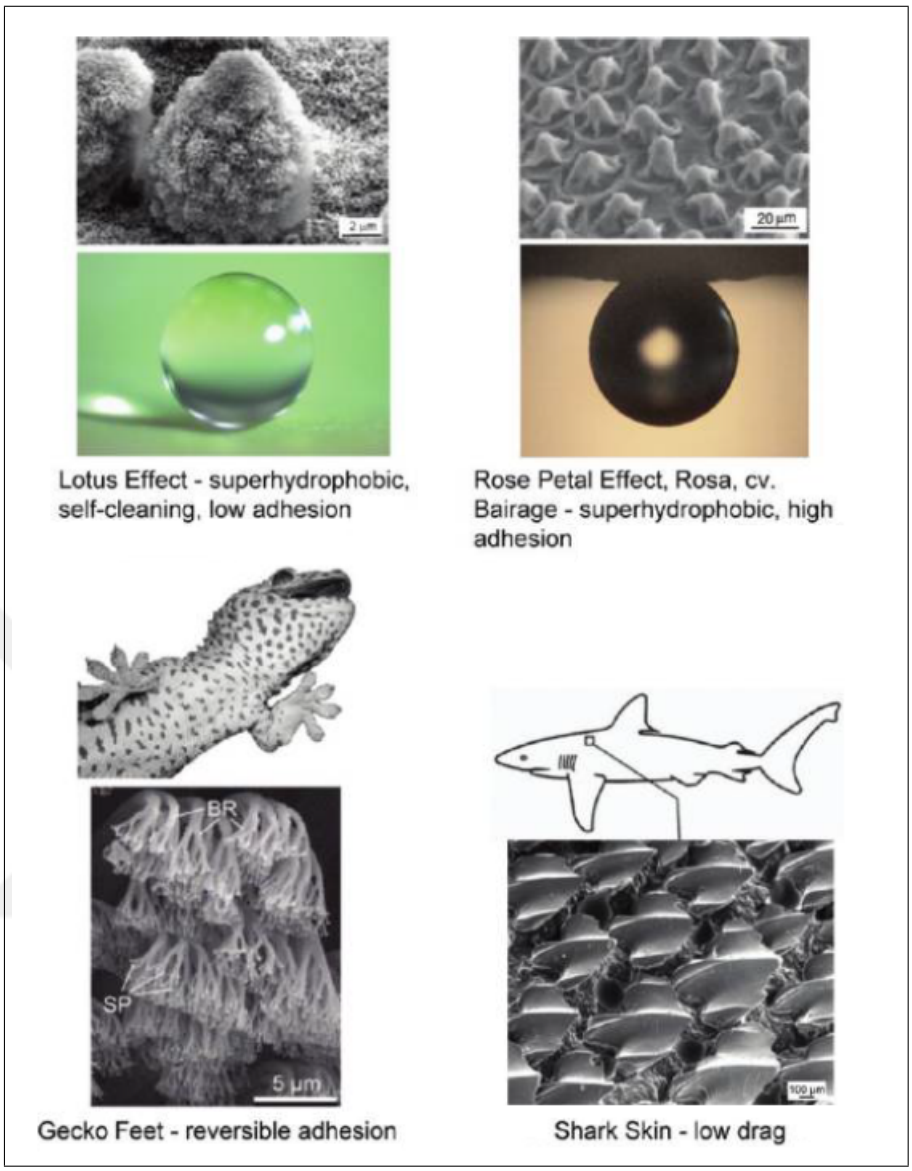

Figure 2.1 Montage of Four Examples from Nature With Remarkable Features [1].

petal can be explained by the different designs in the surface hierarchical micro- and nanostructures [10].

Biological evolution over a long period of time has led to the optimization of leg attachment systems in some animals such as many insects, spiders, and lizards. Attachment pads of these animals are capable of attaching to and detaching from a variety of surfaces and are used for locomotion, even on vertical walls or across the ceiling [12]. This dynamic attachment ability is referred to as reversible adhesion or smart adhesion [11]. The attachment pads of geckos have been the most widely studied

due to the fact that they have the highest body mass and exhibit the most versatile and effective adhesive known in nature. The structure of Gecko feet proved to have very strong adhesive capability to almost any kind of surface. Hence a great interest among the scientific community have been going on for past several years to create surfaces that replicate the adhesion strength of gecko feet [1].

Among the major treats of wild life was and still is, bacterium. Bacteria and fungi during evolution of nature have always survived with little or in some case no alterations. Bacterial and fungal contaminations have been controlled by the nature using naturally developed structures with unique geometrical and chemical structure. Sharks are one of the species that have the capability of defending themselves against bacterial and fungal contaminations and infections using nothing but their skin as the primary defense system. It has been investigated and learned that skin of sharks, of all type, is free of any adhered or penetrated bacterial as long as the skin is intact. Recent studies have hypothesized and some even have proved that the micro-morphology of the skin plays the main role in the defense rather than its chemical composition [1, 2, 9, 11, 13–16].

In the light of these discoveries over that past couple of decades, science has developed various methods to fabricate structures most similar to natural structures such as biomimetic and bioinspiration. Biomimetic is noteworthy since it involves an equal trade between human beings and the environment. Scientists mimic the designs that nature has spent billions of years perfecting [7]. Biomimetic techniques enable researchers to replicate natural structure with almost exact precision and quality [1]. Among techniques used in the field of biomimetic there are soft lithography methods which have been tested and proved effective in replication of sharkskin since an exact replica of sharkskin was obtained in the end. Micro-embossing and micro-molding are examples of these procedures [2,11,17]. A schematic illustration of using micro-molding using PDMS for mimicking sharkskin micro-patterns is shown in Figure 2.2.

The fact that sharkskin microstructure has unique properties makes it of great interest for research purposes.

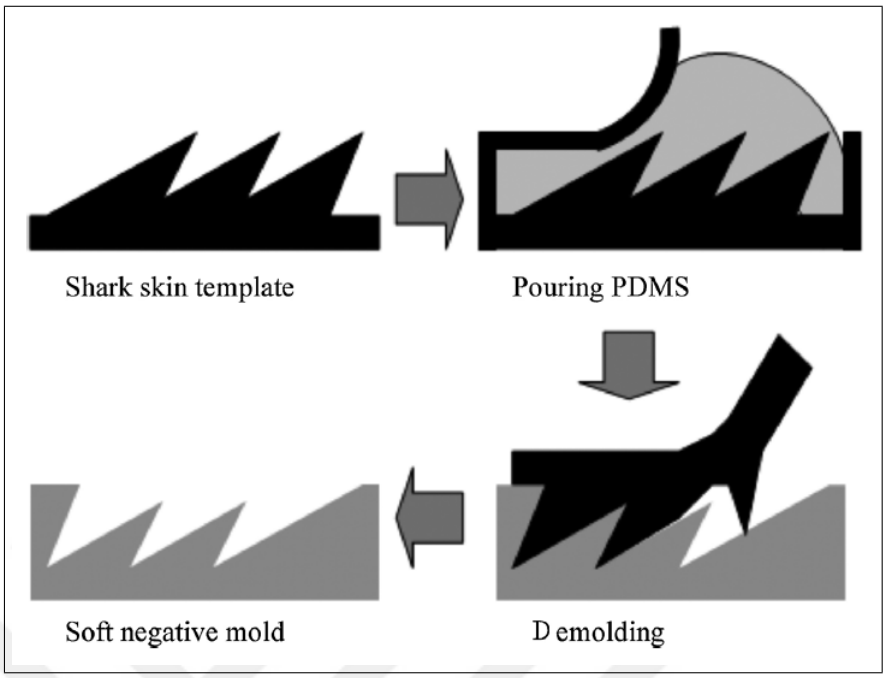

Figure 2.2 Schematic Illustration of Sharkskin Replication Using Micro-Molding Method [2].

2.2 Shark Skin: A Natural Structures with Antibacterial Surface Topography

Sharks are one of the fastest swimmers among marine animals [18]. The skin of sharks possesses excellent performance in drag reduction, so-called shark skin effect which is the main reason of high speed of swimming [11, 14]. Sharks are commonly described as cartilaginous fishes and the reasons of their high speed has mistakenly been attributed to this feature. Whereas they are in fact covered by numerous small dermal tooth-like elements termed placoid scales or denticles [2, 14, 15]. Figure 2.3 illustrates the shape of a single denticle.

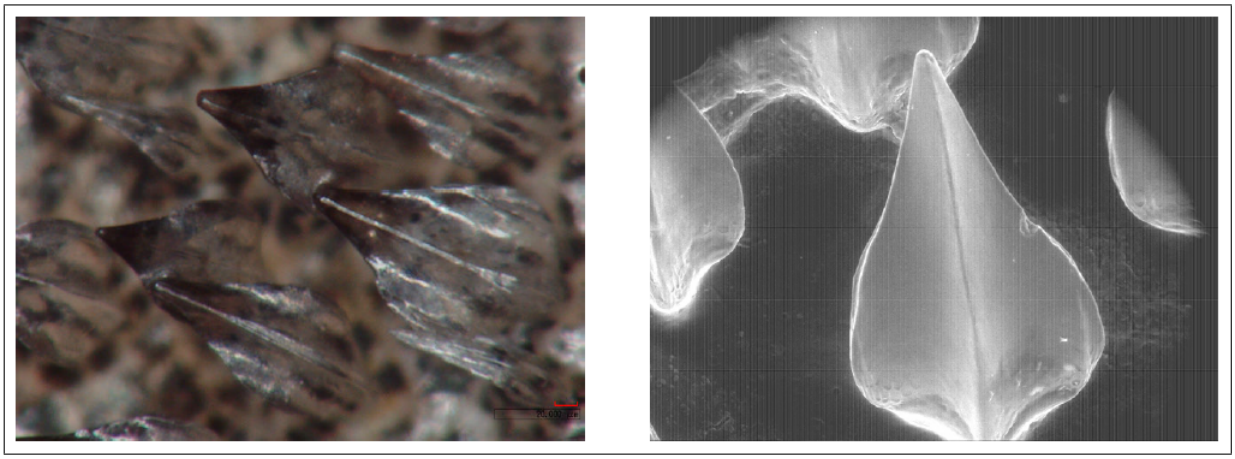

Figure 2.3 3D Video Microscope image of living shark skin (×150) (*left*), ESEM pictures of living shark skin (×200) (*right*) [19].

The surface structure of each denticle consists of a base plate, and spine consists of grooves and riblets as shown in Figure 2.4. The shape of denticles are not the same all over the body, depending on the position of each section of the body and its function, the shape of denticles change. The shapes of denticles also differ based on the species of the shark. Figures 2.5 and 2.6 illustrate the differences in shape of denticle in different sharks [1].

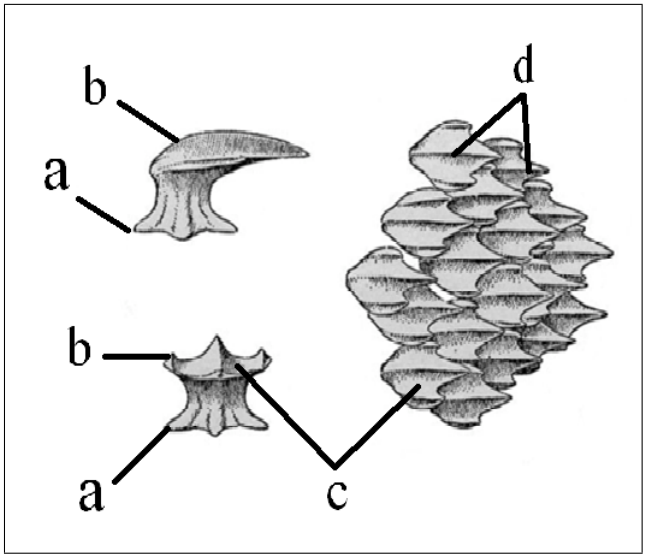

Figure 2.4 Single Denticle of Sharkskin: a) Base Plate, b) Spine, c) Grooves, and d) Riblets [1].

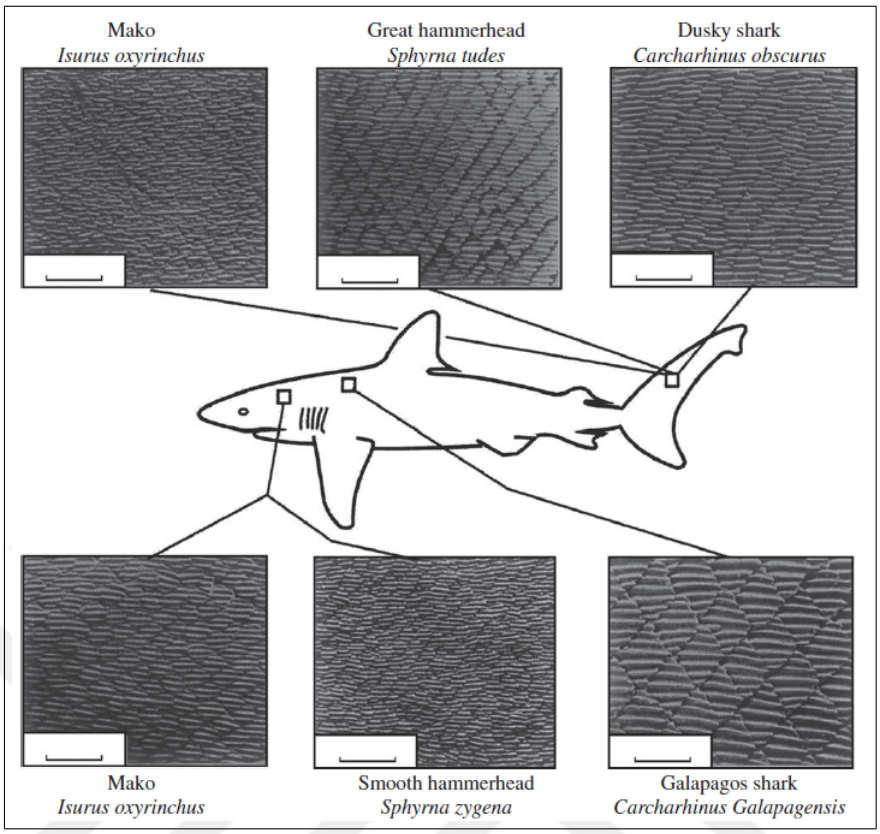

Figure 2.5 Scale patterns on fast-swimming sharks (scale bar, 0.5 mm) [11].

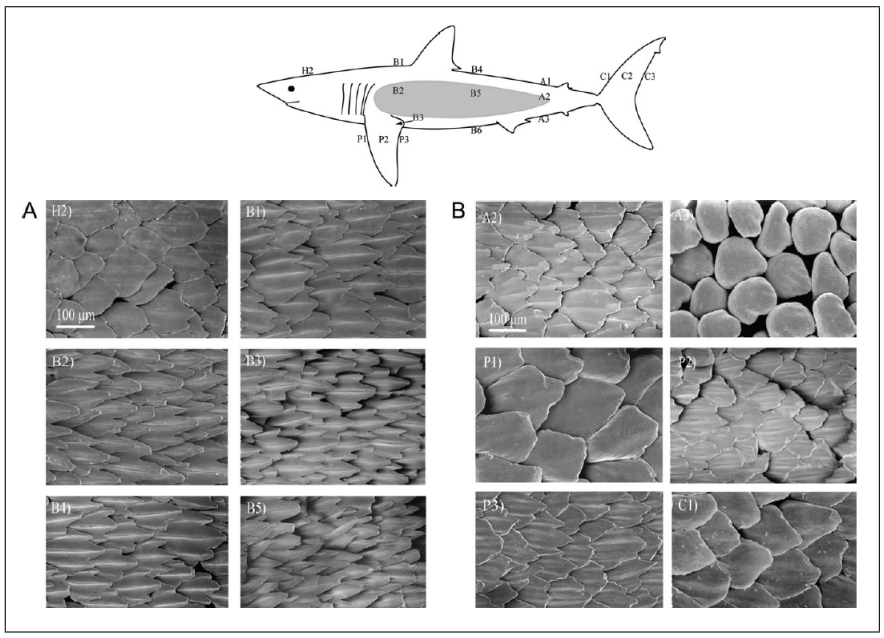

Figure 2.6 Dorsal view of placoid scales from a male shortfin mako Isurus xyrinchus (magnification 200X). The scale crowns on regions P1, C1, and A3 are almost or completely smooth and lacking riblets; the crowns in regions B3, B6, A3 and B5 are long and narrow. Anterior is to the left [16].

Reasons of high swimming speed of sharks have been thoroughly investigated. The results of these studies proved that the shape of the denticles, in particular riblets and grooves on the surface, are responsible for reduction of drag force on the skin, leading to faster flow of water on the skin and faster movement, in other words higher speed [15].

While some researches revealed that morphology of the skin of sharks is responsible for higher speed, another study focused on the fact that sharks unlike other large marine animals are free of any microorganism attachment, a phenomena commonly known as biofouling. In this phenomena, marine organisms settle, attach, and grow on submerged marine surfaces of both animals and ships. It is a usually seen phenomenon for the ocean-going ships and submarines and it can decrease the range, speed, and maneuverability of these vessels and increase the fuel consumption. This fact was investigated and it was reported in two independent and unique theories. From the mechanical engineering and fluid mechanics point of view, the reduced drag on the surface results in a high-speed flow right at the interface of skin and water. The high-speed flow of water during movement prevents organisms of settling to the skin in the first place. Hence the skin stays clean and free of marine organisms [1, 11, 14, 20].

In the second theory, it is proposed and proved that shape of each denticles along with gathering of denticles together have antibacterial properties, solely due to surface morphology [11, 16].

Bioinspired by the shape and design of sharkskin denticles, numerous studies has been going on concerning the veracity of the second theory. Based on the results obtained by several groups, bioinspired sharkskin templates showed significant decrease in the amount of bacterial colonies on the surface, verifying the proposed hypothesis. Figure 2.7 is an illustration of the results of a bacterial culturing test performed on smooth(plain) surface vs. sharkskin-bioinspired surface alone with an illustration of the bioinspired designed surface [8, 10].

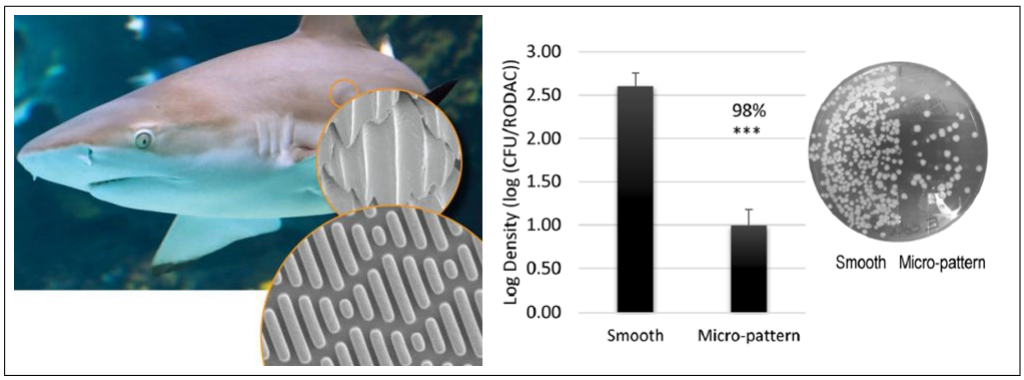

Figure 2.7 Sharkskin Bioinspired surfaces Design Patterns (*left*), and results of bacterial test performed on plain surface vs. sharkskin bioinspired polymeric surface [21].

So far, the extraordinary design of sharkskin and its effects have been tested for many different applications. Unfortunately the mechanism of antifouling still remains unknown but the beneficial and optimum developments are found everyday and uses of sharkskin morphology in biomedical studies has become a growing research field.

2.3 Antibacterial Materials in Nature: A General Overview on Chitosan and Graphene Oxide

Graphene oxide (GO), a well known derivative of graphite, is in the form of pseudo-two-dimensional oxygen-containing sheets or flakes at nano-scale thickness which possesses multiple functional groups, namely hydroxyl, epoxy, and carboxyl [17]. Carboxylic groups are located at the edges of flakes and phenol hydroxyl and epoxide groups on its basal plane [22]. These functional groups significantly alter the van der Waals interactions between the layers of graphene giving it the potential and characteristic of desired solubility in water and some organic solvents which in turn leads to convenient and uncomplicated methods of fabrication of graphene-based materials by solution casting [23]. This carbon based nanomaterial, consists of a single layer of sp2-bonded carbon atoms arranged in a hexagonal crystal structure, enabling it to have significantly vast specific surface area (calculated value, 2630m^2/g) with numerous functional groups spread homogenously over the surface and around the edges.

Moreover, GO flakes own nano-scale surface roughness [22, 23]. It is well known that nano-scaled materials with high surface area could impose strong geometric restrictions to the mobility of polymer molecules. Furthermore, the nano-scale surface roughness may result in an enhanced mechanical interlocking with other functional groups consequently, leading to better adhesion and therefore enhanced mechanical properties. Over the past decade, GO has attracted serious attention of researchers ever since it was reported that GO exhibits strong antibacterial activity [24, 25].

Recent studies have attributed antibacterial effect of GO to membrane stress induced by sharp edges of its flakes, which may result in physical damages on cell membranes, leading to the loss of bacterial membrane integrity and the leakage of RNA [26]. Another study also suggested that GO may enforce oxidative stress on neural cells of PC12 [27]. An extensive and detailed study on toxic effects of graphite derived nanomaterials, compared antibacterial effect of graphite, graphite oxide, GO and reduced GO [23]. According to results of this study, GO showed the highest antibacterial activities, dependant on time and GO concentration, demonstrating the importance, effectiveness and potentials of GO [23]. Extraordinary mechanical properties of GO in addition to its remarkable antibacterial activities, made it a very interesting research subject.

The ease of dissolving GO in water and some organic solvents provided many straightforward and accessible method of conjugating GO to vast group of synthetic and natural polymers. According to results of numerous studies regarding nanocomposites containing GO, addition of GO affected mechanical properties considerably [28]. Among potential natural polymers that have extraordinary characteristics, CH outstands as one of the most abundant biodegradable natural polymers. There have been extensive studies regarding blending chitosan with GO] [6, 7, 23, 24, 29]. According to results of these studies, functional groups of chitosan including carboxylic, amino and hydroxyl groups, provide the means of interacting with GO on a molecular basis. This means that addition of GO to chitosan and dispersing its flakes inside the polymer, does not result in merely physical dispersion, but also chemical bond, hydrogen bonding in particular are created between functional groups of both materials. Figure 2.8

is a schematic illustration of chemical interaction of CH chains with GO flakes.

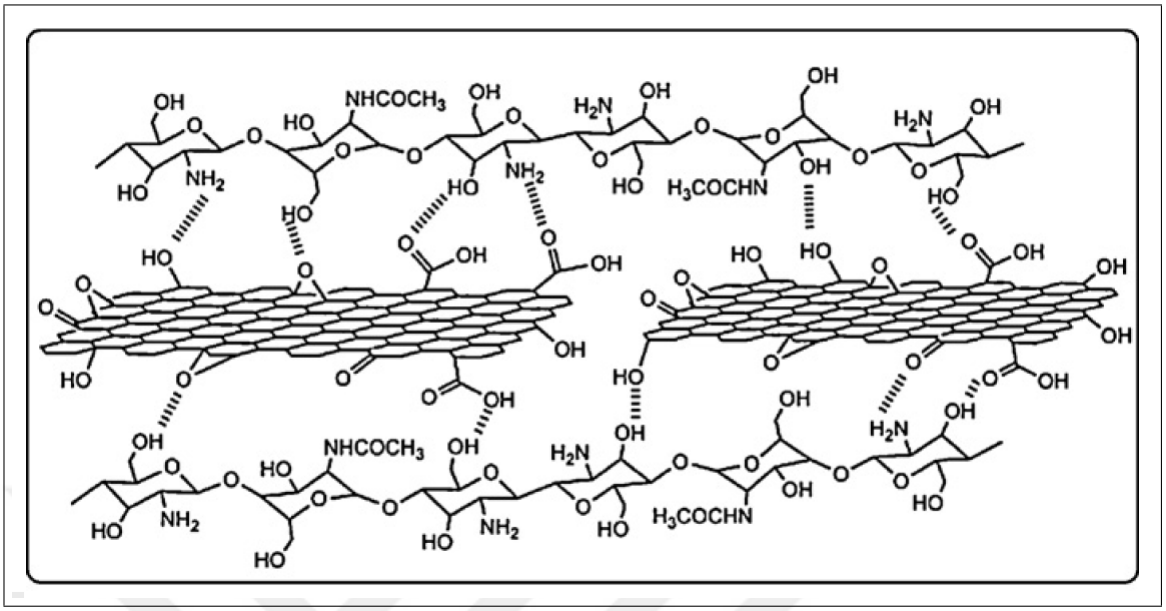

Figure 2.8 Schematic Illustration of Chemical Interactions Between GO and CH [6].

The fact that GO can be easily dispersed in water and its flakes can be exfoliated by rapid heating or ultrasonic homogenization, provides many methods of fabricating chitosan/GO nanocomposites such as solvent casting, also known as solution casting method in which chitosan based solutions containing desired amounts of GO are prepared and casted onto any desired surface [5, 6, 16].

Despite GO's ease of usage, it is known that antibacterial effect of GO along with its impact on chemical, mechanical and biological properties of composites, when mixed with chitosan, is greatly affected by GO concentration [22, 23] Therefore productive research regarding effects of GO concentration on chitosan/GO nanocomposites have been conducted over the past few years [5, 28]. So far, it has been proved that in low concentration of GO in chitosan, less than 0.3%w/w, proper dispersion of GO in chitosan solution results in aligned parallel positioning of GO between chains of plain thin membranes of chitosan/GO composites which were obtained via solvent casting method [3, 11]. It was also reported that aligned parallel positioning of GO flakes take place at the interface of the membranes and the plate upon which the solution was casted and dried [5]. Figure 2.9 illustrates positioning of GO flakes inside chitosan

plain membrane obtained via solvent casting method.

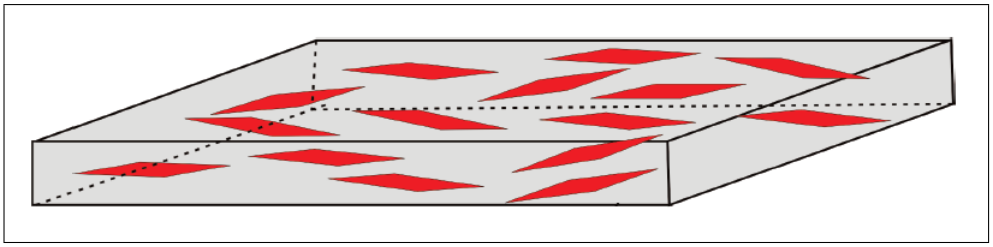

Figure 2.9 Schematic of Aligned and Parallel Positioning of GO Flakes to Chitosan Membranes' Surface [4].

A great number of studies have been done about CH/GO nanocomposites at different concentrations and their numerous potential applications namely their enhanced mechanical performance, antibacterial membranes and hydrogels preparation for various applications both ex-vivo and in-vivo [3, 4, 29]. Selection of CH as the primary polymer of nanocomposites has not just been due to its abundance in nature. CH, as a copolymer of [1,4]-linked 2-acetamido-2-deoxy-D-glucopyranose and 2-amino-2-deoxy-D-glucopyranose, is a deacetylated derivative of chitin [4].

Main reasons chitosan's widespread use both in scientific research and industry include its acceptable level of biodegradability, high biocompatibility, haemostatic properties, nontoxicity, bioactivity and solubility in aqueous medium [3, 4]. Due to simultaneous assembly of all these extraordinary characteristics in chitosan, it has attracted significant interest in a broad range of applications such as water treatment, separation membrane, food package, tissue engineering, biomedicine and so on [30,31].

In spite of remarkable chemical and biological properties of CH, its mechanical properties are not good enough to meet this extensive range of applications. A noticeable number of researches have been done on enhancing mechanical properties of chitosan membranes and scaffolds by addition of plasticizers or cross-linkers [32,33]. Based on these studies, mechanical properties of chitosan thin films, membranes and scaffolds can be improved extensively by adding chemicals such as Polyethylen glycol(PEG), Glycerol, Sorbitol and GO [3, 30, 31]. In addition to commonly used plasticizers, GO has great potentials as cross-linker for enhancement of mechanical properties.

Also, GO particularly holds great promise for tissue engineering applications, due to its unique physicochemical properties of hydrophilicity in addition to its good mechanical characteristics. Researches have revealed that surface wettability (water contact angle) plays a fundamental role in cellular and bacterial interactions with polymeric substrates [33, 34]. According to the literature, surface wettability of plain chitosan membrane is approximately 90° which causes chitosan to behave as a hydrophobic material [35]. In many in-vivo and in-vitro applications, a degree of hydrophilicity is required in order to optimize properties of the biomaterial to be as similar to real conditions inside the body as possible. In some cases this means less wettability and in some cases, more [34, 36]. GO has great influence on wettability properties of biomaterials. Due to existence of carboxylic(-COOH) and hydroxyl(OH) groups in the structure of GO, great tendency towards interactions with water molecules is one of the chemical properties of it, but not by affecting the water contact angle, but with easing the dispersion of GO flakes in water or aqueous solutions [11,37] In cases where GO was blended with CH, amino(NH_2) as well as carboxylic(-COOH) and hydroxyl(OH) groups of CH interacts with functional groups of GO resulting in an increase in number of NH_3^+ groups which in turn increases the number of functional groups with high potential of interacting with water molecules which leads to higher swelling ratio of water and decrease in water contact angle when compared to pristine CH [35, 37].

In the field of biomedicine and tissue engineering, CH is mostly preferred due to its high antibacterial activity and biocompatibility. Almost all chemical, mechanical, biological and antibacterial properties of chitosan are affected by its chemical composition, meaning that factors like molecular weight(MW), degree of deacetylation(DDA) and pH, change the characteristics of CH considerably [36, 38].

It has been investigated and reported that the antibacterial activity of neutral or alkaline chitosan suspension was lower than that of acidic chitosan solution. According to the results of this study, the optimal pH value of chitosan solution was 6.0 for the highest bactericidal activity [36, 39, 40]. This suggests that acidic solution of chitosan would be ideal choices in order to achieve highest antibacterial level. However the inflammatory effects of biomaterials with low or very low pH must not be neglected.

Hence optimization will always be necessary.

Many of chitosan's physicochemical properties are affected by molecular weight among other affecting factors [34, 41]. Based on the results of extensive studies regarding effects of chitosan's MW on its characteristics, low molecular weight (LMW) and ultra high molecular weight (UHMW) chitosan have shown highest antibacterial properties as well as promising mechanical and chemical characteristics. It is quite interesting that the antibacterial activity of chitosan with UHMW just like LMW, was due to the amino protonation and subsequently cationic formation on its molecular side chain in acidic solution [34, 41, 42].

Even though chitosan's characteristics and therefore performance is affected by many diverse factors, it still remains one of the most popular biopolymers with a wide range of applications in the field of biomedical.

3. MATERIALS AND METHODS

3.1 Shark Skin Mimicked Polymeric Membrane Preparations

In the presented thesis, shark skin was obtained, chemically fixated and used in order to fabricate biodegradable polymer based membranes with sharkskin surface morphology. Firstly the skin was harvested and subjected to an initial treatment prior to use according to methods presented in the literature [15,43]. Afterwards, pretreated skin parts were used to prepare negative mold using soft lithography method and Polydimethylsiloxane (PDMS) as the suitable material for replication. Thereafter the obtained PDMS negative molds were used to prepare shark skin mimicked polymeric membranes.

Among all biodegradable biopolymers, chitosan was used to prepare shark skin mimicked polymeric membranes. Some additives were added to chitosan solution in order to enhance the antibacterial and mechanical properties of the shark skin replicated membranes such as Graphene Oxide (GO) with various concentrations. Then all chemical and antibacterial properties of the fabricated membranes were investigated including mechanical properties at which point an elimination took place and the remaining experimental groups were used in in-vitro cell culture studies. The following is detailed explanation of each step.

3.2 Shark Skin Pretreatment

Shark skin in its fresh and original form could not be used due to excess flesh and slippery nature of the skin, hence the skin was cleaned and chemically fixated prior to use. Pre-treatment of the shark skin is an essential step in replication since it maintains skin‘s micro-grooved structure as well as improving its strength as the molding (replication) template. The pre-treatment process of the shark skin follows

six steps: cleaning, rigidity fixing, chemical fixing, rinsing, dehydration and drying. To prevent the shark skin from shrinking and deforming during pre-treatment, it was fixed on a rigid plate with nails or clamps before cleaning [15].

After obtaining a 40 cm long pup shark, the skin was removed completely using a scalpel. Then, dermis and subcutaneous tissue was scraped clean and a thin layer of sharkskin template was attained. Afterwards sharkskin template was rinsed five to eight times with de-ionized water in order to wash any impurities and blood and dermis residue off. Then the template was cut into 5 cm x 5 cm pieces followed by flattening and nailing to a rigid plate prior to chemical fixation process. Stabilization protects the skin from being deformed as a reaction to chemicals [14].

For chemical fixation of sharkskin, the templates were placed in 2.5% Glutaraldehyde ($C_5H_8O_2$) for 3 hours to maintain its original micromorphology. Afterwards, the chemically fixated sharkskin templates were rinsed for 1hour by three to four changes of a 0.1 mol/L phosphate buffer solution (pH 7.2) followed by three to four times wash with clear and de-ionized water so as to rinse off any residual solution. Excessive and rapid water loss during drying phase would have resulted in template deformation, which was prevented by conducting gradient dehydration. At this step, chemically fixated sharkskin templates were immersed in 30% v/v, 50% v/v, 75% v/v, 80% v/v, 95% v/v and 100% v/v ethanol solutions to dehydrate them step by step, each for 15 to 30 min. Finally, the samples were kept inside a drying oven at 60 °C for 12 hours, which completed the pretreatment procedure of the sharkskin template pieces [13].

3.2.1 Preperation of Shark Skin Mimicked Negative Mould via Soft Lithography Methods

After collecting dried sharkskin samples, the inverse (negative) surface topography of the sharkskin was replicated via usage of PDMS as the material and Soft Lithography as the method. In this regard, PDMS (Sylgard 184; Dow Corning, Midland, MI) was used with the desirable ratios of Silicone Elastomer 184 to Curing Agent

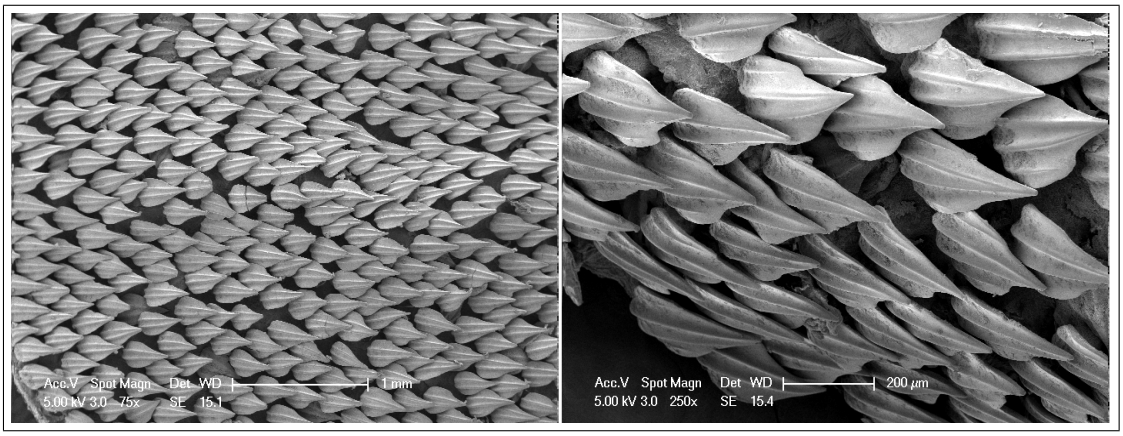

Figure 3.1 SEM Image of Micro-grooves of sharkskin after pre-treatment ($Left : TopView, Right : Sideview$) [19].

184 in order to obtain a mold with best replication and acceptable flexibility. For our studies 15 to 1 ratio of silicone elastomer to curing agent was tested and proved to be efficient. The PDMS solution was prepared, degassed and poured onto the sharkskin and put at 60 °C for 5.5 to 6 hours to cure. Thereafter, the PDMS polymer layer was detached from the sharkskin by simply peeling it off. The confirmation of precision and quality of replication was done by comparing Scanning Electron Microscope (SEM) images of shark skin and negative PDMS mold. The PDMS negative mold which was achieved at this step, was coated by a 50nm thick gold layer and imaged via SEM (Philips XL30 ESEMFEG/EDAX). Then it was stored at RT further use in the following steps. Figure 3.2 show PDMS mold preparation steps schematically [43].

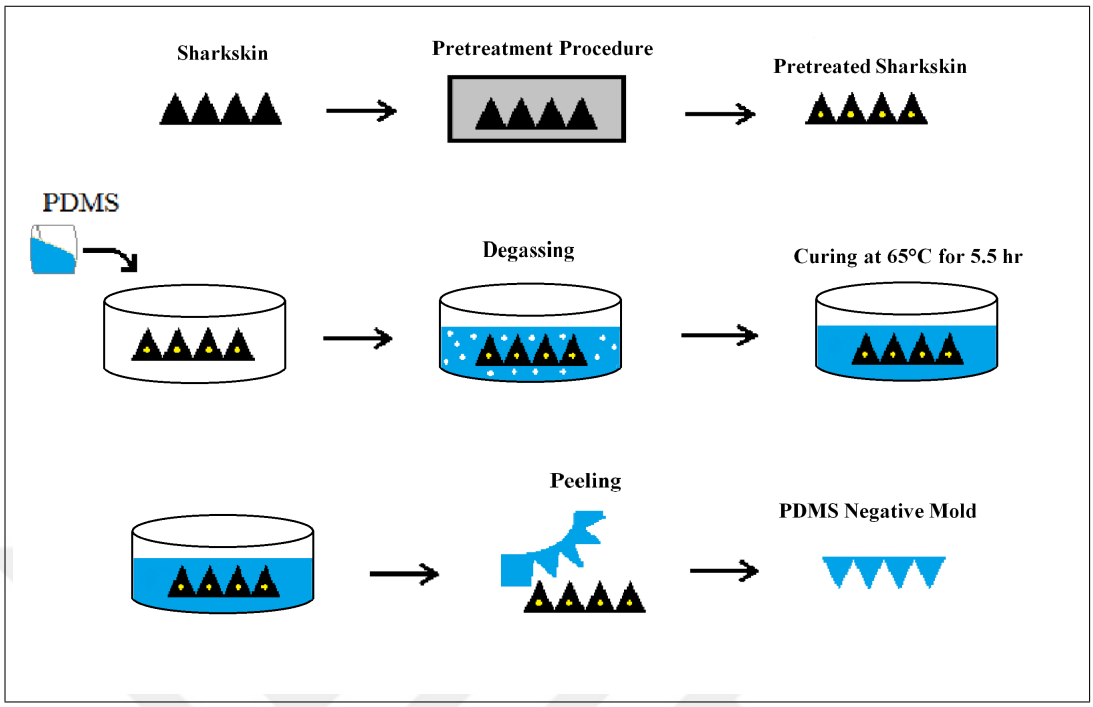

Figure 3.2 Schematic Illustration of PDMS Mold Preparation Steps.

3.3 Chitosan Purification

Low molecular weight chitosan which was used as the main material in this study, was purchased from Sigma Aldrich. This polymer had some impurities which could have caused problems in characterization and cell culture experiments, which is why chitosan was purified to prevent occurrence of any complications and unreliable results [44, 45].The purification process was designed and performed in six main steps:

Step 1) Preperation of 1%wt CH solution

Since chitosan only dissolves in dilute acidic solution, firstly 1 liter of 1% v/v aqueous acetic acid solution was prepared. Then 1 gram of chitosan was dissolved in the acid solution and mechanically mixed overnight.

Step 2) Removal of insoluble impurities by filtration

The next day, the solution was filtered using a Whatman filter paper Grade

41 with pore size of 20 to 25 μm. The filtered solution was collected and stored at room temperature.

Step 3) Reprecipitation of chitosan using Sodium Hydroxide (NaOh) solution

In order to reprecipitate chitosan, the pH of the solution needed to be in the ranges of 10 to 12, therefore a solution of 1M NaOH was prepared in order to increase the pH. Then, NaOH solution was added to chitosan solution while mixing until the pH was set [44].

Step 4) Collecting the precipitated CH

Afterwards, the precipitated CH solution was centrifuged in order to collect the precipitated pure chitosan. At this point, there was residuals of both unreacted acetic acid and NaOH solution which needed to be extracted.

Step 5) Removing any residual solvents and excess solutions

In order to extract all residual solutions, the collected CH was dispersed in deionized (DI) water and mixed for 10min followed by centrifugation. This step was repeated 3 times at which point all residual chemicals were taken out of the polymer.

Step 6) Collecting the purified CH and drying it

After 3 times wash with DI water, the obtained polymer is collected into a clean and sterile cup and kept at -20°C for 24 hours. Afterwards the frozen chitosan was dried by putting the polymer on hotplate for 48 hours at +40°C. At this stage the purified chitosan was ready to used at all other steps of the project [44].

3.3.1 Chitosan-Based Membrane Preparation

In order to prepare chitosan based membranes with and without surface micro-topography, purified chitosan was used and the polymer solution of 2%wt concentration

was prepared using 2%v/v acetic acid solution as the solvent. The dried pure chitosan powder of desired amount was dissolved in acidic solution and mixed overnight by magnetic stirring. Then this solution was used to fabricate both plain and sharkskin mimicked (SSM) polymeric membranes. Solvent-casting method was used, which implies to pouring of the polymer solution directly onto the surface. Figure 3.3 is a schematic illustration of solvent casting of chitosan on negative PDMS mold.

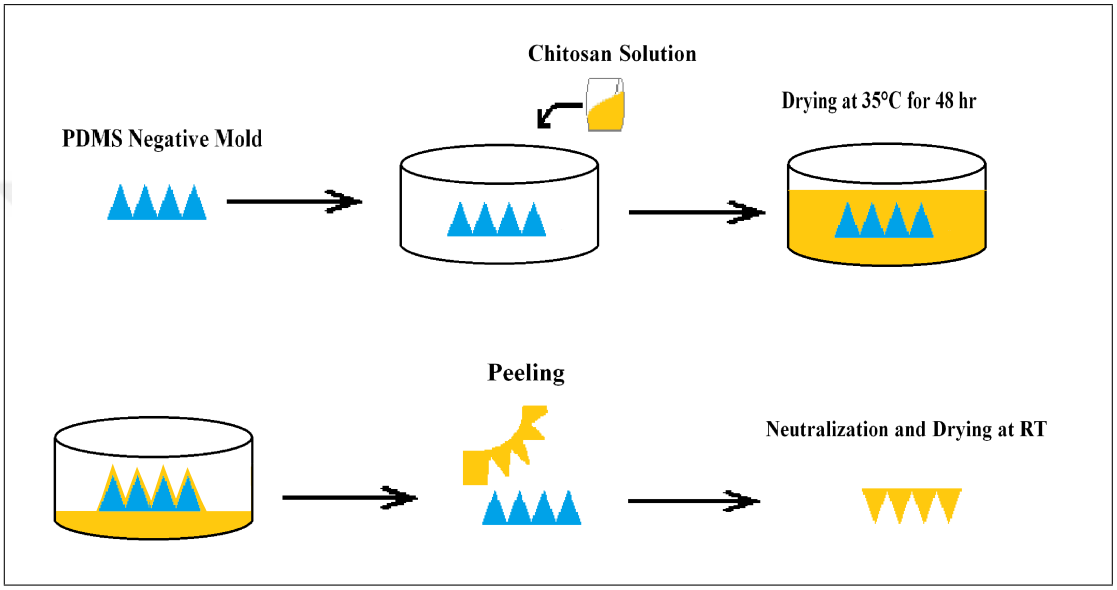

Figure 3.3 Schematic Illustration of Solvent Casting of Chitosan on Negative PDMS

3.3.2 Plain Membrane Preparation

In order to prepare chitosan membranes with absolutely no surface topography, a thin layer of PDMS was cast on glass and after solidification of PDMS, the surface of it was modified by Polyethylene Glycol (PEG) in order to make the surface hydrophilic. The hydrophilicity of the surface is imperative due to hydrophilic-hydrophilic interactions that are needed for better dispersion of polymer solution on the surface so as to obtain a homogeneous layer of chitosan membrane with approximately equal thicknesses at every point [45].

In this procedure, PDMS surface was cleaned with Isopropanol and deionized water, dried with compressed air. Then it was placed in Oxygen Plasma Sterilizer for 30

seconds. Plasma treatment was performed at 200mT and 50sccm flow of oxygen in order to form hydroxyl groups on the surface of PDMS. After that, PEG was immediately applied onto the oxidized PDMS surface and it was immediately placed on a hot plate set at 150°C for 25min. PDMS surface was then cooled, washed water to remove residual PEG and dried. The success of this process was checked by Water Contact Angle (WCA). At this point, CH solution was cast upon the modified plain PDMS surface and the solution was placed onto a hotplate at +35°C for 36 hours to dry [45].

After drying, the membrane was detached from the PDMS surface by simply peeling it off. Then NaOH solution was used again in order to neutralize acetic acid still exciting in the membrane. NaOH treatment was done by immersing CH membrane in NaOH 1M solution for 4-6 hours. Afterwards, the membrane was taken out of the NaOH solution and washed with DI water and immersed in DI water twice each time for 3-4 hours. This step is essential because without neutralizing both excess acetic acid molecules inside the polymer chains and the reacted acetic acid molecules, the membrane would have dissolved in aqueous environments which was present during water contact angle, cell culture and bacterial culture studies [46].

Finally, washed and cleaned membrane was placed onto a layer of filter papers so that while the membrane is drying, the water loss would be gradual and slow and nailed to the surface beneath the filter papers so that while drying the shrinkage of the membrane would not result in deformation of its physical appearance. The membrane packed by filter paper was left to dry at room temperature for 24 to 36 hours.

3.3.3 Sharkskin Mimicked Membrane Preparation

Preparation of sharkskin mimicked chitosan membranes was done using previously prepared negative PDMS molds. These molds were modified with PEG just like plain PDMS using the same method. Afterwards, 3%wt chitosan solution was prepared and casted onto the mold and was placed onto a hotplate at + 35 °C for 36 hours to dry. After drying, the membrane was detached from the mold by peeling it off. Then it

was immersed in NaOH 1 M solution for 4-6 hours followed by 2 times immersion in DI water each for 3-4 hours. Just like plain chitosan membrane, the neutralized sharkskin mimicked membrane was placed onto a layer of filter papers and nailed to the surface beneath the filter papers and left to dry at room temperature for 24-36 hours [44].

Only plain chitosan membranes were cut into strips of 1cm x 5cm for mechanical tests as the first characterization. The mechanical properties of polymeric membranes of all groups are based on the data obtained from plain films.

3.3.4 CH/GO Nanocomposite Membranes Preparation

Dried Chitosan membranes obtained showed very poor mechanical properties which demanded the need for additional chemicals in order to improve their mechanical properties. This demand arose from the results of mechanical tests. In order to ipmrove mechanical properties of chitosan membranes, GO was chosen as an additive with promising mechanical properties [19, 47–49].

During preparation of chitosan solution, GO was added to the solution in order to enhance the biological, chemical and mechanical properties of membranes. GO can be dispersed through functionalization, or chemically converted to make different graphene-based nanocomposites with excellent mechanical and thermal properties. GO can be evenly dispersed in chitosan matrix through the formation of amide linkages between them [50].

GO was obtained from Sigma Aldrich in the form of a 2mg/ml aqueous solution. To fabricate CH membranes enriched with GO sheets, various concentrations of CH/GO solutions was prepared. Table 3.1 shows GO concentrations selected in our experiments and their designations.

Necessary amount of commercial GO aqueous solutions (2mg/ml) was taken and treated with ultrasonic homogenization by Omni Sonic Ruptor 4000 Ultrasonic

Table 3.1
CH/GO Composite Concentrations Groups and Their Designations

Designations	CH Content (gr)	GO Content (mg)	Concentrations (WGO/WCH)
CH/GO 1	2	2	0.1% w/w
CH/GO 2	2	4	0.2% w/w
CH/GO 3	2	6	0.3% w/w

Homogenizer, for 30 min. Previously prepared CH 2 %wt solution in 2 %v/v acetic acid was used. The ultrasonication separated GO sheets and shattered then into smaller pieces making it much easier for GO sheets to settle between polymer chains. Dispersion of GO sheets inside the solution and between polymer chains was accomplished by an additional hour of ultrasonic homogenization. The solution was then stirred at 400-500 rpm for 3 hours. After stirring, the GO/CH suspension was poured onto both plain and sharkskin mimicked PDMS negative molds followed by placing them onto hotplate at 30-35 °C for 24-36 hours, allowing water to evaporate for membrane formation. After drying, these membranes were treated with NaOH 1M solution and 2 washes of DI water for 4-6 hours and 3-4 hours respectively as well. The neutralized membranes were placed onto a layer of filter papers and nailed to the surface beneath the filter papers in order to prevent membrane deformation during drying. The membrane packed by filter paper was left to dry at room temperature for 24-36 hours [51].

Covalent bonding of GO to chitosan was checked via Raman, XPS, Swelling ration in DI water and WCA analysis. In this group as well as before, plain membranes were cut in 1cm x 5cm pieces for mechanical tests as well.

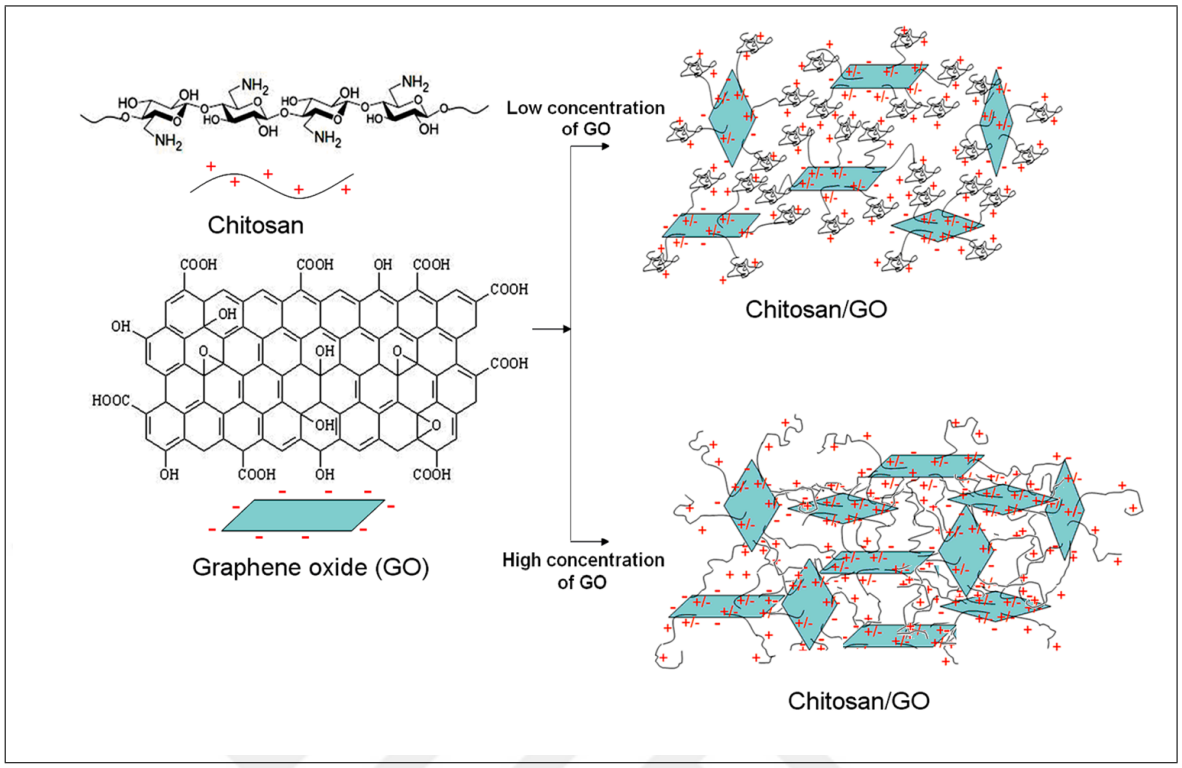

Figure 3.4 Schematic illustration of dispersion of GO sheets in chitosan solution [19].

Table 3.2
Experimental Groups For Chemical, Mechanical and Morphological Characterizations

Designations	GO Content (mg)/CH Content (gr)
CH	0.0% w/w
CH/GO 1	0.1% w/w
CH/GO 2	0.2% w/w
CH/GO 3	0.3% w/w

Table 3.3
Experimental Groups For Cell and Bacterial Culture Experiments

Designations	Chitosan Content (gr)	GO Content (mg)
CH[a]	0.0% w/w	-
CH/GO 1	0.1% w/w	2
CH/GO 2	0.2% w/w	4

[a]CH designated group was the control group

3.4 Surface Characterizations

Surface characterization of experimental groups was divided in three distinct categories:

1. Mechanical Characterizations (Elongation at Break, Tensile Strength)
2. Morphological Characterizations (SEM)
3. Chemical Characterizations (Raman, XPS, WCA, Swelling)

For mechanical tests, 1cm x 5cm strips of membrane were used. As for morphological tests, the membranes were obtained by replicating one specific PDMS negative mold so that comparison would be possible. On the other hand for chemical characterizations, sample membranes were cut in square shape with 1cm x 1cm dimensions. All samples were kept in 60% RH and at RT prior to use [51].

3.4.1 Characterization of Mechanical Properties of Chitosan Based Membranes

Mechanical Characterization included tensile strength and elongation at break measurement. In order to obtain these data CH membranes were prepared and average

thickness of each sample was measured by using 5 random points on each strip and calculating the average value. For mechanical tests, 30 samples of each group were used. In all measurements, the samples were placed between flanges of the instrument in a way that 1cm^2 from top and 1cm^2 from bottom. The rate at which measurements were done was 0.5mm/s with 5kN load. All experiments were done at room temperature and tests stopped when samples broke. The data extracted from this measurement are reported at the results section [52].

3.4.2 Characterization of Morphological Properties of CH Based Membranes

The aim of morphological characterization was to ensure that patterns of sharkskin were replicated along with determination of quality of replication. In order to attain this information, a piece of sharkskin was selected. After pretreatment and prior to PDMS replication, a reference point was created on the surface of the skin. Afterwards PDMS negative mold was obtained and all types of sharkskin mimicked chitosan membranes were fabricated using the same negative mold with reference point.

After drying, membranes were coated with a thin layer of gold with 50nm along with reference sharkskin and the negative PDMS mold prior to SEM imaging. SEM images were captured at 5.00kV voltage and 15mm working distance with various magnifications ranging from 100x to 800x. After SEM imaging was conducted by comparing reference points on chitosan membranes with counterpart points on PDMS negative mold and sharkskin pieces, which provided information about quality of replication. Additionally, SEM images of surface and cross-section of plain membranes was done in order to investigate effects of GO on surface topography and internal structure of plain membranes [13].

3.4.3 Characterization of Chemical Properties of CH Based Membranes

3.4.3.1 Raman Spectroscopy

After preparation of CH membranes, Raman spectroscopy was used to provide information regarding elemental analysis of CH and GO [53].

Room temperature FT Raman spectra (RS) were measured in the 600-1800 $cm^{-1}$and 2400-330 cm^{-1} spectral range with the Nd:YAG excitation and 2cm^{-1} resolution by a Raman spectroscopy, Witec Alpha 300S, Raman Module at laser excitation of 785nm (Ar-ionlaser). The spectroscopic measurements of all samples were independently done from sharkskin mimicked membranes at room temperature [29].

3.4.3.2 X-Ray Photoelectron Spectroscopy (XPS)

Thermo Scientific K-Alpha X-Ray Photoelectron Spectrometer (base pressure of 1x10-10 Torr) was used for XPS measurements. All spectra were collected with an angle of 65° to the analyzer. This condition provided, the deepest sampling (ca. 100 A°) into the films. Angles between 65° and 10° was used to get variable angle XPS spectroscopy in order to monitor spectral changes on the C1s, O1s and N1s region of the spectra as a function of tilting angle. Survey spectra were taken with a pass energy of 165 eV over the range of 1200 and 0 eV. High resolution spectra on the regions of interest were taken in a 20 eV window with a pass energy of 5.85 eV. The envelopes from high resolution spectra were curve-fitted using standard fitting routines with Gaussian-Lorentzian bands and by selecting a linear background [54].

3.4.3.3 Water Contact Angle Measurements

Water contact angle as a good indicator of the degree of hydrophilicity of films and membranes was used to investigate the degree of hydrophilicity/hydrophobicity

of chitosan based membranes and investigate the effect of sharkskin microstructure, surface modification and chemical additives on this property. Since chitosan is a kind of material with water absorption tendency, hence states of a water drop on the film surface varies at various time points, thus were taken as an indication of surface wettability. To this end, 1cm x 5cm strips of all experimental groups of chitosan membrane of both plain and sharkskin mimicked type were prepared. Contact angle of water was measured using DI water at room temperature. Samples were put on a movable sample stage and leveled horizontally; then a drop of about 5 μL of distilled water was placed on the surface of the film using a micro-syringe. The contact angles were measured using a Contact Angle Measurement Instrument (CAM 100, KSV) in a conditioned room by recording contact angle values [55].

3.4.3.4 Swelling Ratio

In order to investigate liquid absorption capacity of chitosan membranes, swelling ration experiment was conducted. Dried chitosan membranes were cut into square shaped pieces with area of $1cm^{-1}$. The dried sheets were conditioned in a vacuum oven for 24 hours prior to use. Swelling test was done with DI water. After dried sheets were weighed, the swelling ratio was determined by immersing membranes in glass bottles containing 10ml of DI water at room temperature. The membranes were then taken out at designated time points of t = 5min, 10min, 30min, 60min, 2h and 4h. Then excess water was removed carefully with filter paper from the surface prior to weighing [56].

The swelling ratio (Q) will be calculated from the equation: Q(%) = ((Wt -Wo) x 100)/W_0 where Wt is the weight of membrane after time point t and Wo will be the weight of initial dry membrane.

3.5 Cell Culture Studies

In order to investigate the behavior of cells towards chitosan based membranes and observe the effects of GO with different concentration on cell attachment and proliferation, fibroblast cell line (L929, ATCC, USA) was cultured on the plain membranes and the viability of cultured cells was measured using MTT assay. The cell culture studies were carried out by culturing approximately 1.5x104 fibroblast cells onto each of the samples which were placed into wells of 24-well plate. RPMI culture medium was used containing 10%v/v Fetal Bovine Serum (FBS) and 1%v/v antibiotic. All samples were sterilized using 2 washes of 70%v/v Ethanol for 15min, each followed by 15min exposure to UV light. Afterwards, ethanol was removed and in order to extract remaining ethanol absorbed by the samples, 3 times washes of PBS was performed each for 2hr followed by final immersion in cell-free medium overnight. Then the cells were cultured on the samples and the plates were placed in an incubator at 37 with 5% CO2 gas concentration inside. Viability of cells was measured on 7th day using MTT assay. Cell culture was performed for 3 treatment groups of plain membranes (CH, CH/GO1 and CH/GO2) and tissue culture plate. (Based on the results obtained with SEM imaging of plain membranes, CH/GO3 membrane group was eliminated.) [57].

MTT assay is a calorimetric method, used to measure level of cell viability by determining the activity of mitochondrial enzymes in living cells. In this method, NAD(P)H-dependent cellular oxidoreductase enzymes are believed to have capability of reflecting the number of viable cells present by reducing the tetrazolium dye 3-(4,5-dimethylthiazol-2-yl) -2,5- diphenyltetrazolium bromide (MTT) to its insoluble formazan, which has a purple color.

After culturing the membranes with L929 cells with density of 1.5x104 cells/well and incubation at 37°C and 5% CO2 for 7 days, MTT assay was performed by preparation of 5mg/ml MTT solution using sterilized DI water and addition of 40μl of it to the medium of each well. Then the plates were incubated for another 3 hours prior to measurement. Afterwards, the MTT solution-containing medium was removed and 250μl Dimethyl Sulfoxide (DMSO) was added to each well and after few minutes, 75μl of each

well's solution was taken and transferred to 96-well plate. Cell viability was calculated by measuring the optical density of the formazan dissolved DMSO solution at 570nm and 750nm as reference wavelengths using a Micro-plate Reader Spectrophotometer (BIO-RAD iMark, Microplate Reader).

4. RESULTS

4.1 Morphological Characterization Results

SEM was used to investigate the quality of mimicking sharkskin surface microtopography using PDMS and CH as materials for negative and positive molds, respectively. Additionally, SEM images provided information regarding effect of chemical additives (GO) on surface topography of plain membranes as well as quality of replication of sharkskin mimicked membranes [15].

Figures 4.1 to 4.4 represent sharkskin, PDMS negative mold and sharkskin mimicked CH Based membrane at 100x to 800x magnification.

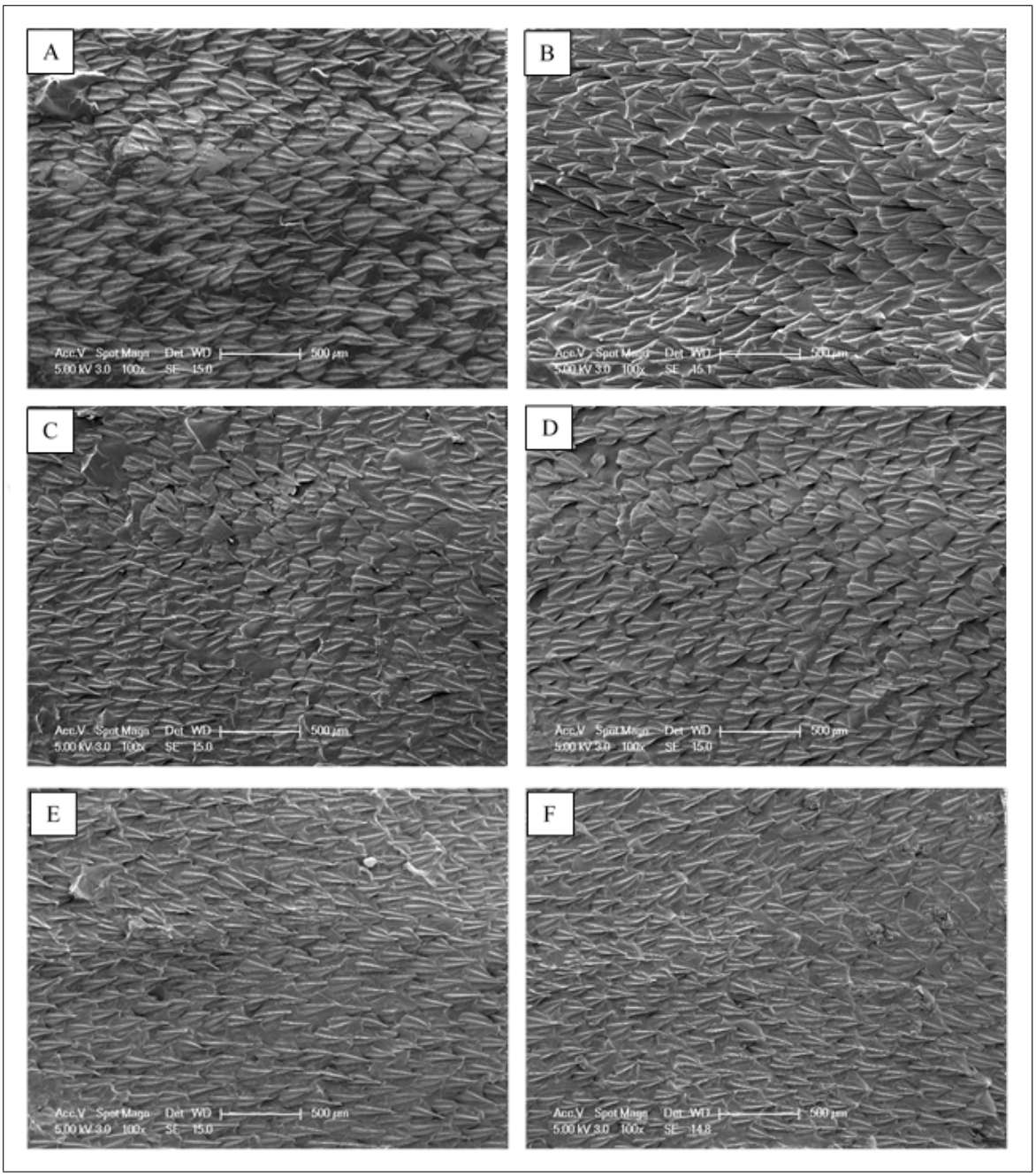

Figure 4.1 Sharkskin, PDMS Negative Mould and Sharkskin Mimicked CH Based Membranes at 100x Magnification: A) Sharkskin, B) Negative PDMS mold, C) Sharkskin Mimicked CH, D) Sharkskin Mimicked CH/GO1, E) Sharkskin Mimicked CH/GO2, F) Sharkskin Mimicked CH/GO3.

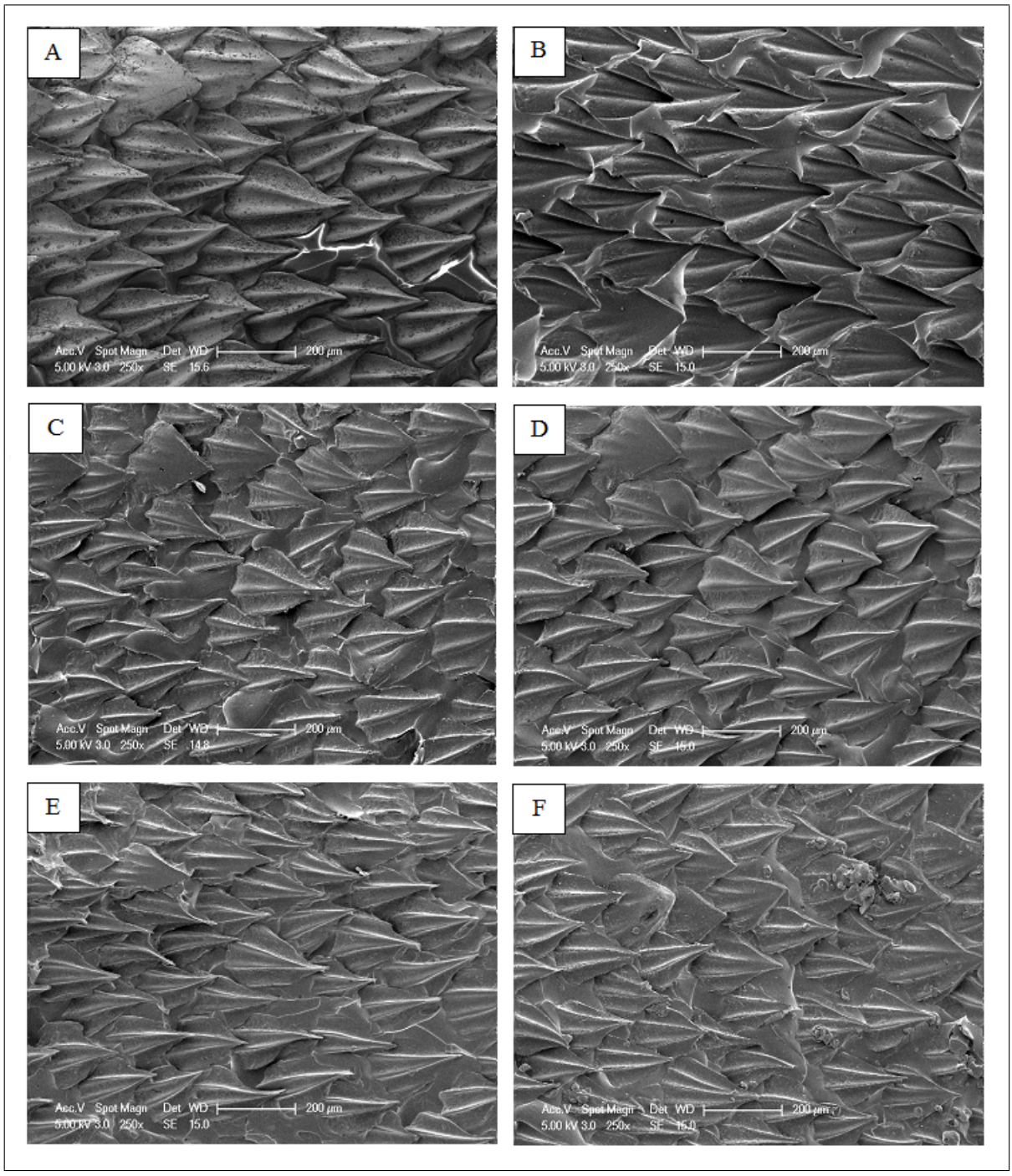

Figure 4.2 Sharkskin, PDMS Negative Mould and Sharkskin Mimicked CH Based Membranes at 250x Magnification: A) Sharkskin, B) Negative PDMS mold, C) Sharkskin Mimicked CH, D) Sharkskin Mimicked CH/GO1, E) Sharkskin Mimicked CH/GO2, F) Sharkskin Mimicked CH/GO3.

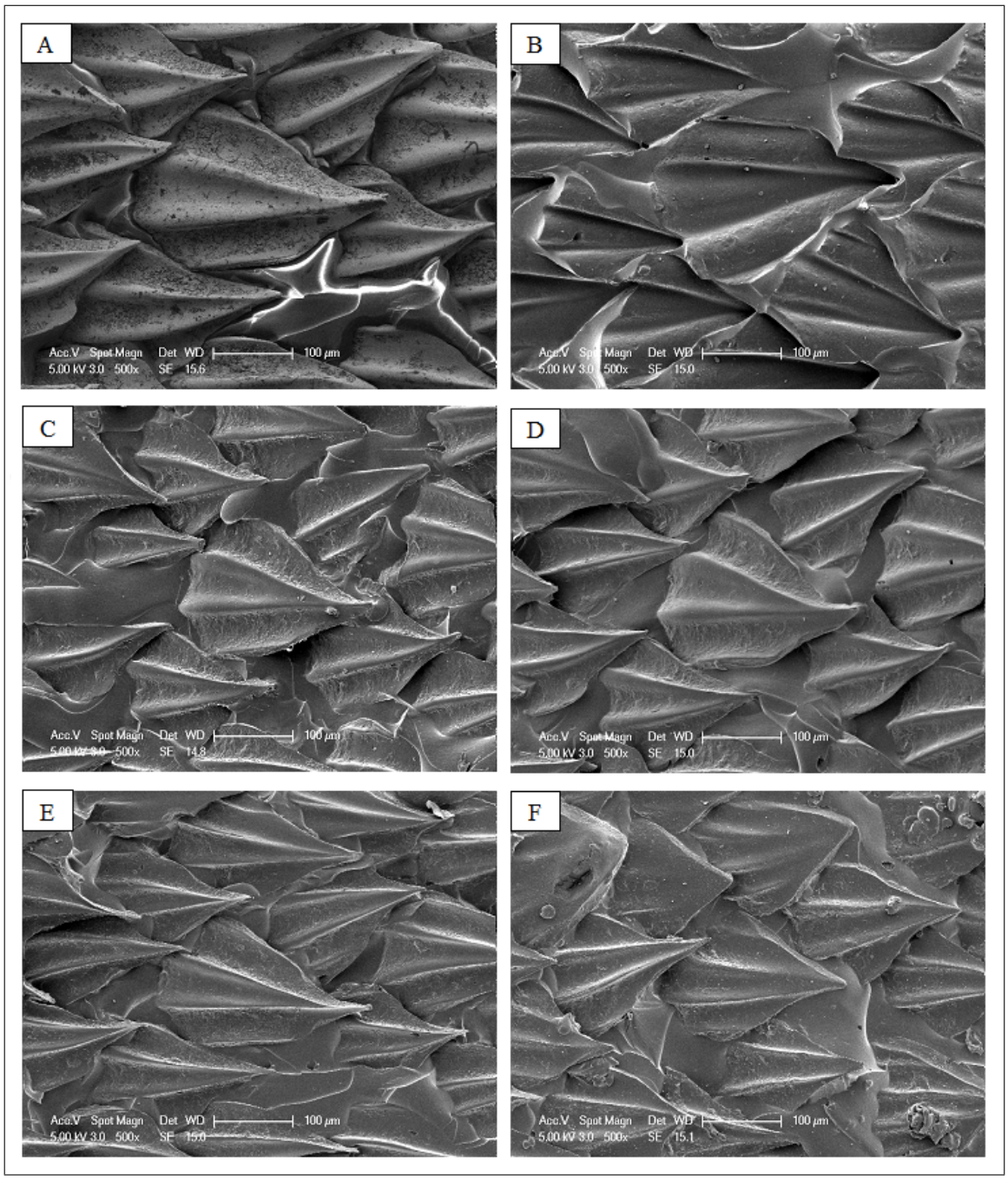

Figure 4.3 Sharkskin, PDMS Negative Mould and Sharkskin Mimicked CH Based Membranes at 500x Magnification: A) Sharkskin, B) Negative, PDMS mold, C) Sharkskin Mimicked CH, D) Sharkskin Mimicked CH/GO1, E) Sharkskin Mimicked CH/GO2, F) Sharkskin Mimicked CH/GO3.

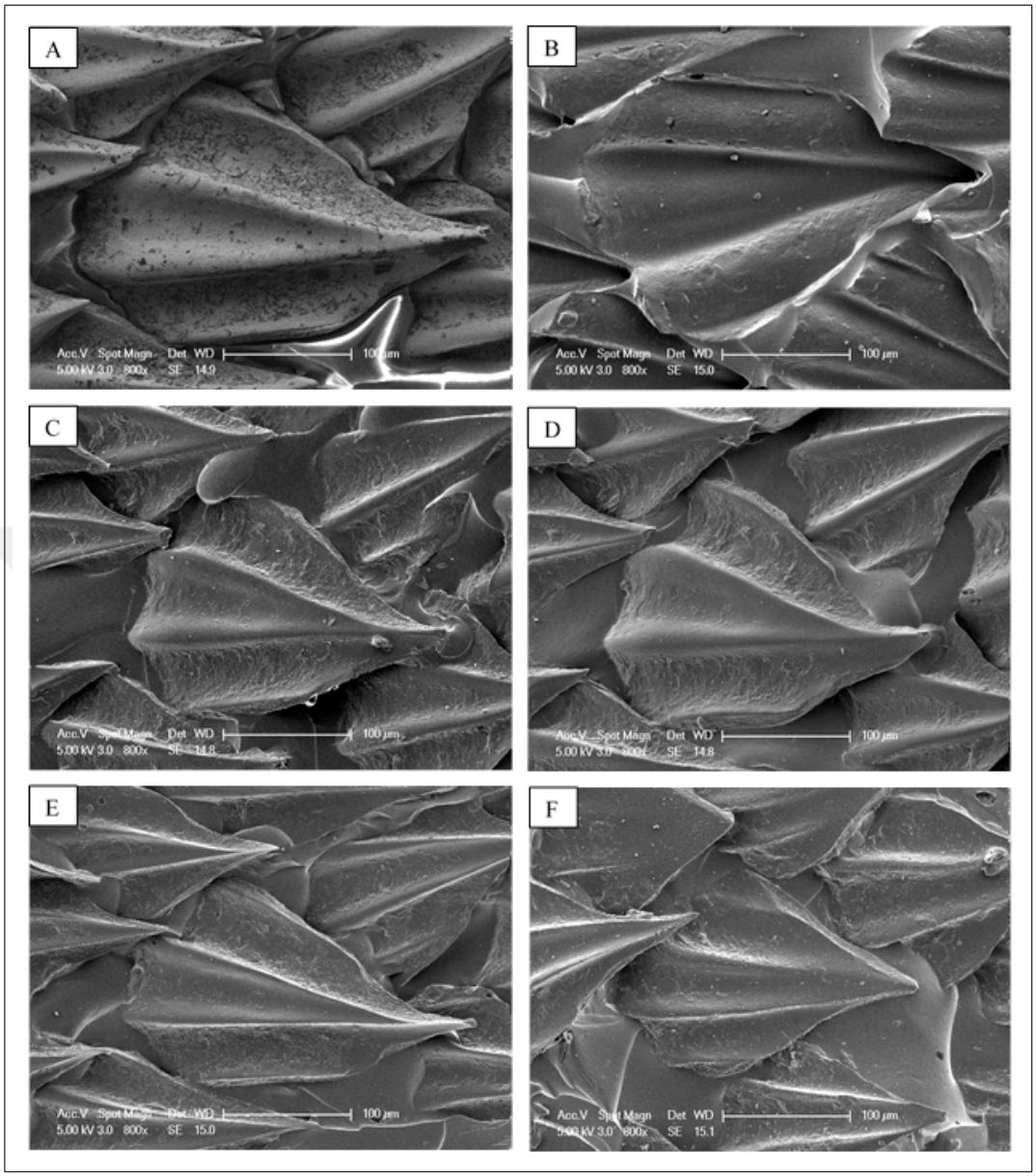

Figure 4.4 Sharkskin, PDMS Negative Mould and Sharkskin Mimicked CH Based Membranes at 800x Magnification: A) Sharkskin, B) Negative PDMS mold, C) Sharkskin Mimicked CH, D) Sharkskin Mimicked CH/GO1, E) Sharkskin Mimicked CH/GO2, F) Sharkskin Mimicked CH/GO3.

From Figures 4.1 to 4.4 , it was observed that mimicking the surface micro-topography of sharkskin was possible using PDMS as a negative mold and CH as a positive membrane. Although the mimicking seemed with high quality using pristine CH, but after addition of GO, in low concentrations, (0.1 and 0.2 %w/w) the quality of replication was increased. However, in high concentration of GO (0.3%w/w) the quality of replication was decreased again.

Effects of GO on structural properties of CH based plain membranes were studied via cross-sectional as well as surface imaging of membranes, which are presented by Figures 4.5 to Figure 4.11.

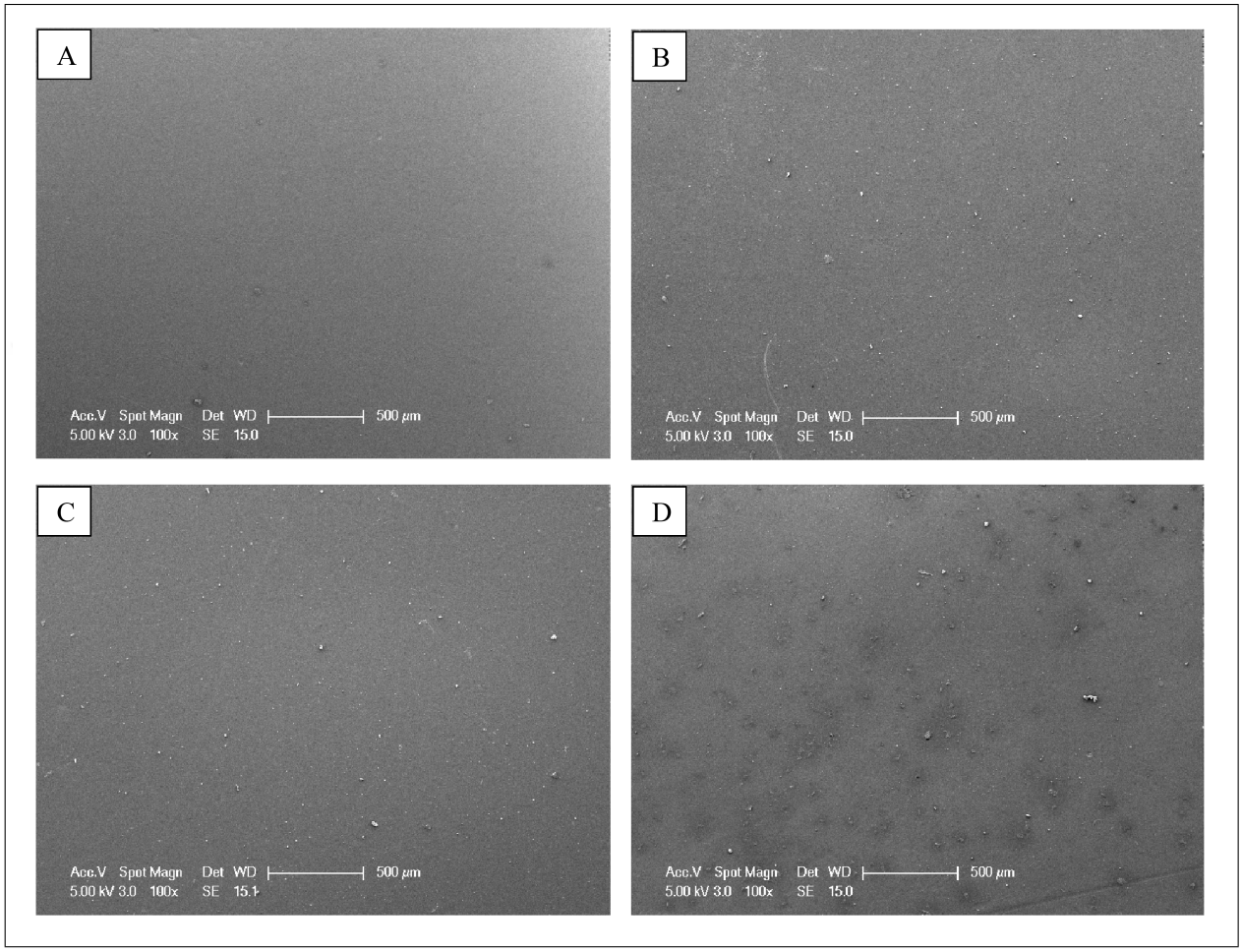

Figure 4.5 Surface Images of CH Based Membranes at $100x$ Magnification: A) Plain Pristine CH, B) Plain CH/GO1, C) Plain CH/GO2 and D) Plain CH/GO3.

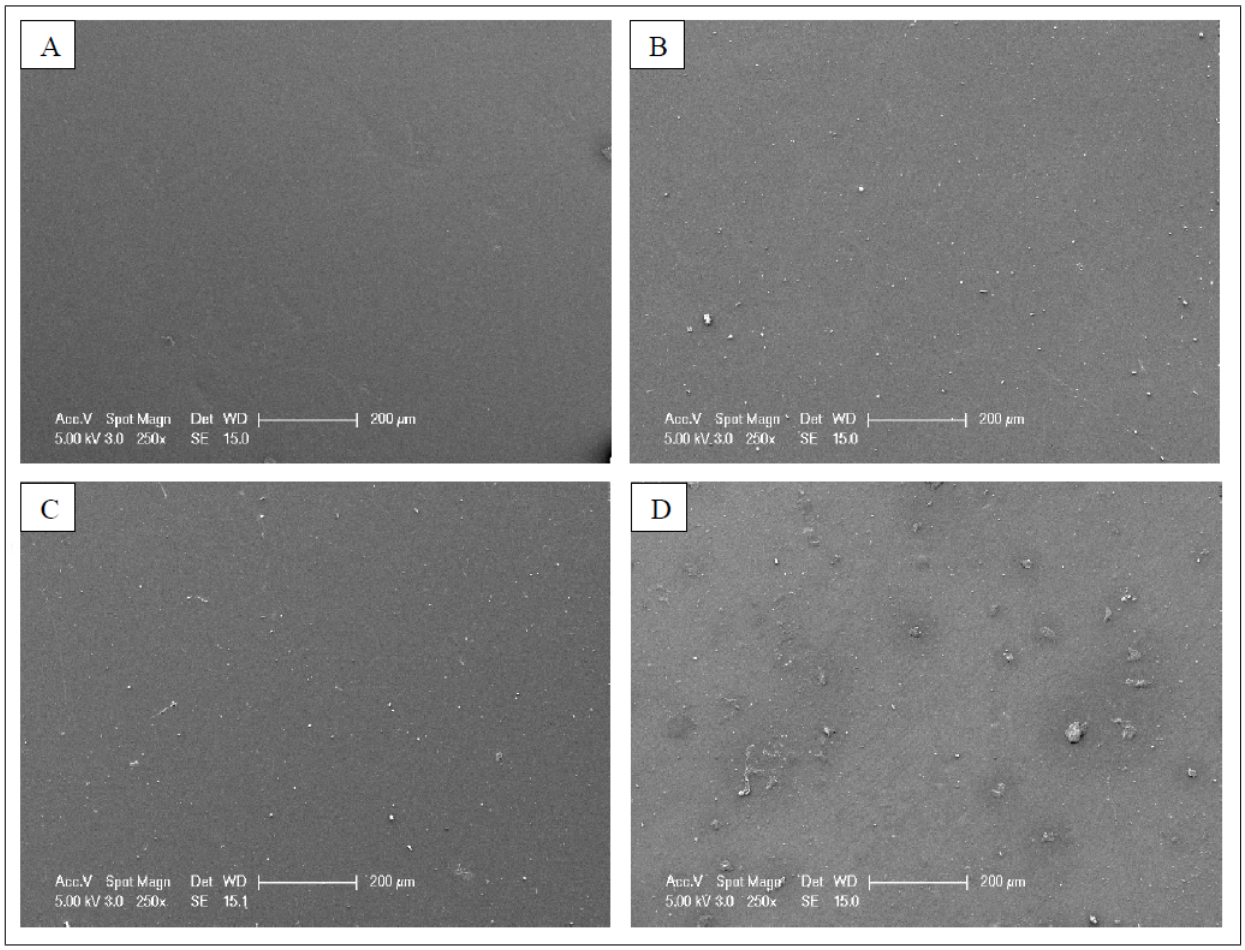

Figure 4.6 Surface Images of CH Based Membranes at 250x Magnification: A) Plain Pristine CH, B) Plain CH/GO1, C) Plain CH/GO2 and D) Plain CH/GO3.

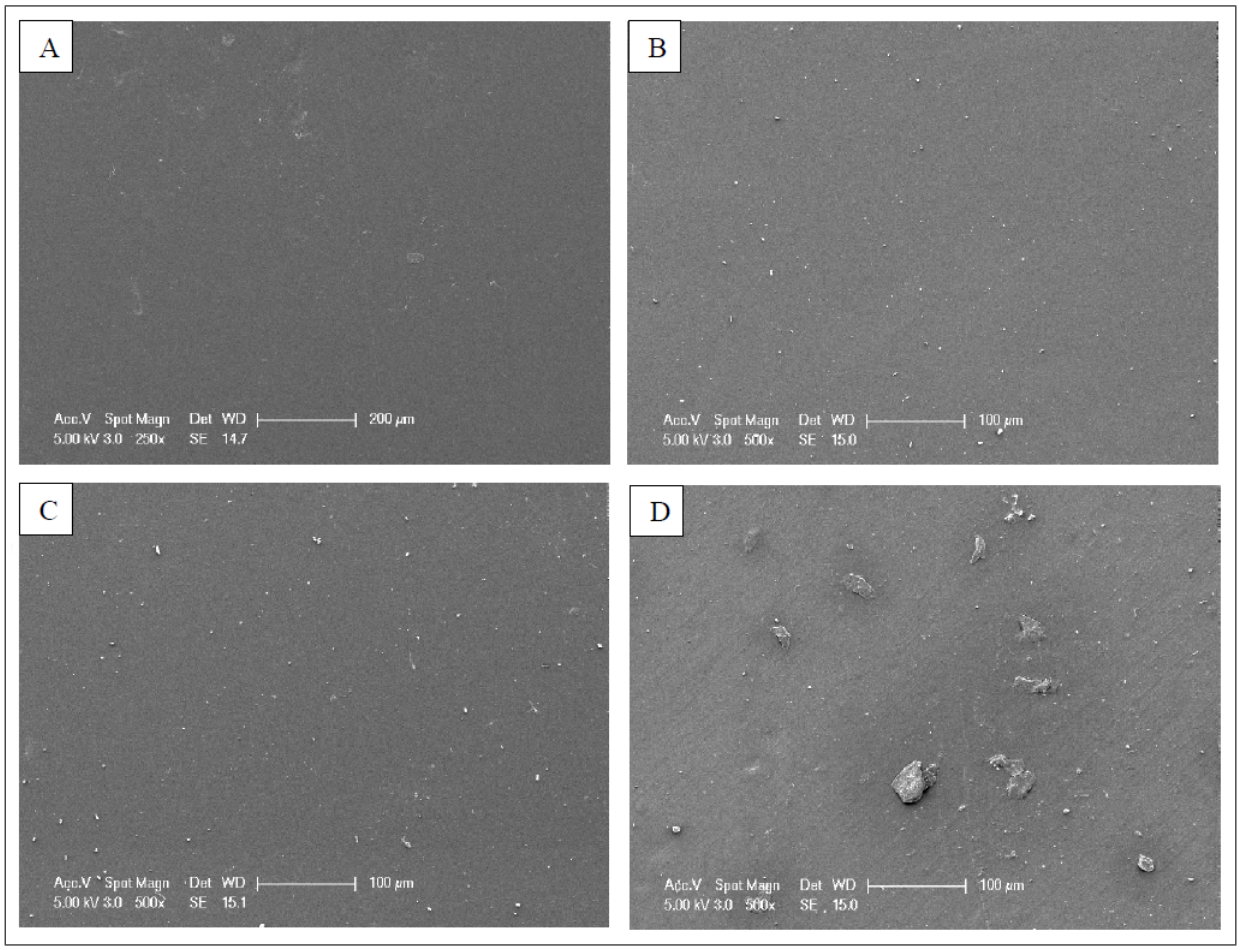

Figure 4.7 Surface Images of CH Based Membranes at 500x Magnification: A) Plain Pristine CH, B) Plain CH/GO1, C) Plain CH/GO2 and D) Plain CH/GO3.

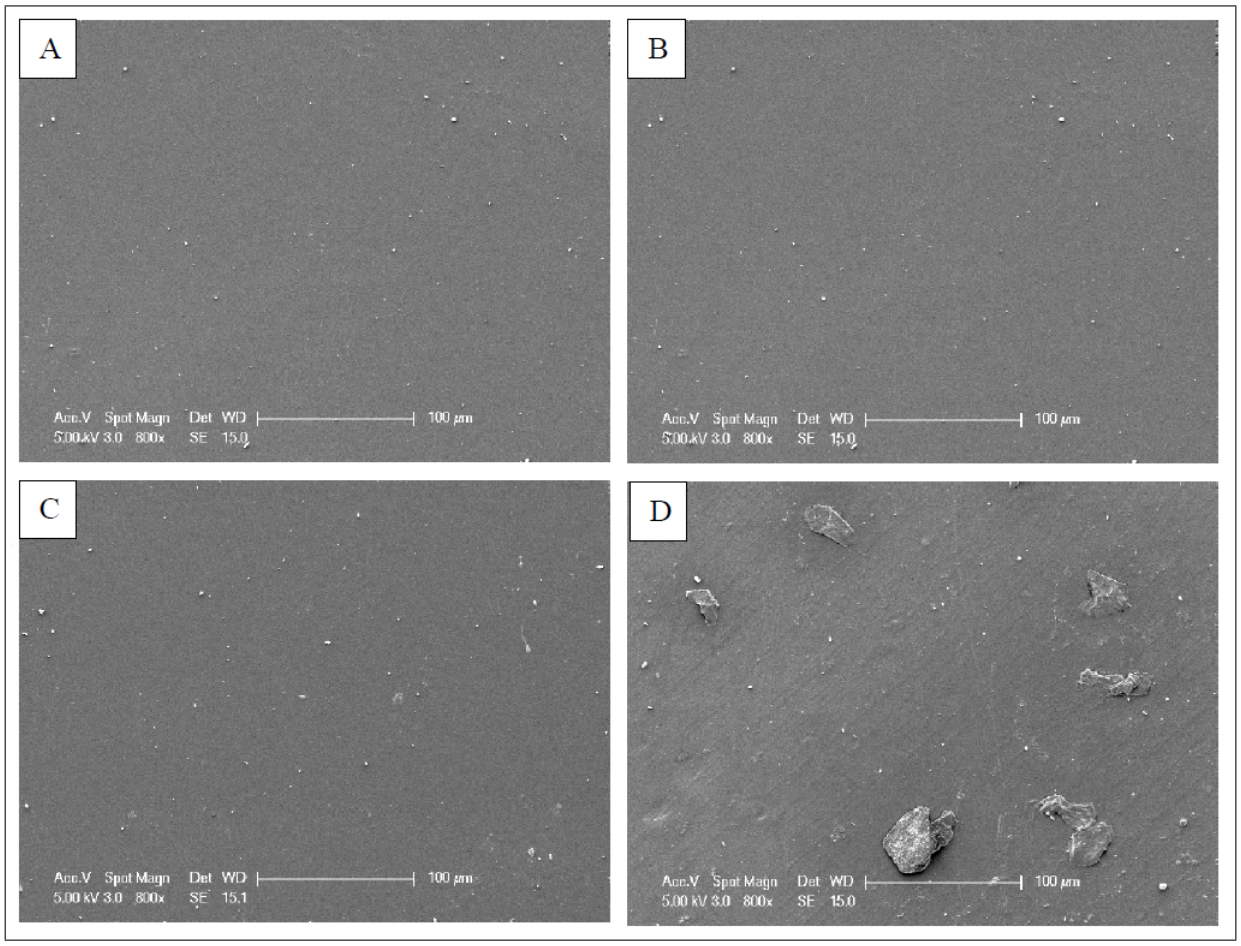

Figure 4.8 Surface Images of CH Based Membranes at 800x Magnification: A) Plain Pristine CH, B) Plain CH/GO1, C) Plain CH/GO2 and D) Plain CH/GO3.

According to images presented in Figures 4.5 to 4.8, GO did not change the surface topography of CH based plain membranes. All membranes were free of any kind of surface morphology, proving the effectiveness of PEG coated PDMS plain mold as a good substrate for plain membrane preparation.

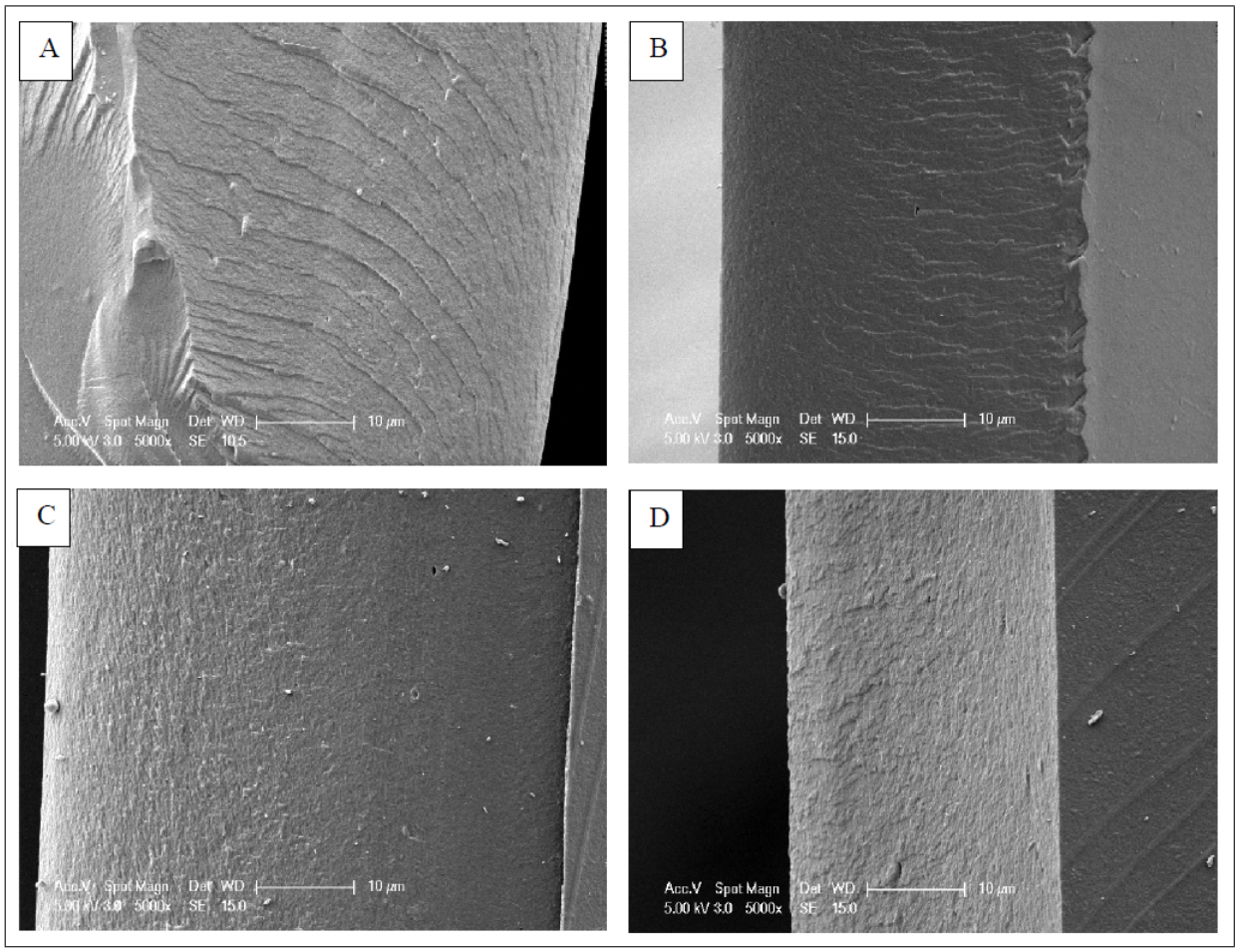

Figure 4.9 Cross-Sectional Images of CH Based Membranes at 5000x Magnification: A) Plain Pristine CH, B) Plain CH/GO1, C) Plain CH/GO2 and D) Plain CH/GO3.

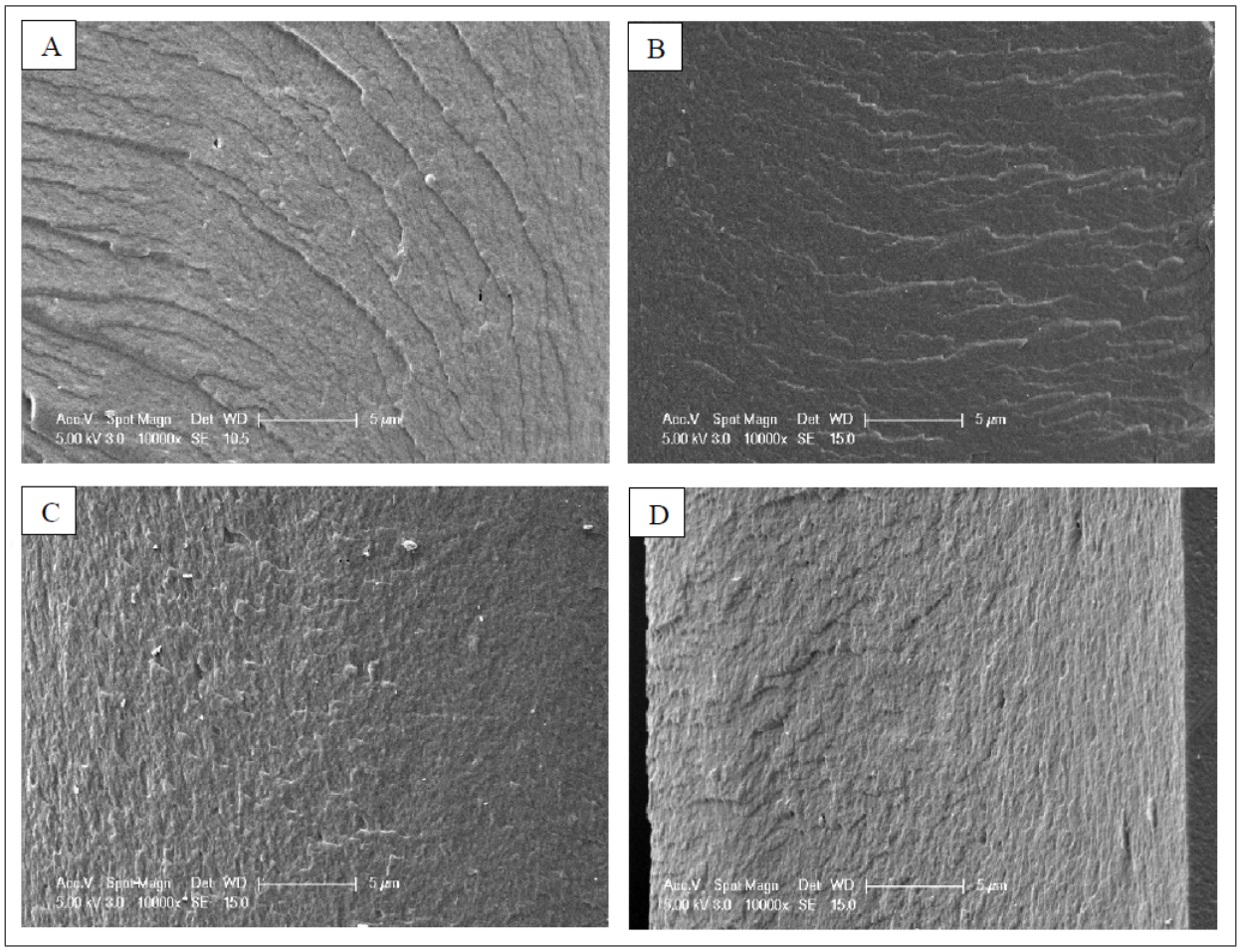

Figure 4.10 Cross-Sectional Images of CH Based Membranes at 10000x Magnification: A) Plain Pristine CH, B) Plain CH/GO1, C) Plain CH/GO2 and D) Plain CH/GO3.

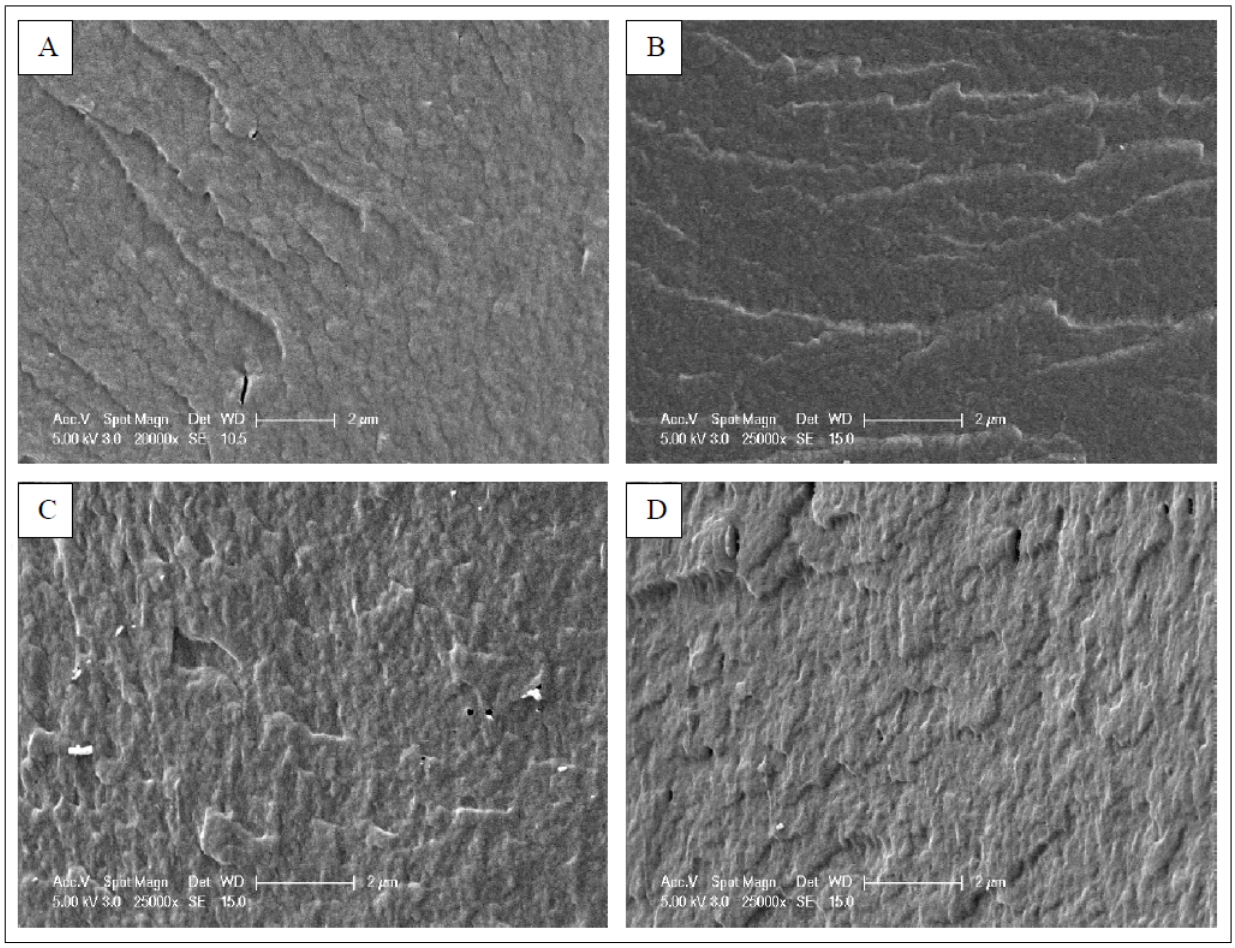

Figure 4.11 Cross-Sectional Images of CH Based Membranes at 25000x Magnification: A) Plain Pristine CH, B) Plain CH/GO1, C) Plain CH/GO2 and D) Plain CH/GO3.

Due to the fact that concentrations of GO inside the membranes were very low, GO was not able to alter the internal structure of CH based membranes; hence cross-sectional images appear to be very alike.

4.2 Mechanical Characterization Results

In order to investigate mechanical properties of CH based membranes with and without GO, Tensile Strength and Elongation at Break tests were performed using 30 samples of 1cm x 5cm dimensions with similar average thicknesses. The measurements

were conducted at RT and samples were at dry state.

4.2.1 Homogeneity Checking (Gaussian Distribution)

Statistical analyses were performed prior to experimentation in order to have samples as much similar to each other as possible and homogeneity of samples was proved by fitting the experimental data to Normal (Gaussian) Distribution. Calculated results are presented in Figures 4.12.

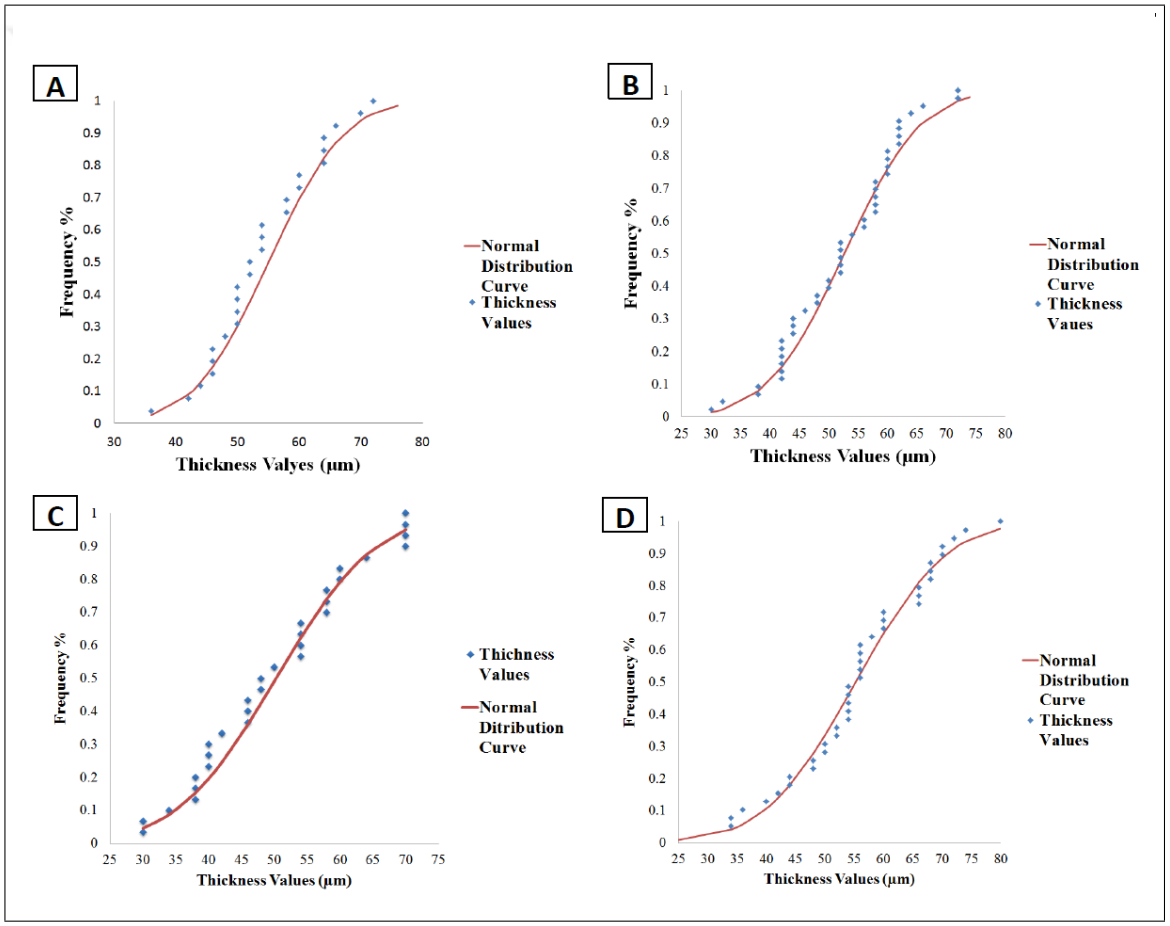

Figure 4.12 Normal Distribution of Membrane Thickness Values: A) Plain CH, B) Plain CH/GO1, C) Plain CH/GO2 and D) Plain CH/GO3.

According to the normal distribution results, all four groups were suited to be statistically analyzed using ANOVA due to the homogenous distribution of valued

around the mean.

4.2.2 Elongation at Break

Elongation at Break(%) is a measurement of mechanical properties representing limits of flexibility of the material. 1cm x 5cm samples were pulled by 0.5mm/s speed at room temperature and in their dry state. Data were obtained from 30 samples in each group and presented in Figure 4.13 Statistical analysis was performed and presented in Table 4.1 [58].

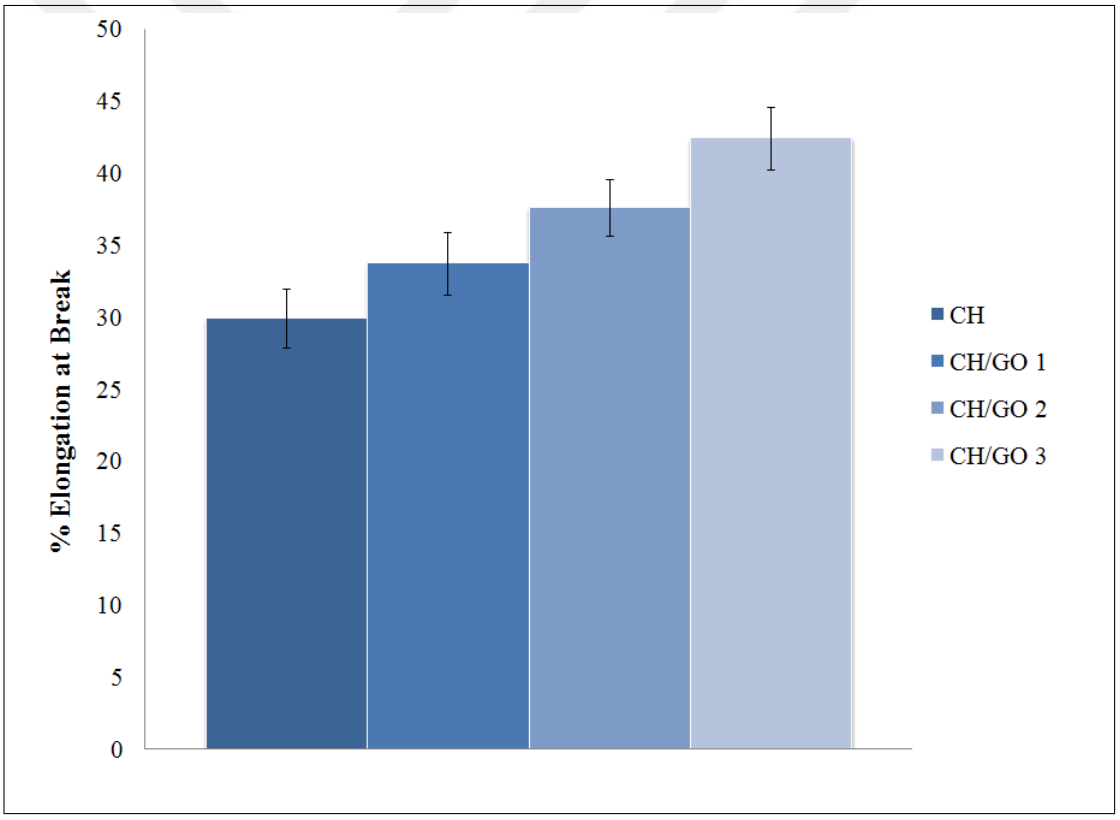

Figure 4.13 Elongation at Break (%) of Plain Membranes. Data are expressed in means ± SE.

Table 4.1
Statistical Analysis of Elongation at Break Data.

Treatments Pair Gropus	One Way ANOVA p-Value (Tukey)	One Way ANOVA Results (Tukey)
CH vs CH/GO 1	0.6866283	Insignificant
CH vs CH/GO 2	0.1932165	Insignificant
CH vs CH/GO 3	0.0074302	$p<0.01$
CH/GO 1 vs CH/GO 2	0.6429162	Insignificant
CH/GO 1 vs CH/GO 3	0.0510281	Insignificant
CH/GO 2 vs CH/GO 3	0.5400516	Insignificant

The purpose of addition of GO to chitosan was to change the fragile nature of CH membranes and make them more flexible. As shown in Figure 4.13, adding GO even at very low concentrations increased the elongation of CH based membranes. Although increase in not found significant according to statistical analysis results but the effectiveness of GO is well illustrated.

4.2.3 Tensile Strength

As well as Elongation at Break, Tensile Strength is also a measurement of mechanical properties of polymeric membranes. Tensile strength of CH membranes along with CH/GO nanocomposites were measured simultaneously with elongation measuring. Obtained data and their statistical analysis results are presented in Figure 4.14 and Table 4.2 respectively [58].

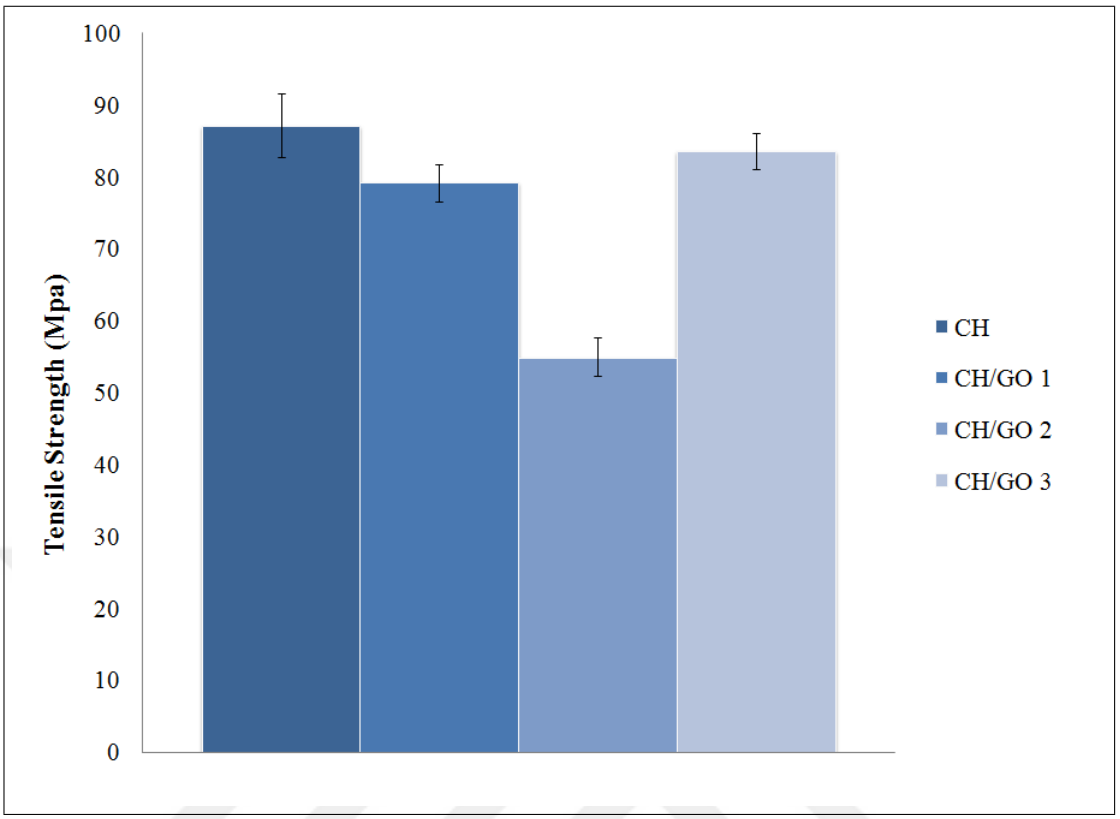

Figure 4.14 Tensile strength of of Plain Membranes (Mpa). Data are expressed in means ± SE.

Table 4.2
Statistical Analysis of Tensile Strength (Mpa) Results.

Treatments Pair Gropus	One Way ANOVA p-Value (Tukey)	One Way ANOVA Results (Tukey)
CH vs CH/GO 1	0.2969210	Insignificant
CH vs CH/GO 2	0.0010053	$p<0.01$
CH vs TCP	0.8938506	Insignificant
CH/GO 1 vs CH/GO 2	0.0010053	$p<0.01$
CH/GO 1 vs CH/GO 3	0.6727818	Insignificant
CH/GO 2 vs CH/GO 3	0.0010053	$p<0.01$

By examining the results of Tensile Strength experiments, it was concluded that addition of GO decreased Tensile strength of CH. As the concentration of GO in chi-

tosan increased, the tensile strength decreased more and more except for CH/GO3 group in which tensile strength is approximately as high as CH group which was an unexpected phenomena and might have occurred due to the increased chemical interactions between GO flakes and chitosan polymer chains [58].

4.3 Chemical Characterization

4.3.1 Raman Spectroscopy

Raman spectroscopy as one of the spectroscopic techniques was used to observe vibrational, rotational, and other low-frequency modes in a system, which provided a fingerprint by which molecules could be identified [58]. All samples were subjected to the measurement within one day and at RT. Since CH based membranes were transparent, sharkskin mimicked samples were chosen for this test due to the ease of contrast on patterned surface rather than plain surface.

Obtained results are presented in Figure 4.15 and 4.16.

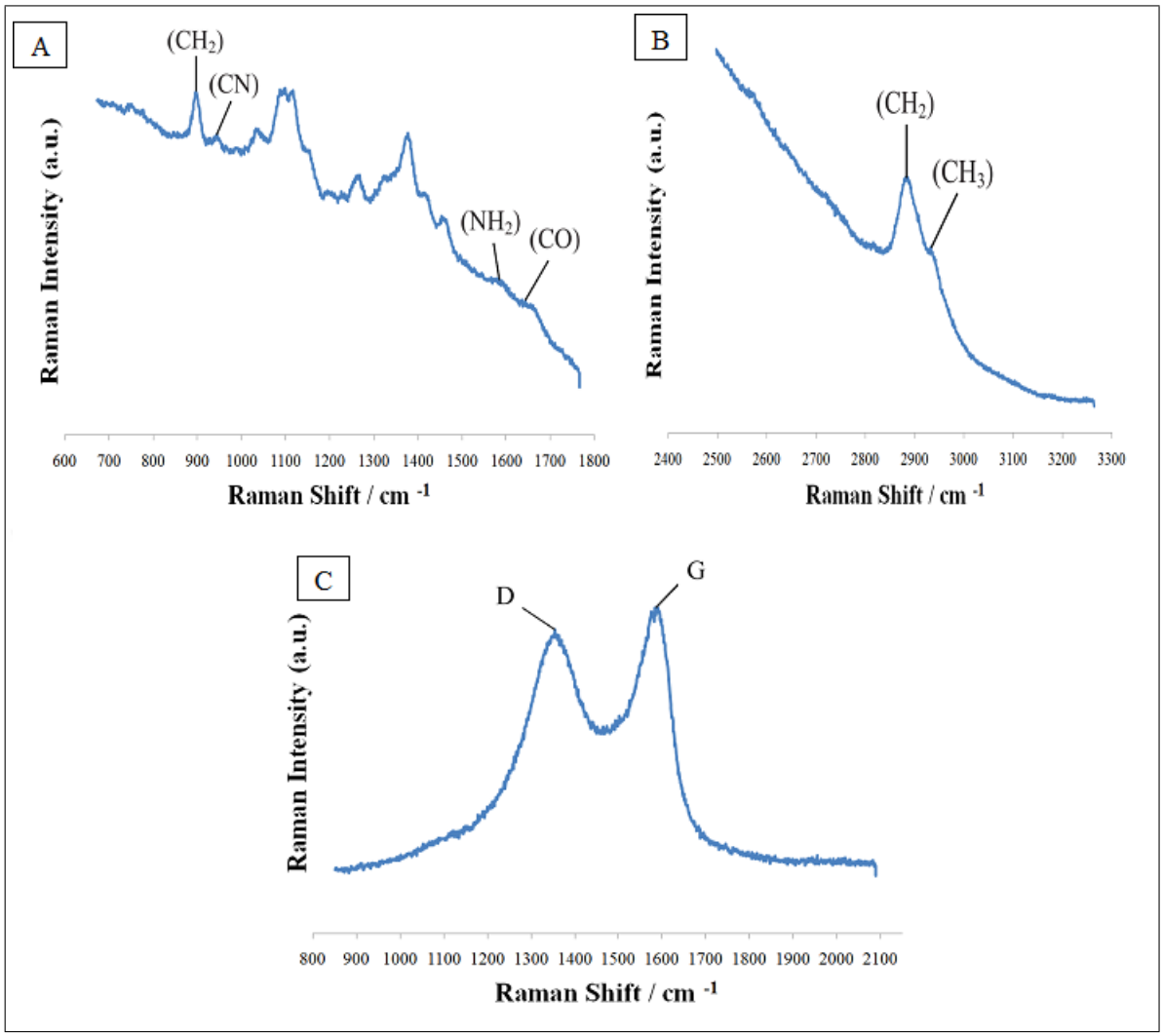

Figure 4.15 A) Raman Spectrum of CH at 600-1800 cm^{-1} Range, B) Raman Spectrum of CH at 2400-3300 cm^{-1} Range and C) Raman Spectrum of GO at 800-2200 cm^{-1} Range.

Investigating chemical structure of chitosan membrane provided information regarding elements based on wavelength of chemical bond.(Figure 4.15 (a) and (b)) Specific band along with their wavenumbers are shown in Table 4.3.[81]

There were slight shifts observed which were due to purification process that was initially performed on chitosan [53].

Table 4.3
Statistical Analysis of Tensile Strength (Mpa) Results [59].

Band Assignment	Observed Wavenumber cm^{-1}	Expected Wavenumber cm^{-1}
υCH_2	2887	2885
CH_3	2934	2932
CO	1662	1654
CN	944	936
NH_2	1590	1591
ρCH_2	897	896
CH + CH_2 + OH	1462	1458

Raman spectrum of GO was presented in Figure 4.15(c). Since GO is derived from Graphite, it is essentially a carbonic product therefore in the Raman spectra only D and G bands were of importance; hence spectrum was recorded only in 800 - 2200 cm^{-1} range.

The ratio of I_D to I_G was calculated at 0.93 for pristine GO. G band appeared at 1578.4 cm^{-1} and D band at 1349.7 cm^{-1} whereas they should have appeared at 1580 cm^{-1} and 1350 cm^{-1} respectively. Observed shifts were considered normal as they were slight changes [59].

For CH/GO nanocomposites membranes, Raman spectrums were recorded at 600-1800 cm^{-1} and 2400-3300 cm^{-1} range and obtained are presented in Figure 4.16.

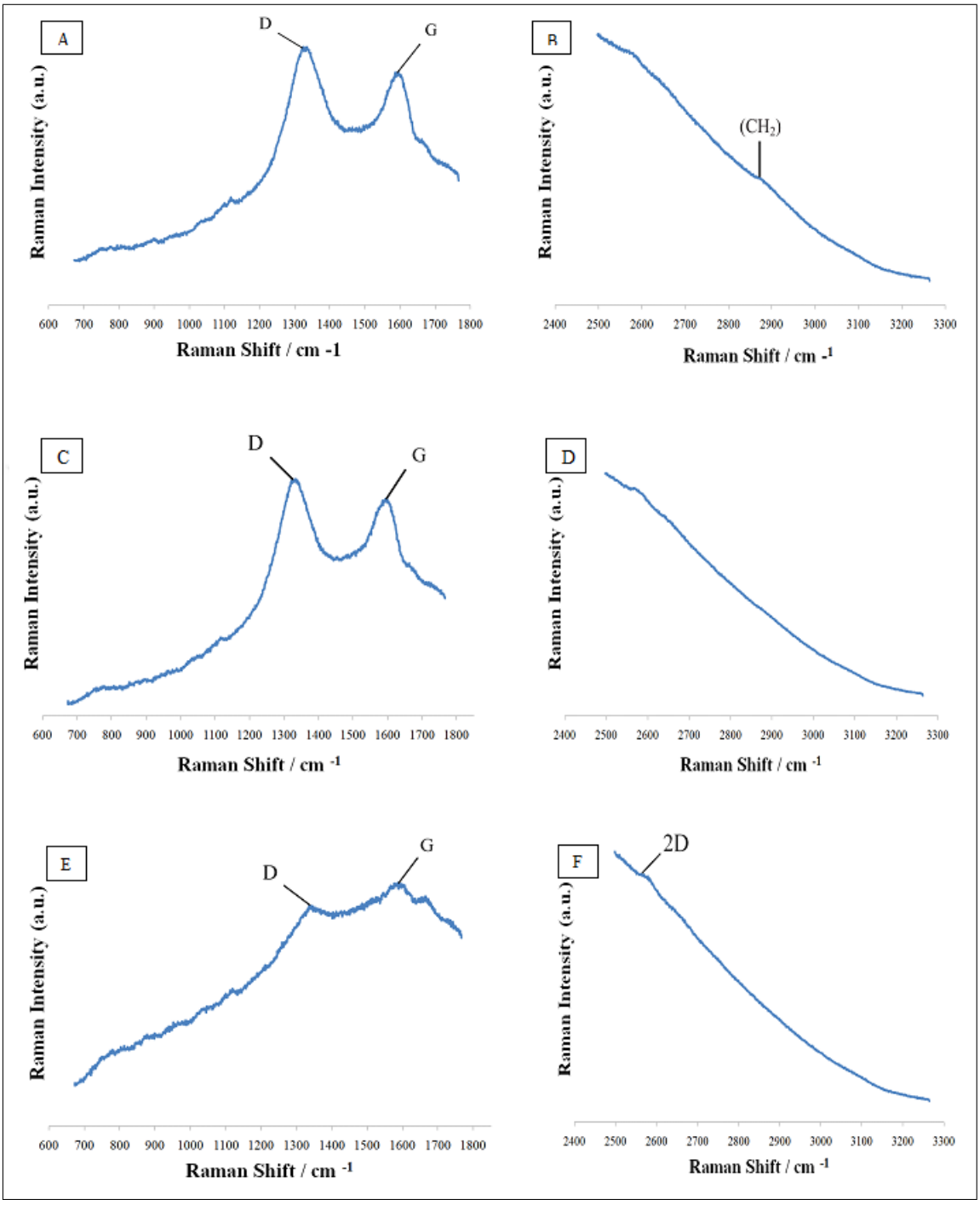

Figure 4.16 A) Raman Spectrum of CH/GO1 at 600-1800 cm-1 Range, B) Raman Spectrum of CH/GO1 at 2400-3300 cm-1 Range, C) Raman Spectrum of CH/GO2 at 600-1800 cm-1 Range, D) Raman Spectrum of CH/GO2 at 2400-3300 cm-1 Range, E) Raman Spectrum of CH/GO3 at 600-1800 cm-1 Range and, F)Raman Spectrum of CH/GO3 at 2400-3300 cm-1 range [19].

According to the data obtained from the spectrum (Fig 4.16), it was concluded that none of the major peaks of CH were detectable meaning that all were suppressed by

GO's D and G band. The D band appeared at 1327 cm^{-1} and the G band appeared at 1595 cm^{-1} which were noticeably dispositioned which were due to interactions between GO flakes and chitosan chains. In the range of 2400 to 3300 cm^{-1} the CH_2 peak of chitosan is still detectable at 2871 cm^{-1} which also shifted. I_D/I_G was calculated at 1.04 [15, 53, 59].

In case of CH/GO2, D and G band appeared at 1326 cm^{-1} and 1593 cm^{-1} with very little shifts compared to CH/GO2, whereas CH_2 peak of chitosan in the range of 2400 to 3300 cm^{-1} had almost completely disappeared. I_D/I_G was calculated at 1.03.

In the highest GO concentration, 2D peak of GO had appeared at 2579 cm^{-1} in addition to significant shifts of D and G band which were detected at 1338 cm^{-1} and 1585 cm^{-1} respectively. I_D/I_G was calculated at 0.97 [15, 53, 59].

4.3.2 X-Ray Photoelectron Spectroscopy (XPS)

In order to measures the elemental composition at the parts per thousand range, empirical formula, chemical state and electronic state of the elements that exist within a material XPS was used as a surface-sensitive quantitative spectroscopic technique [60]. XPS survey spectrum along with high resolution spectrums and deconvolution curves of C1s, O1s and N1s core levels were measured and illustrated in Figures 4.17 to 4.21.

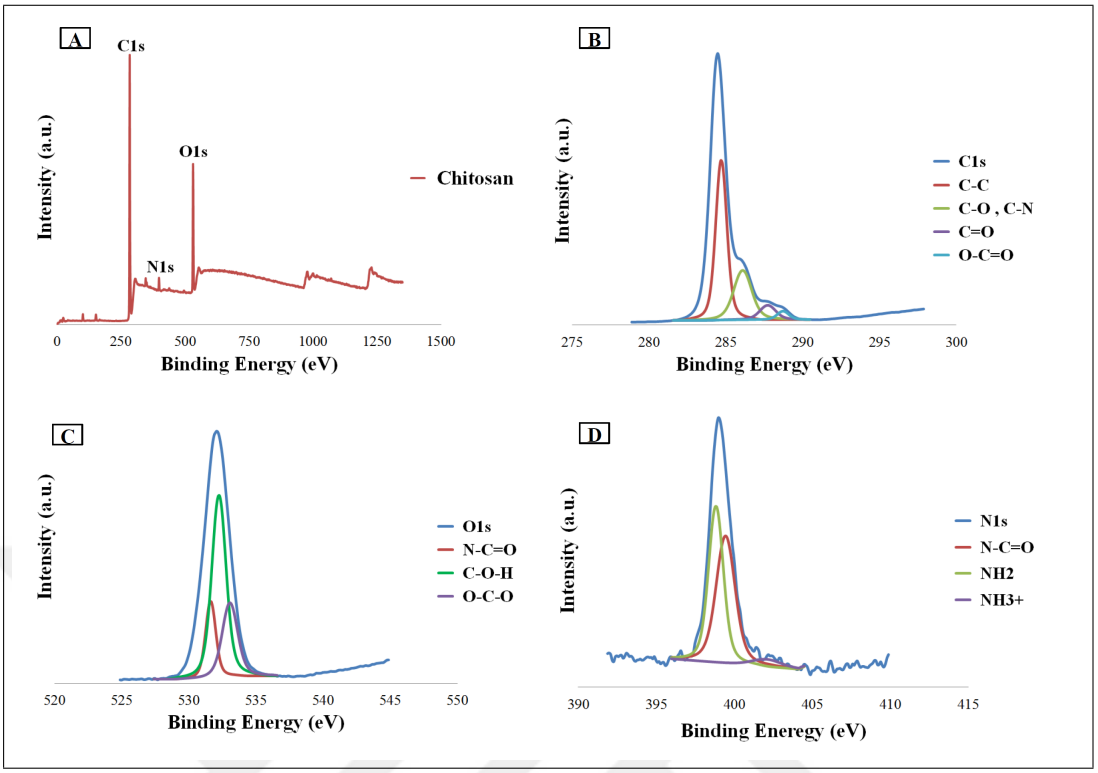

Figure 4.17 A) XPS Survey Spectrum of CH, B) High-Resolution Spectrum of Carbon Peaks (C1s) of CH, C) High-Resolution Spectrum of Oxygen Peaks (O1s) of CH, D) High-Resolution Spectrum of Nitrogen Peaks (N1s) of CH.

Based on the data obtained from survey spectrum of pristine chitosan, C1s, O1s and N1s peaks appeared at 285 eV, 532.26 eV and 399.25 eV respectively. Table 4.4 illustrates atomic percentages of elements in chitosan [6, 60].

Table 4.4
Measured Atomic % of C, O and N in Pirsitine CH.

Atom	Measured Atomic %
C	81.06
O	16.47
N	2.47

XPS spectrum of C1s core level was obtained and 6 peaks were identified in

total, C-C, C-H, C=O and COO- which were found at 284.71 eV, 284.32 eV, 287.73 eV and 288.73 eV respectively as well as C-N and C-OH peaks that were both assigned to 286.1 eV. Table 4.5 illustrates parameters of measured peaks [6, 60].

Table 4.5
C1s Measured Peaks Parameters (Binding Energy(eV), Height Ratio, Full at Half Maximum (eV)) in CH.

Designation Band	Peak BE (eV)	Height Ratio	FWHM (eV)
C-N , C-OH	286.1	0.31	1.38
C=O	287.73	0.09	1.23
COO-	288.73	0.05	0.9
C-C	284.71	1	0.86
C-H	284.32	0.74	0.72

XPS spectrum of O1s core level was also obtained and 3 peaks were identified appearing at 532.24 eV, 533.06 eV and 531.63 eV and were assigned to C-O-H, O-C-O and N-C=O bands respectively. Table 4.6 illustrates parameters of measured peaks [6, 60].

Table 4.6
O1s Measured Peaks Parameters (Binding Energy(eV), Height Ratio, Full at Half Maximum (eV)) in CH.

Designation Band	Peak BE (eV)	Height Ratio	FWHM (eV)
C-O-H	532.24	1	1.26
O-C-O	533.06	0.4	1.36
N-C=O	531.63	0.42	0.9

XPS spectrum of N1s core level was recorded resulting in identification of three peaks in total, N-C=O, NH_2 and NH_3^+ which were found at 399.44 eV, 398.83 eV and 402.05 eV respectively. Table 4.7 illustrates parameters of measured peaks [6, 60].

Table 4.7
N1s Measured Peaks Parameters (Binding Energy(eV), Height Ratio, Full at Half Maximum (eV)) in CH.

Designation Band	Peak BE (eV)	Height Ratio	FWHM (eV)
N-C=O	399.44	0.81	1.44
NH_2	398.83	1	1.12
NH_3^+	402.05	0.05	2.23

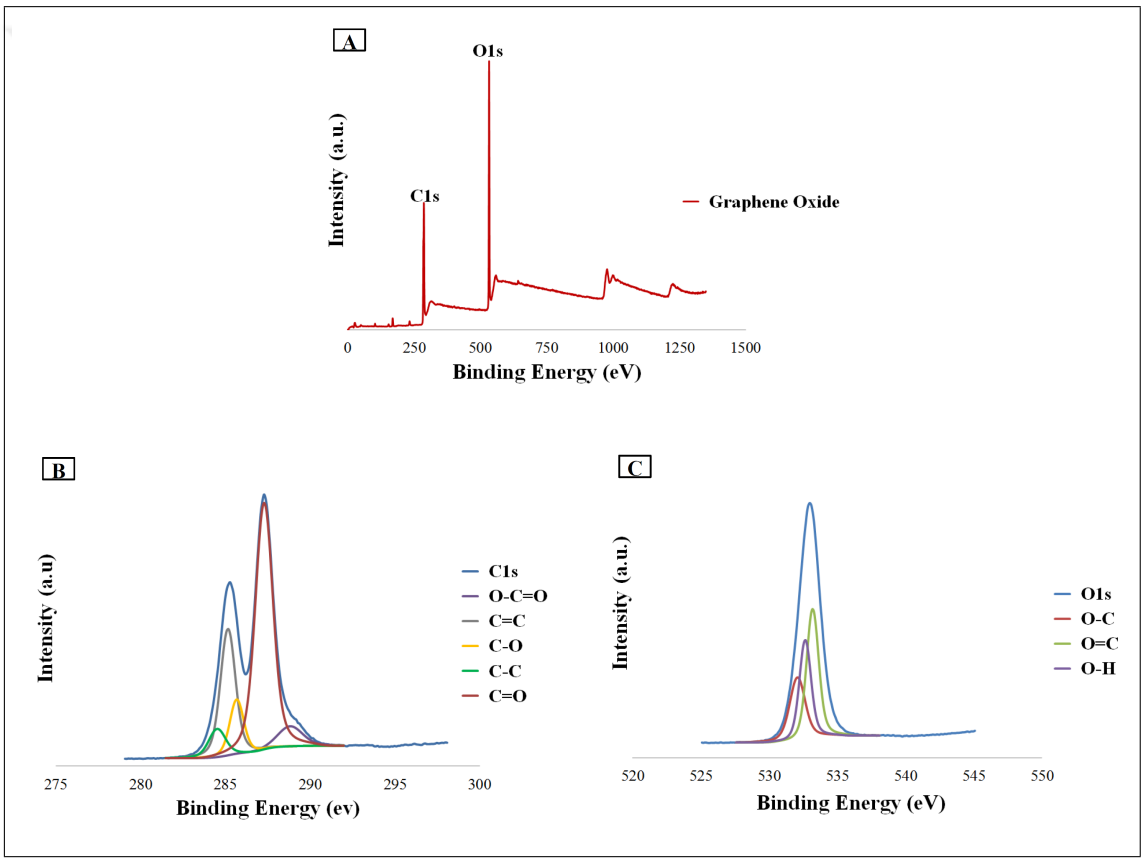

Figure 4.18 A) XPS Survey Spectrum of GO, B) High-Resolution Spectrum of Carbon Peaks (C1s) of GO, C) High-Resolution Spectrum of Oxygen Peaks (O1s) of GO.

XPS survey spectrum of pristine GO was obtained O1s and C1s peaks appeared at 533.13 eV, and 286.75 eV respectively. Table 4.8 illustrates atomic percentages of elements in pristine GO.

Table 4.8
Measured Atomic % of C and O in Pirsitine CH.

Atom	Measured Atomic %
C	35.02
O	64.98

XPS spectrum of C1s core level was obtained and five peaks were identified in total, C=O, C-C, O-C=O, C=C and C-O which were found at 287.29 eV, 284.52 eV, 288.82 eV, 285.15 eV and 285.67 eV respectively. Table 4.9 illustrates parameters of measured peaks [23, 61].

Table 4.9
C1s Measured Peaks Parameters (Binding Energy(eV), Height Ratio, Full at Half Maximum (eV)) in GO.

Designation Band	Peak BE (eV)	Height Ratio	FWHM (eV)
C=O	287.29	1	1.22
C-C	284.52	0.11	1.19
O=C-O	288.82	0.08	1.73
C=C	285.15	0.51	1.05
C-O	285.67	0.22	0.98

XPS spectrum of O1s core level was also obtained and 3 peaks were identified appearing at 532.08 eV, 533.19 eV and 532.65 eV and were assigned to O-C, O=C and O-H bands respectively. Table 4.10 illustrates parameters of measured peaks [23, 61].

Table 4.10
O1s Measured Peaks Parameters (Binding Energy(eV), Height Ratio, Full at Half Maximum (eV)) in GO.

Designation Band	Peak BE (eV)	Height Ratio	FWHM (eV)
O-C	532.08	0.49	1.35
O=C	533.19	1	1.05
O-H	532.65	0.77	1.01

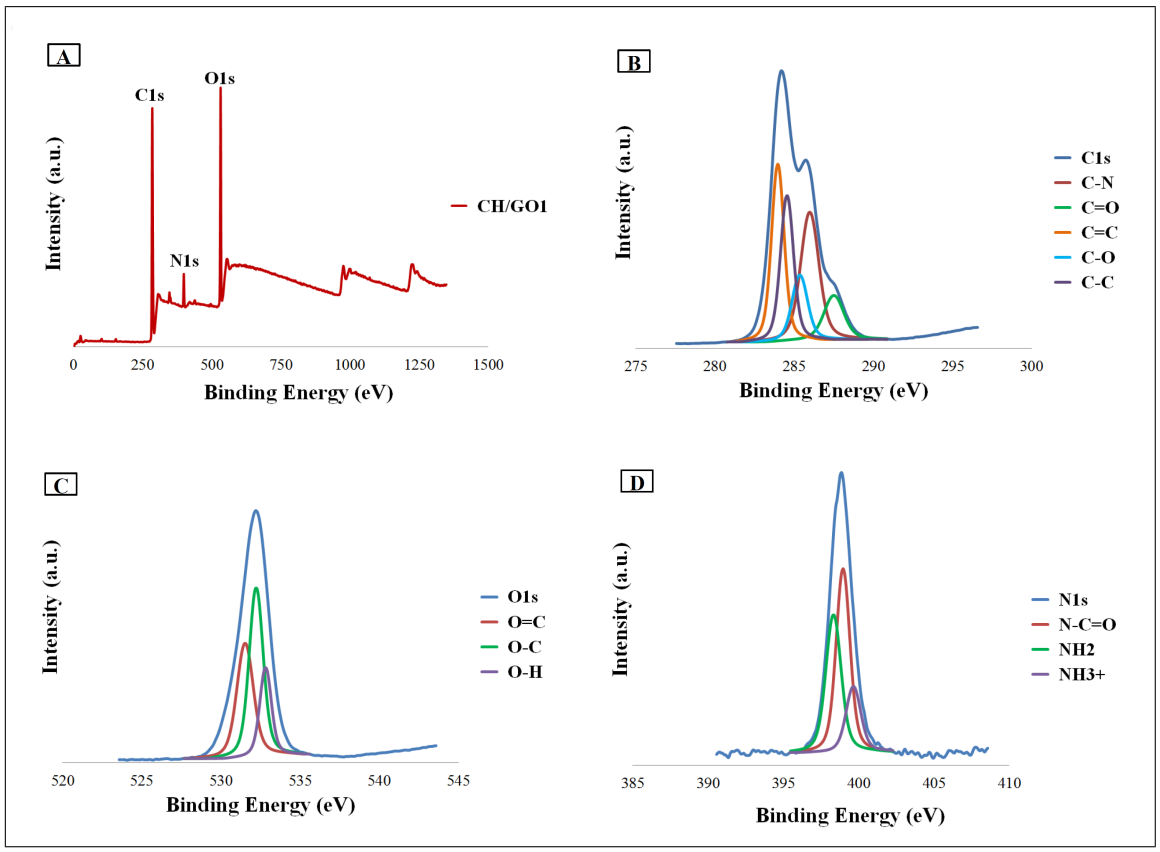

Figure 4.19 A) XPS Survey Spectrum of CH/GO1, B) High-Resolution Spectrum of Carbon Peaks (C1s) of CH/GO1, C) High-Resolution Spectrum of Oxygen Peaks (O1s) of CH/GO1, D) High-Resolution Spectrum of Nitrogen Peaks (N1s) of CH/GO1.

Based on the data obtained from survey spectrum of CH/GO1, C1s, O1s and N1s peaks appeared at 291.57 eV, 537.57 eV and 404.47 eV respectively. Table 4.11 illustrates atomic percentages of elements in CH/GO1.[83-86]

Table 4.11
Measured Atomic % of C, O and N in Pirsitine CH/GO1.

Atom	Measured Atomic %
C	72.90
O	22.39
N	4.71

XPS spectrum of C1s core level of CH/GO1 was obtained and five peaks were identified in total, C-N, C=O, C=C, C-C and C-O which were found at 285.99 eV, 287.51 eV, 283.97 eV, 284.55 eV and 285.36 eV respectively. Table 4.12 illustrates parameters of measured peaks [6, 60].

Table 4.12
C1s Measured Peaks Parameters (Binding Energy(eV), Height Ratio, Full at Half Maximum (eV)) in CH/GO1.

Designation Band	Peak BE (eV)	Height Ratio	FWHM (eV)
C-N	285.99	0.72	1.36
C=O	287.51	0.25	1.49
C=C	283.97	1	0.94
C-C	284.55	0.82	0.98
C-O	285.36	0.37	1.16

XPS spectrum of O1s core level of CH/GO1 was also obtained and 3 major peaks were identified appearing at 531.53 eV, 532.22 eV and 532.82 eV and were assigned to O=C, O-C and O-H bands respectively. Table 4.13 illustrates parameters of measured peaks [6, 60].

Table 4.13
O1s Measured Peaks Parameters (Binding Energy(eV), Height Ratio, Full at Half Maximum (eV)) in CH/GO1.

Designation Band	Peak BE (eV)	Height Ratio	FWHM (eV)
O=C	531.53	0.68	1.23
O-C	532.22	1	1.05
O-H	532.82	0.52	0.87

Table 4.14
N1s Measured Peaks Parameters (Binding Energy(eV), Height Ratio, Full at Half Maximum (eV)) in CH/GO1.

Designation Band	Peak BE (eV)	Height Ratio	FWHM (eV)
N-C=O	398.97	1	1.09
NH_2	398.34	0.75	1.2
NH_3^+	399.66	0.36	1.16

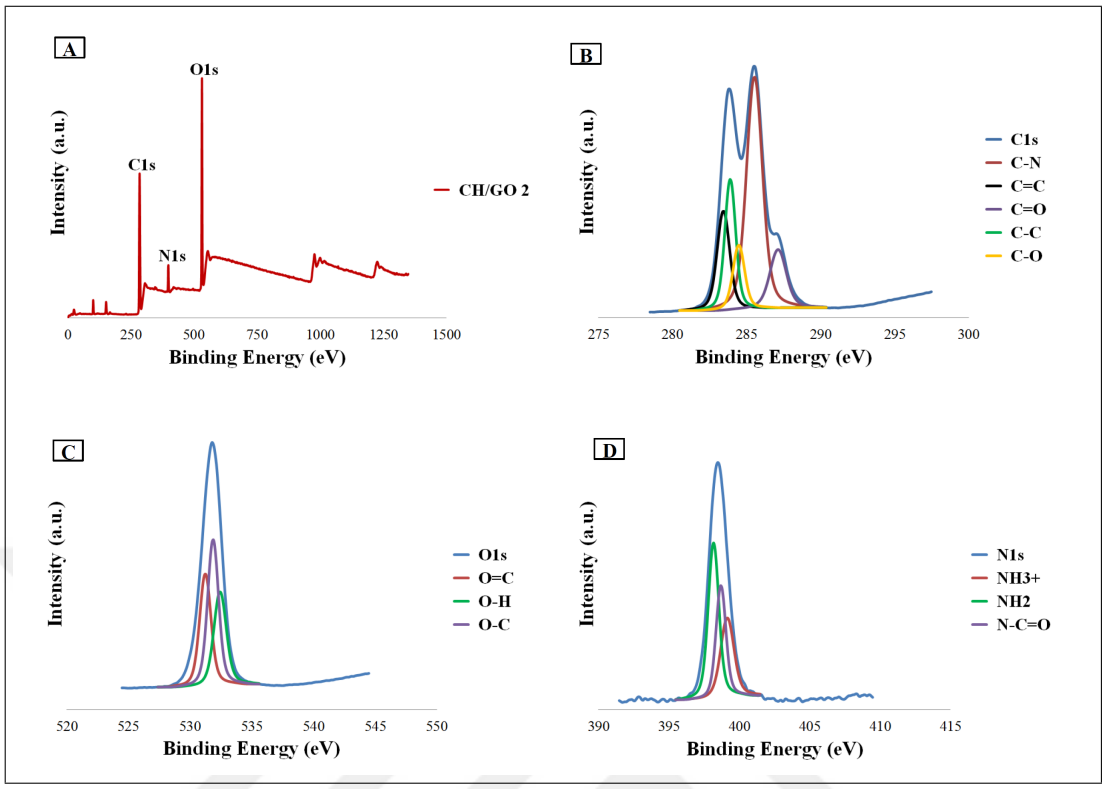

Figure 4.20 A) XPS Survey Spectrum of CH/GO2, B) High-Resolution Spectrum of Carbon Peaks (C1s) of CH/GO2, C) High-Resolution Spectrum of Oxygen Peaks (O1s) of CH/GO2, D) High-Resolution Spectrum of Nitrogen Peaks (N1s) of CH/GO2.

XPS survey spectrum of CH/GO2 was obtained and based on the data, C1s, O1s and N1s peaks appeared at 291.08 eV, 538.08 eV and 405.58 eV respectively. There were noticeable shifts in binding energy of C1s, O1s and N1s peaks compared to peaks which appeared in survey spectrum of CH/GO1, which were due to increase of GO content. Table 4.15 illustrates atomic percentages of elements in CH/GO2 [6, 60].

Table 4.15
Measured Atomic % of C, O and N in Pirsitine CH/GO2.

Atom	Measured Atomic %
C	65.71
O	28.80
N	5.49

XPS spectrum of C1s core level of CH/GO2 was obtained and five peaks were identified in total, C-N, C=C, C=O, C-C and C-O which were found at 285.54 eV, 283.44 eV, 287.13 eV, 283.9 eV and 284.48 eV respectively. There were noticeable shifts in binding energy of obtained peaks comparing to peaks which appeared in C1s deconvolution curve of CH/GO1 which could be due to increase of GO content and therefore increase in the amounts of C and O in the material. Table 4.16 illustrates parameters of measured peaks.

Table 4.16
C1s Measured Peaks Parameters (Binding Energy(eV), Height Ratio, Full at Half Maximum (eV)) in CH/GO2.

Designation Band	Peak BE (eV)	Height Ratio	FWHM (eV)
C-N	285.54	1	1.27
C=C	283.44	0.43	1.01
C=O	287.13	0.25	1.31
C-C	283.9	0.56	0.87
C-O	284.48	0.28	0.94

XPS spectrum of O1s core level of CH/GO2 was also obtained and three major peaks were identified appearing at 531.23 eV, 532.42 eV and 531.86 eV and were assigned to O=C, O-H and O-C bands respectively. Slight shifts were detected in all three peaks that were results of increase of GO content. Table 4.17 illustrates parameters of measured peaks [6,60].

Table 4.17
O1s Measured Peaks Parameters (Binding Energy(eV), Height Ratio, Full at Half Maximum (eV)) in CH/GO2.

Designation Band	Peak BE (eV)	Height Ratio	FWHM (eV)
O=C	531.23	0.77	1.09
O-H	532.42	0.64	1.2
O-C	531.86	1	1.05

XPS spectrum of N1s core level of CH/GO2 was recorded and deconvolution resulted in identification of three peaks in total, N-C=O, NH_2 and NH_3^+ which were found at 398.7 eV, 398.18 eV and 399.15 eV respectively. Table 4.18 illustrates parameters of measured peaks [6, 60].

Table 4.18
N1s Measured Peaks Parameters (Binding Energy(eV), Height Ratio, Full at Half Maximum (eV)) in CH/GO2.

Designation Band	Peak BE (eV)	Height Ratio	FWHM (eV)
NH_3^+	399.15	0.5	1.12
NH_2	398.18	1	0.89
N-C=O	398.7	0.72	0.83

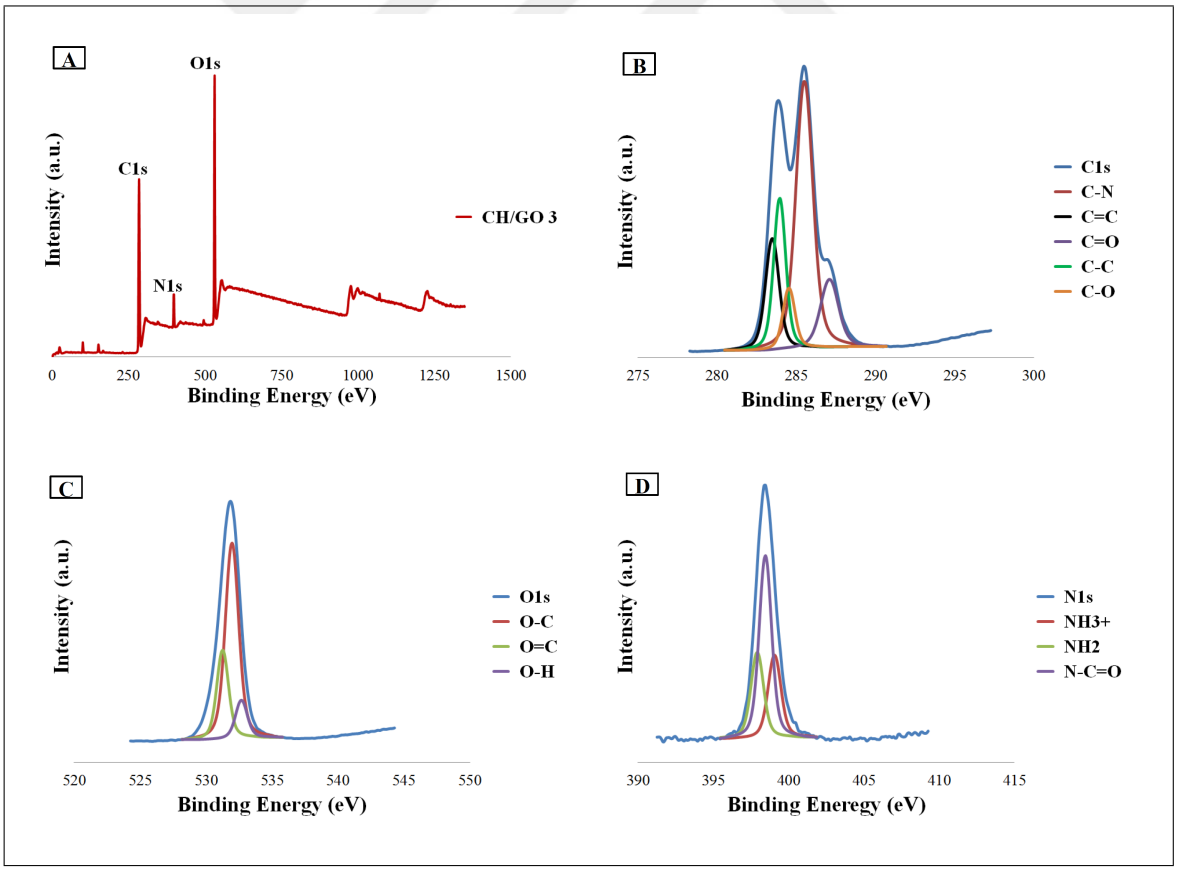

Figure 4.21 A) XPS Survey Spectrum of CH/GO3, B) High-Resolution Spectrum of Carbon Peaks (C1s) of CH/GO3, C) High-Resolution Spectrum of Oxygen Peaks (O1s) of CH/GO3, D) High-Resolution Spectrum of Nitrogen Peaks (N1s) of CH/GO3.

XPS spectrum of CH/GO3 was obtained and based on the data, C1s, O1s and N1s peaks appeared at 291.08 eV, 537.58 eV and 405.08 eV, respectively. There were slight shifts in binding energy of C1s, O1s and N1s peaks compared to peaks which appeared in survey spectrum of CH/GO2, which were due to increase of GO content. Table 4.19 illustrates atomic percentages of elements in CH/GO3 [6,60].

Table 4.19
Measured Atomic % of C, O and N in CH/GO3.

Atom	Measured Atomic %
C	66.59
O	27.62
N	5.79

XPS spectrum of C1s core level of CH/GO3 was obtained and five peaks were identified in total, C-N, C=C, C=O, C-C and C-O which were found at 285.52 eV, 283.49 eV, 287.1 eV, 283.96 eV and 284.54 eV respectively. There were noticeable shifts in binding energy of obtained peaks comparing to peaks which appeared in C1s deconvolution curve of CH/GO2 which were due to increase of GO content and therefore increase in the amounts of C and O in the material. Table 4.20 illustrates parameters of measured peaks [6,60].

Table 4.20
C1s Measured Peaks Parameters (Binding Energy(eV), Height Ratio, Full at Half Maximum (eV)) in CH/GO3.

Designation Band	Peak BE (eV)	Height Ratio	FWHM (eV)
C-N	285.52	1	1.27
C=C	283.49	0.42	1.02
C=O	287.1	0.25	1.35
C-C	283.96	0.57	0.9
C-O	284.54	0.23	0.9

XPS spectrum of O1s core level of CH/GO3 was also obtained and three major peaks were identified appearing at 531.26 eV, 532.68 eV and 531.97 eV and were assigned to O=C, O-H and O-C bands respectively. Slight shifts were detected in all three peaks that were results of increase of GO content. Table 4.21 illustrates parameters of measured peaks [6,60].

Table 4.21
O1s Measured Peaks Parameters (Binding Energy(eV), Height Ratio, Full at Half Maximum (eV)) in CH/GO3.

Designation Band	Peak BE (eV)	Height Ratio	FWHM (eV)
O-C	531.97	1	1.2
O=C	531.26	0.45	1.05
O-H	532.68	0.19	1.05

XPS spectrum of N1s core level of CH/GO3 was recorded and deconvolution resulted in identification of three peaks in total, N-C=O, NH_2 and NH_3^+ which were found at 398.47 eV, 397.93eV and 399.08 eV respectively. Slight shifts were detected in binding energy of all three peaks, which were due to increase of GO content. Table 4.22 illustrates parameters of measured peaks [6,60].

Table 4.22
N1s Measured Peaks Parameters (Binding Energy(eV), Height Ratio, Full at Half Maximum (eV)) CH/GO3.

Designation Band	Peak BE (eV)	Height Ratio	FWHM (eV)
NH_3^+	399.08	0.45	1.01
NH_2	397.93	0.47	1
N-C=O	398.47	1	0.98

4.3.3 Water Contact Angle Measurements

Water contact angle measurements were performed for all experimental groups in order to obtain information regarding hydrophobic/hydrophilic properties of the samples. All measurements were done at RT using DI water and the volume of the water droplet was approximately 3μl. Table 4.23 represents the results at the 10th second after settling of the droplet on the surface.

Table 4.23
Water Contact Angle Measurement Results of CH Based Membranes.

Experimental Group	Plain	Sharkskin Mimicked (SSM)
CH	90° ±1.87	102.1°±1.98
CH/GO 1	89.87°±4.53	100.63°±5.03
CH/GO 2	87.30°±4.31	98.6°±5.11
CH/GO 3	84.57°±3.69	94.35°±5.21

Based on the data obtained from the experiment, GO increased the tendency of the surface towards water and decreased the contact angle of water. On the other hand, surface topography of sharkskin considerably increased the contact angle of water resulting in a hydrophobic surface [35, 36, 62].

4.3.4 Swelling Ratio

Based on desired applications of polymeric membranes, their capacity of liquid absorption must be investigated. CH based membranes' capacity for absorbing DI water was investigated and presented in Figures 4.22 to 4.26. Both plain and sharkskin mimicked membranes were subjected to this experiment.

In order to investigate the effects of morphology and GO concentration, all treatment groups were subjected to swelling ratio measurement experiment. Figure

4.22 presents the experiment results for understanding effect of GO concentration for both plain and sharkskin mimicked membranes separately [63, 64]

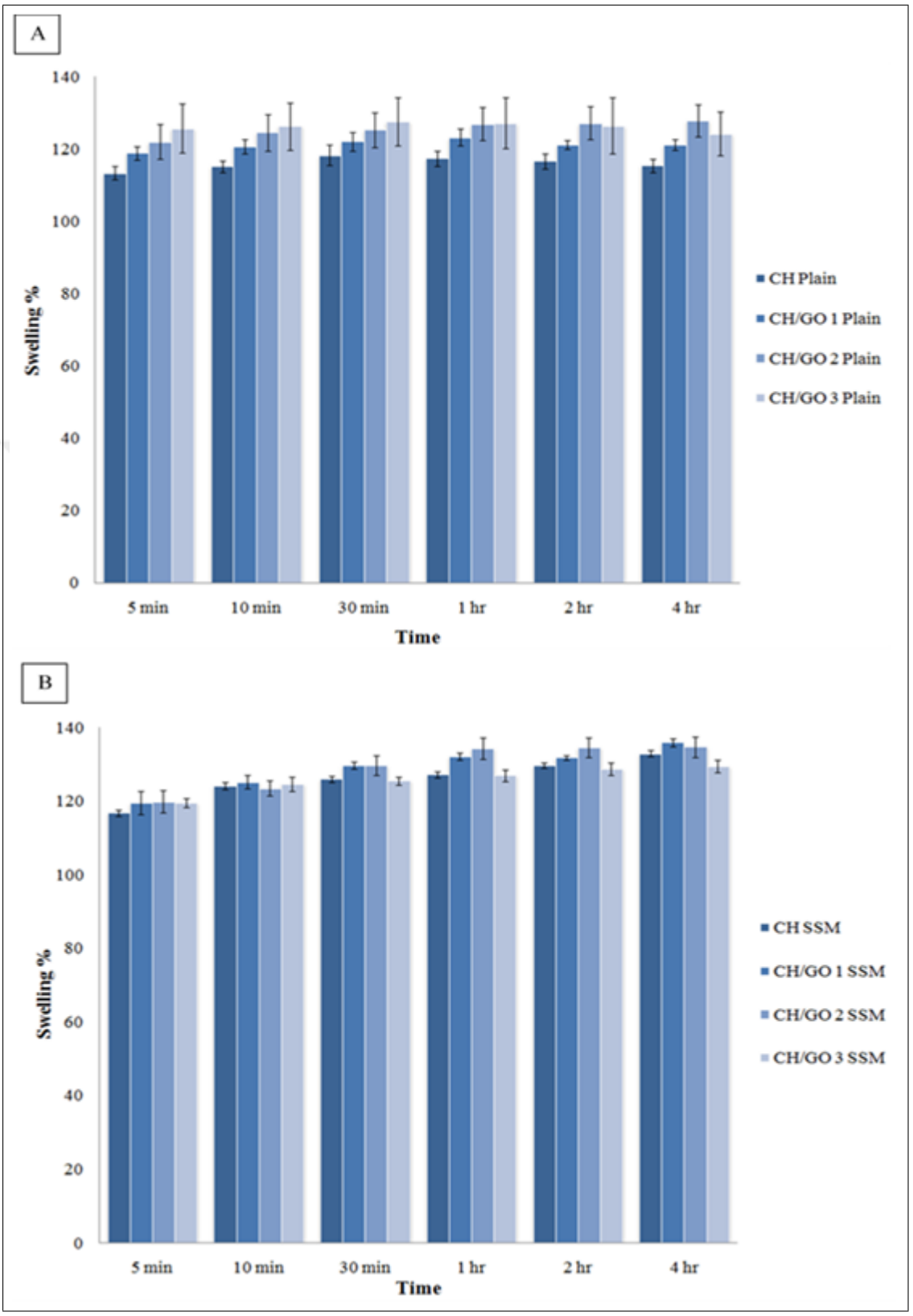

Figure 4.22 A) Swelling Ration of Plain CH Based Membranes. B) Swelling Ration of Sharkskin Mimicked (SSM) CH Based Membranes. Data are expressed in means ± SE.

In both groups, an increase in water absorption was observed as GO was added and it became even more as the concentration of GO increased. In plain membranes, this increase was steady until 10th minute but after that as the immersion duration increased, samples started to stabilize and chemical interactions caused a decrease in absorbed water content of CH/GO3 membranes.

As for sharkskin mimicked membranes, swelling ratio of CH/GO1 kept increasing until 4th hour whereas CH/GO1 and CH/GO2 continued without any decrease or increase after maximum swelling capacity was reached approximately at 1st hour and 2nd hour respectively.

The effect of surface topography was studied by comparing plain and sharkskin mimicked membranes with same chemical compositions were presented in Figure 4.23 to 4.26.

Table 4.24
Swelling Ratio (%) of Plain Membranes of CH and CH/GO nanocomposite in DI Water. Data are expressed as Mean ± SD.

Time	5 min	10 min	30 min	1 hr	2 hrs	4 hrs
CH	113.45±1.95	115.19±1.55	118.37±2.80	117.41±2.15	116.78±2.10	115.44±1.92
CH/GO1	118.94±1.86	120.81±1.97	122.14±2.62	123.27±2.35	121.12±1.23	121.13±1.49
CH/GO2	122.00±4.83	124.60±5.12	125.29±4.77	126.97±4.61	127.24±4.52	127.85±4.40
CH/GO3	125.71±6.75	126.29±6.51	127.69±6.62	127.21±7.06	126.49±7.84	124.24±5.98

Table 4.25
Swelling Ratio (%) of Plain Membranes of CH and CH/GO nanocomposite in DI Water. Data are expressed as Mean ± SD.

Time	5 min	10 min	30 min	1 hr	2 hrs	4 hrs
CH	116.85±0.80	124.15±0.92	126.04±0.83	127.25±0.87	129.81±0.70	133.01±0.88
CH/GO1	119.53±3.12	125.27±1.87	129.78±1.06	132.26±0.91	131.94±0.61	135.99±1.09
CH/GO2	119.90±2.99	123.59±1.97	129.82±2.72	134.37±2.85	134.66±2.71	134.75±2.86
CH/GO3	119.53±1.17	124.72±2.01	125.56±1.15	127.04±1.62	128.77±1.76	129.55±1.64

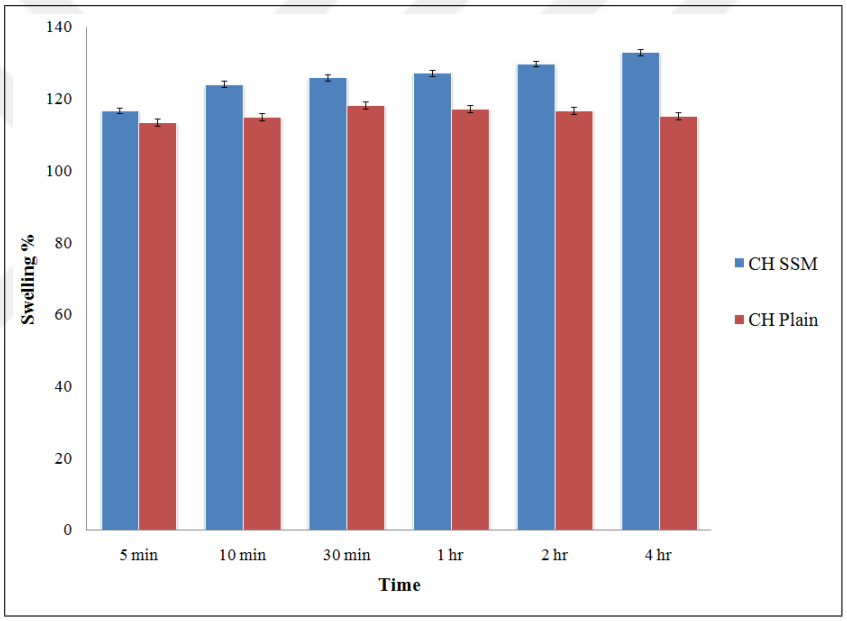

Figure 4.23 Swelling Ratio of CH Membranes. (Surface Morphology Effect). Data are expressed in means ± SE.

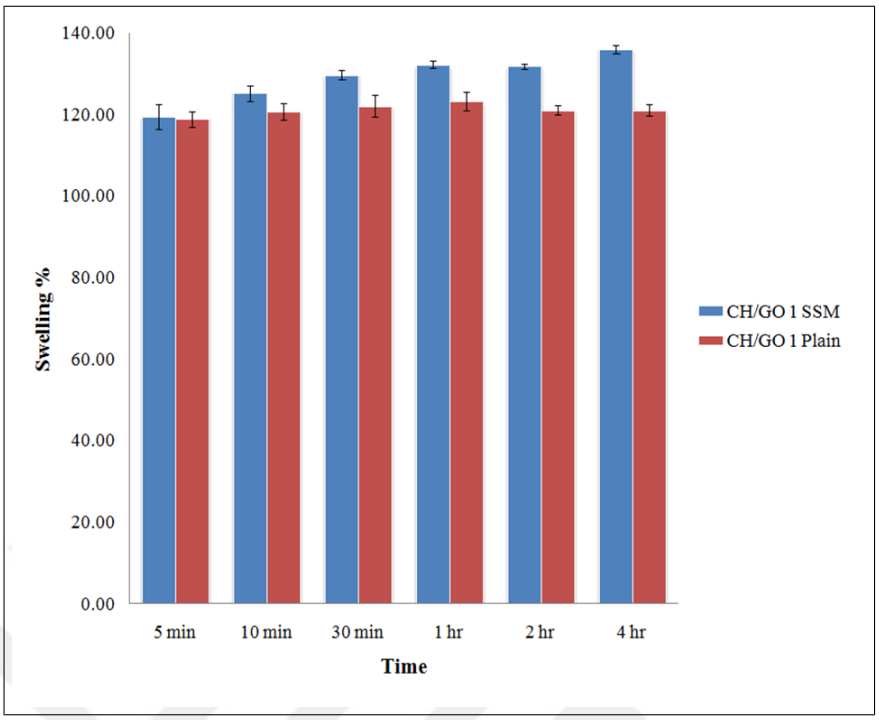

Figure 4.24 Swelling Ratio of CH/GO1 Membranes (Surface Morphology Effect). Data are expressed in means ± SE.

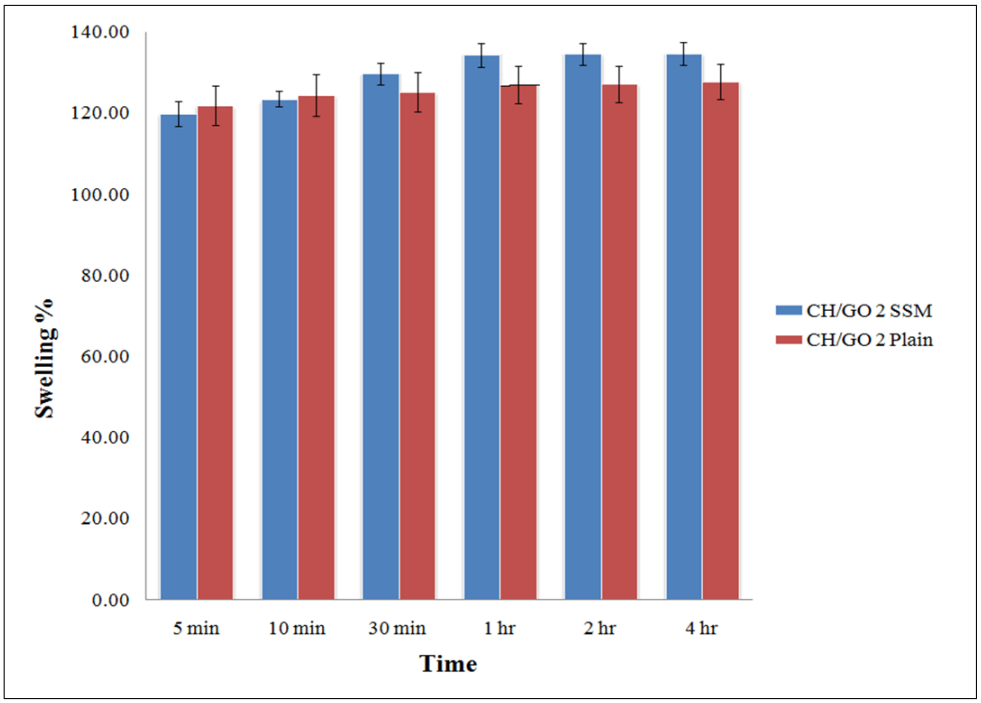

Figure 4.25 Swelling Ratio of CH/GO2 Membranes (Surface Morphology Effect). Data are expressed in means ± SE.

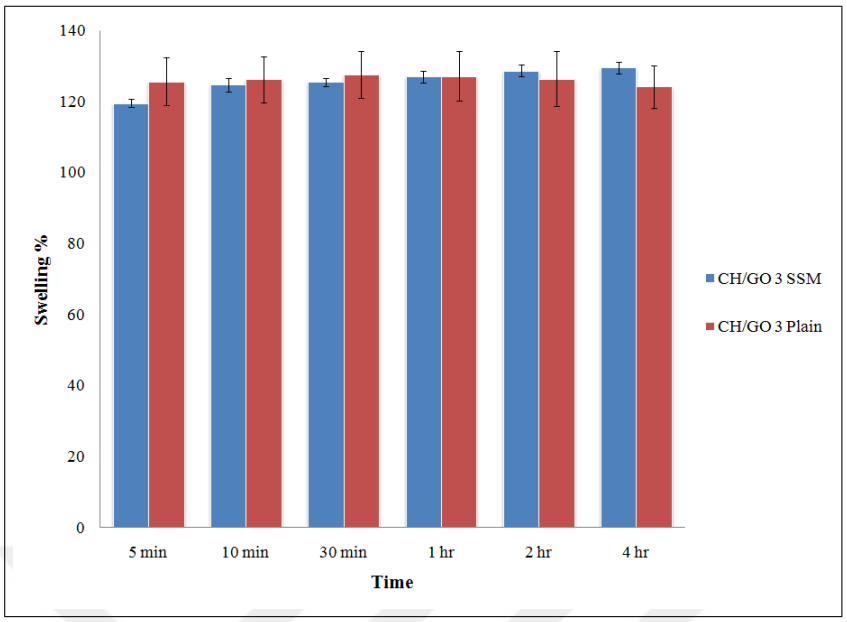

Figure 4.26 Swelling Ratio of CH/GO3 Membranes (Surface Morphology Effect). Data are expressed in means ± SE.

Based on the data obtained for swelling ratio, surface topography has great influence on water absorption of CH and CH/GO nanocomposite membranes. Also, the observed decrease of swelling ratio of samples of plain membranes after 10th minute did not occur for sharkskin mimicked samples.

In addition, the enhancing effect of surface morphology due to sharkskin micro-pattern was suppressed as the concentration of GO increased.

4.4 Cell Culture Studies (MTT Assay)

The effect of GO concentration on cell viability was investigated by using MTT assay. Fibroblast cells (L929 - ATCC) were culture on CH membranes as treatment groups along with tissue culture plate as the control groups. $1.5x10^4$ cells were cultured into each well of 24 well-plates and viability of cells were measured on day 7 with the aim of detecting cellular behavior towards different concentrations of GO in addition to any possible cytotoxic effects of GO [57].

Treatment groups that were chosen for cell culture experiments were: CH, CH/GO1 and CH/GO2. This elimination was concluded based on the SEM results on mimicking quality of membranes.

According to the obtained data, at day 7, calculated metabolic activity of cells were calculated and represented in Table 4.26 and Figure 4.27.

Table 4.26
MTT Assay Results at Day 7 (n=8). Data are expressed in mean±SD.

Treatment Gropus	Cell Viability %
CH	22.42 ± 6.26
CH/GO 1	43.86 ± 7.39
CH/GO 2	33.41 ± 6.35
TCP	100.00 ± 24.41

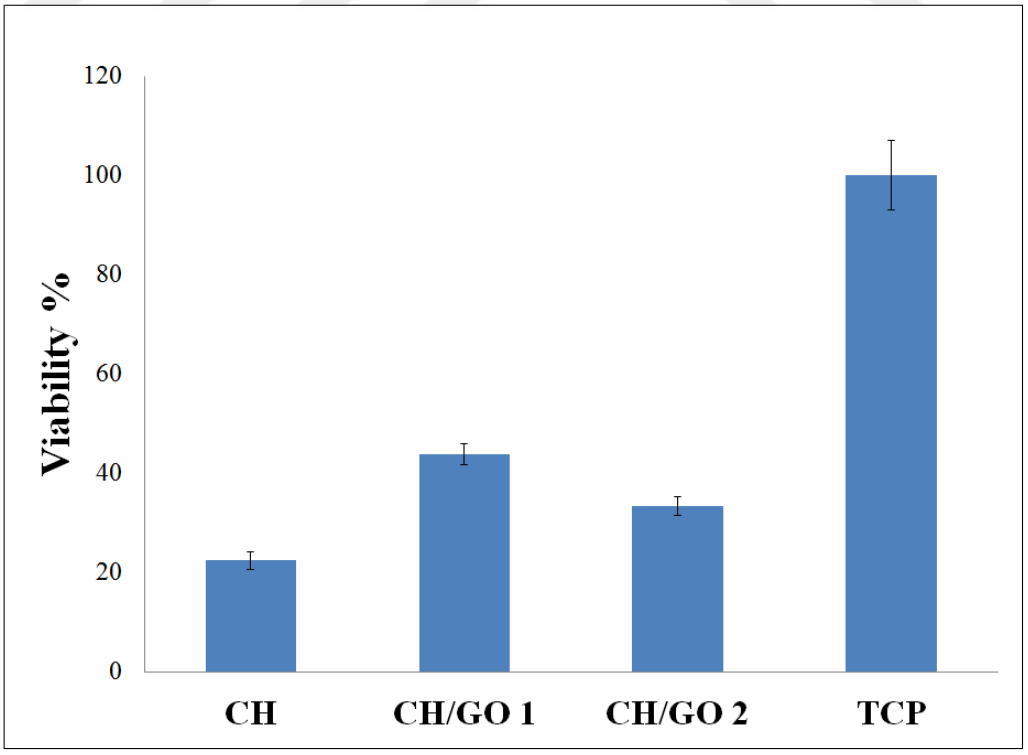

Figure 4.27 MTT Assay Results at Day 7 (n=8). Data are expressed in means ± SE.

According to the obtained data, it was observed that cell viability on CH membrane was very low whereas addition of GO by 0.1%w/w resulted in a remarkable increase. However, positive effect of GO on cell viability faded away by increasing GO concentration to 0.2%w/w, which caused a noticeable decrease in cellular activity. ANOVA was chosen as a suitable statistical method to compare and find statistical significances between experimental groups and results are represented in Table 4.27.

Table 4.27
Statistical Analysis of Cell Viability Results.

Treatments Pair Gropus	One Way ANOVA p-Value (Tukey)	One Way ANOVA Results (Tukey)
CH vs. CH/GO 1	0.0018618	$p<0.01$
CH vs. CH/GO 2	0.2066043	Insignificant
CH vs. TCP	0.0010053	$p<0.01$
CH/GO 1 vs. CH/GO 2	0.2453055	Insignificant
CH/GO 1 vs. CH/GO 3	0.0010053	$p<0.01$
CH/GO 2 vs. CH/GO 3	0.0010053	$p<0.01$

Based on information attained from statistical calculations, a significant difference between CH, CH/GO1 and TCP was detected whereas no significant difference was detected between CH and CH/GO2 confirming the conclusions made by comparison results derived from Figure 4.27.

5. DISCUSSION

Recent studies have shown numerous applications and advantages of biomimicked structures and their crucial role on cellular and bacterial behavior such as adhesion, growth, migration and proliferation.[93] Inspired from nature and its ways to balance chemical and biological activities of microorganisms via geometry and chemistry, sharkskin, CH and GO outstood as highly potential factors for our purposes since each have unique and extraordinary characteristics.

The main objective of the presented thesis were to:

1. Preparation of biomimicked polymer based membranes with the inspiration of natural surface topography, sharkskin via biomimicking.
2. Combining sharkskin morphology with a natural primary polymeric substrate with extraordinary properties, CH, with the aim of enhancing the desired chemical and biological properties.
3. Using an additional carbon based additive with remarkable chemical, mechanical and biological properties, GO, in order to improve mechanical and biological properties of polymeric membranes.
4. Characterization and optimization of obtained membranes prepared by combining sharkskin micro-topography, CH and GO regarding mechanical and chemical properties so as to gain an insight to characteristics of sharkskin micro-topography and GO at various concentrations.
5. Investigating the effects of concentration of GO on cellular viability

In the presented study, sharkskin micro-patterned CH and CH/GO nanocomposites membranes were prepared along with plain membranes and common characterization techniques including SEM, Elongation at Break, Tensile Strength, Raman

spectroscopy, XPS , Water Contact Angle and Swelling Ration were used to obtain information about morphology, mechanical properties and chemistry of prepared membranes.

5.1 Morphological Characterization

SEM imaging technique was conducted to observe the natural shape and structure of pretreated sharkskin‘s micron-scale features, quality of mimicking sharkskin surface patterns via PDMS, chitosan and CH/GO nanocomposites along with possible effects of GO on topography and internal structure of polymeric membranes [2,14,15,17] Replicating the sharkskin topography using soft lithography and PDMS provided a negative mold with high quality which was basically the mirror image of sharkskin itself. Therefore obtained SEM images of negative PDMS mold and sharkskin were mirror image of each other as well.(Figure 4.1 to 4.4) SSM polymeric membranes were prepared using CH, CH/GO1(0.1%w/w), CH/GO2(0.2%w/w), and CH/GO3(0.3%w/w) nanocomposites. Despite the fact that negative PDMS mold was nearly the exact mirror image of sharkskin, fabrication of SSM chitosan based membranes was affected by the concentration of polymer and GO. According to images presented in Figure 4.1 to 4.4, it was concluded that CH/GO1 seemed more alike to sharkskin than other experimental groups followed by CH/GO2 as the second best mimicked membrane [2,15] It seemed like, as the GO content in the membranes increased from 0.1%w/w to 0.2%w/w and then to 0.3%w/w, the quality of mimicking reduced. This conclusion was also verified by SEM images of plain CH/GO3 membranes, which appeared with some superficial defects (most probably groups of large GO flakes on the surface) that were associated to effect of high GO content. In addition to SSM images, SEM images of plain membranes were obtained both from the surface and cross-section. The aim of surface SEM imaging was to observe effects of various GO contents on the morphology. According to Figures 4.5 to 4.8, there was absolutely no feature on the surface of plain pristine CH and CH/GO1 membranes. As the concentration of GO increased from 0.1%w/w in CH/GO1 nanocomposite to 0.2%w/w in CH/GO2 nanocomposite, some small jut-like features with no specific shape were observed. In CH/GO3, which had

0.3%w/w GO content, the jut-like shapeless features on plain membranes were considerably much larger than those of CH/GO2(Figure 4.8). Observed shapeless features seemed like huge mass of GO flakes, which were reattached to each other during the long, drying phase. The reattachment of GO flakes to one another was associated to the interactions between functional groups of GO triggered by prolonged, gradual heating at 35°C during drying.[98] This phenomena altered the surface topography resulting in elimination of CH/GO3 treatment group for cell culture experiments(Table 3.2 and Table 4.26).

Despite the fact that GO flakes were well dispersed in CH solution via homogenization and therefore it was expected to be seen in the internal structure of CH/GO nanocomposite membranes rather than on the surface, SEM images presented in Figures 4.9 to 4.11, showed no noticeable changes in cross-sectional images of chitosan compared to CH/GO nanocomposites with various GO content suggesting that low amounts of GO (0.1%w/w, 0.2%w/w and 0.3%w/w) did not cause any detectable changes on chitosan internal structure.

5.2 Mechanical Characterization

In order to measure mechanical properties of CH membranes, percentage of elongation at break and tensile strength (Mpa) tests were conducted on plain membranes (Table 3.2). Average thickness of the membranes subjected to these tests was $50\pm5\mu$m. As shown in Figure 4.13 and Table, elongation at break values for CH, CH/GO1, CH/GO2 and CH/GO3experimental groups were calculated at 29.92 $\pm$ 3.72%, 33.73 $\pm$ 2.29%, 37.60 $\pm$ 1.95% and 42.41 $\pm$ 2.20% respectively. Based on obtained data, adding GO to CH even in very low concentrations, increased the extension at the point of break which was interpreted as enhancement of the flexibility of chitosan membranes [51, 52, 65]. Preparation of CH/GO nanocomposites membranes was done via homogeneous dispersion of GO flakes throughout the CH matrix using ultra sonication. Based on the elongation results, it seemed that strong interfacial adhesion between GO flakes and chitosan chains had taken place. Since CH is a biopolymer possessing amino,

primary, and secondary hydroxyl groups in its glucosamine unit, when interacted with GO flakes, also owning superior hydrophilicity because of abundant Oxygen groups on the surface, strong hydrogen-bonds were most probably formed between chitosan and GO flakes. As a result, elongation of CH at the break point enhanced significantly by addition of GO [65].

In addition to measuring percentage of extension at break point, tensile strength of CH based membranes was also measured (Figure 4.14). According to the data obtained for tensile strength, values of 87.15 ± 4.39 Mpa, 79.21±2.58 Mpa, 54.83 ± 2.88 Mpa and 83.57 ± 2.51 Mpa were obtained respectively for CH, CH/GO1, CH/GO2 and CH/GO3. Based on the results of a similar study, in the low concentrations of GO(less than 0.25%w/w), GO flakes were positioned in an aligned and parallel to the surface formation [8]. The aligned and parallel formation and positioning of GO flakes inside the membrane resulted from the method of membrane fabrication (solution casting) used to prepare the nanocomposites in which GO flakes tended to lie down inside the CH solution due to their unique 2D structure and the gravitational attraction. This phenomenon was also found in other procedures involving GO and graphite such as preparation of graphite nanoplates/poly-(vinylidene fluoride) and GO/poly(vinyl alcohol) nanocomposite films [51, 52].

This way of positioning of GO flakes in chitosan at 0.1%w/w and 0.2%w/w concentrations seemed to have changed the integrity of polymer chains in a way that GO flakes might have blocked certain binding sites on chitosan chain decreasing the number of within-chain interactions resulting in decreased internal integrity and eventually leading to a noticeable decrease in tensile strength of the material. GO possesses functional groups to interact with chitosan's amino, primary, and secondary hydroxyl groups, but based on the obtained data, in low GO concentrations(0.1%w/w and 0.2%w/w), apparently there was not enough number of GO flakes between the chains to act as a cross-linker with high mechanical properties [66].

However, as the concentration of GO increased to 0.3%w/w, the tensile strength increased significantly meaning that by increasing the concentration to 0.3%w/w, at

this point, there were enough GO flakes located between the chains that acted as a very strong and effective cross-linker with high mechanical properties and numerous amounts of carboxylic and hydroxyl groups which have bound to the functional groups on chitosan chains via hydrogen bonding resulting in noticeable increase of tensile strength. Also, it is well known that GO flakes have higher specific surface area (calculated value, 2630m^2/g), nano-scale surface roughness and unique two-dimensional (2D) structure [66] Nanoparticles with high surface area could impose strong geometric constraints to the mobility of polymer molecules. Thus nano-scale surface roughness of GO flaks may have caused an enhanced mechanical interlocking with polymer chains, consequently, leading to better adhesion at the interface [66].

5.3 Chemical Characterization

In order to investigate the chemical nature of the materials and obtain information about chemical interactions in nanocomposites, Raman Spectroscopy was conducted. Raman spectra can be used as a standard tool for studying characteristic effect of interactions on the molecular structure of a component present in nanocomposite materials [29]. Based on the data obtained from Raman spectroscopy of pristine CH, 8 major characteristic peaks of chitosan were identified in total. In the range of 600-1800cm^{-1}, at 897 cm^{-1}, 944 cm^{-1}, 1462 cm^{-1}, 1590 cm^{-1} and 1662 cm^{-1}, sharp peaks appeared which were assigned to ρCH_2, CN, CH+CH_2+OH, NH_2 and CO, respectively (Figures 4.15). These peaks were expected at 896 cm^{-1}, 936 cm^{-1}, 1458 cm^{-1}, 1591 cm^{-1} and 1654 cm^{-1}. The shift in the wavenumber of the mentioned peaks are believed to be due to the purification process in which many of unwanted impurities were filtered leading to minor displacement of characteristic peaks of the material. Also in the range 2400-3300 cm^{-1}, two peaks were detected at the wavenumbers of 2887 cm^{-1} and 2934 cm^{-1}, which were supposed to appear at 2885 cm^{-1} and 2932 cm^{-1}. These peaks were assigned to υCH_2 and CH_3 respectively [53]. Shifts of these peaks could be caused by the chemical reactions during the purification process (Figure 4.15).

Raman spectroscopy of GO was also recorded and two major peaks were found.

The G band, which appeared at 1578.4cm^{-1} and the D band at 1349.7 cm^{-1} with slight shifts. These bands are prominent characteristic bands of GO. The G band should have appeared at 1580 cm^{-1} and the G band at 1350 cm^{-1}. G-band corresponded to the first-order scattering of the E2g mode in other word, vibration of the sp2-bonded carbon. The prominent D peak was from the structural imperfections created by the attachment of hydroxyl and epoxy groups on the carbon basal plane in GO. The intensity of the overtone 2D-band with respect to the D and G peaks was small and it appeared more obviously in the CH/GO nanocomposites rather than in the GO spectrum. I_D/I_G for GO was calculated at 0.93 [29,67].

By obtaining Raman spectrum of CH/GO nanocomposites, the interactions between GO flakes and functional groups of chitosan were investigated. According to Figure 4.16, Raman spectrum of CH/GO1 was recorded in two ranges, 600-1800 cm^{-1} and 2400-3300 cm^{-1}. Three main peaks were detected D band at 1327 cm^{-1} , G band at 1595 cm^{-1} and 2D band at 2561 cm^{-1} which was a very small peak. All peaks were noticeably dispositioned when compared to D/G band positions of GO, implying that interactions between GO flakes and chitosan chains have taken place. In the range of 2400 cm^{-1}to 3300 cm^{-1} the CH_2 peak of CH was still detectable at 2871 cm^{-1}, which also had shifted. I_D/I_G was calculated at 1.04. Based on these observations, it was concluded that none of the major peaks of CH were detectable because of GO's D and G band suppressed them all [68,69].

As for CH/GO2, D band appeared at 1326 cm^{-1} and G band appeared at 1593 cm^{-1} and 2D band at 2563 cm^{-1}. CH_2 band at this concentration became undetectable. I_D/I_G was calculated at 1.03 and D, G and 2D bands had very little shifts compared to CH/GO1. In the highest GO concentration, 0.3%w/w, 2D peak appeared at 2579 cm^{-1} in addition to significant shifts of D and G band which were detected at 1338 cm^{-1} and 1585 cm^{-1} respectively. I_D/I_G was calculated at 0.97 and compared to CH/GO1, CH/GO2 and GO the peaks had considerable shifts, leading to the conclusion that the intensity and therefore amount of chemical interactions between GO and CH had increased considerably which in turns verified the results of tensile strength for CH/GO3 experimental group [51,52,65].

Overall noticeable shifts of D,G and 2D peaks in nanocomposites compared to GO, indicated that GO and chitosan had indeed chemically interacted with each other. The shift of peaks as the concentration of GO increased from 0.1%w/w to 0.2%w/w and then to 0.3%w/w, implied that more GO flakes have chemically bonded to chitosan chain's functional groups. By comparing the I_D/I_G ratio between GO and nanocomposite groups, a trend was observed starting from 1.04 for CH/GO1 to 1.03 for CH/GO2 followed by 0.97 for CH/GO3 and ending with 0.93 for GO. These ratios once again verified the results obtained in mechanical characterization section and indicated that CH/GO nanocomposite fabrication was successful [51, 52, 65].

After attaining primary information regarding the chemical state of the membranes, XPS was used to obtain more detailed information. XPS survey spectra of CH, CH/GO1, CH/GO2 and CH/GO3 were obtained. In addition to that, high-resolution spectrum of C1s,O1s and N1s and their deconvolutions were obtained. For GO, survey spectrum was also recorded and since only C and O peaks were detected, high-resolution spectrum of C1s and O1s were recorded. The aim of recording the survey spectrum was to identify all elements present in the material which in case of chitosan, there were C, O and N. The atomic percentages provided information regarding the amount of each element. In chitosan, measured atomic percentages were: 81.06% for C, 16.47% for O and 2.47% for N. Based on the data obtained from survey spectrum of pristine CH, C1s, O1s and N1s peaks appeared at 285 eV, 532.26 eV and 399.25 eV respectively. (Figure 4.17) N1s peaks was found to be not very sharp indicating that amount of nitrogen contaning groups was not much [60, 61].

Figure(4.17) also showed high resolution spectrum of elements along with their deconvoluted peaks. According to C1s core level spectrum of chitosan, five peaks were identified in total, C-C, C=O and O-C=O which were found at 284.71 eV, 287.73 eV and 288.73 eV respectively as well as C-N and C-O overlapping peaks, assigned to 286.1 eV. [111-113] Height ratio of these peaks provided information about their intensity which were 0.09 for C=O band, 0.05 for O-C=O band, 0.31 for C-N and C-O, and 1.00 for C-C band. (Table 4.5) These height ratios show the concentration of each band or in other words, intensity of each band existing in the material [15, 23, 60, 70].

XPS spectrum of O1s core level of chitosan was also obtained and three peaks were identified appearing at 532.24 eV, 533.06 eV and 531.63 eV corresponded to O-H, O-C and C=O bands with height ratios of 1.00, 0.4 and 0.42 respectively.(Table 4.6) [60, 61].

XPS spectrum of N1s core level was also recorded resulting in identification of three peaks in total, N-C, N-H band in NH_2 and N-H band NH_3^+ which were found at 399.44 eV, 398.83 eV and 402.05 eV, respectively(Table 4.7). Height ratios were 0.81, 1.00 and 0.05 accordingly [57, 60, 61]. Obtained data suggested that number of NH_3^+ functional group was very low and negligible with a high acceptance degree.

XPS survey spectrum of pristine GO was obtained in order to identify its elements as well as their composition.(Figure 4.18) O1s and C1s peaks were found at 533.13 eV, and 286.75 eV respectively. Corresponding measured atomic percentages were 35.02% for C and 64.98% for O. In order to determine types and intensity of chemical bands in GO, high resolution spectrums of C and O were obtained and deconvolution peaks were determined.(Table 4.8) [23, 71].

According to the data obtained from high resolution XPS spectrum of C1s core level of GO, five peaks were identified in total, at 287.29 eV, 284.52 eV, 288.82 eV, 285.15 eV and 285.67 eV corresponding with C=O, C=C, O-C-O, C-C and C-O bands.(Table 4.9) Height ratios of determined band were: 1.00, 0.11, 0.08, 0.51 and 0.22 accordingly which indicated that due to high atomic percentage of O, C=O chemical bands are the most abundant [23, 71]. To verify conclusions regarding peak intensities, XPS high resolution spectrum of O1s core level was also obtained and three peaks were identified appearing at 532.08 eV, 533.19 eV and 532.65 eV that were assigned to O-C, O=C and O-H bands respectively.(Table 4.10) Corresponding measured height ratios were 0.49, 1.00 and 0.77 illustrating that majority of O were in chemical interaction with C through double covalent bond (C=O) confirming the high height ratio of C=O found in C1s spectrum and high amount of O calculated in GO survey spectrum [23, 71–73].

XPS survey spectrum of CH/GO nanocomposites were subsequently obtained

and substantial data were obtained and presented in Figures 4.19 to 4.21 and Tables 4.11 to 4.22 including identified peaks, their binding energy (eV), atomic percentages, deconvolution peaks and their height ratios.

In the survey spectrum of CH/GO1, C1s, O1s and N1s peaks were detected at 291.57 eV, 537.57 eV and 404.47 eV respectively.(Table 4.11) Measured atomic percentages for CH/GO1 nanocomposites were calculates at 72.90% for C, 22.39% for O and 4.71% for N. When atomic percentage of C in CH/GO1 was compared to CH chitosan, which was 81.06%, a noticeable decrease was observed. In contrast to that, by comparing atomic percentage of C in CH/GO1 with C atomic percentage in GO, which was 35.02%, a very significant increase was observed. Afterwards atomic percentage of O in CH/GO1 was compared to chitosan which was 16.47%, a noticeable increase was observed indicating that addition of GO as a material with high amounts of oxygen element, even in very low concentrations, affected the atomic percentages of O and C [70]. This explained the atomic percentage of C in CH/GO1 being less than chitosan's and more than GO's. By comparing atomic percentages of N in CH/GO1 to chitosan, a significant rise was observed since atomic percentage of N in chitosan measured at 2.47%, had doubled to 4.71% in CH/GO1 nanocomposite. It was concluded from these observations that chemical interactions between GO and chitosan could have occurred mostly via hydrogen binding of chitosan's amino group to carboxylic and hydroxyl groups of GO at quit high levels [15, 60, 61, 67, 68]. This indeed did not mean that interactions of C and O between chitosan and GO were negligible.

In order to get more accurate information, high-resolution spectrums of C1s, O1s and N1s of CH/GO1 were obtained and deconvolution curves were determined. For C1s core level spectrum, five peaks were identified in total corresponding to C-N, C=O, C=C, C-C and C-O which were found at 285.99 eV, 287.51 eV, 283.97 eV, 284.55 eV and 285.36 eV respectively. Height ratios of detected peaks were calculated at 0.72, 0.25, 1.00, 0.82 and 0.37 accordingly. By comparing band types found in CH/GO1 with that of chitosan's, C=C did not exist in chitosan which has appeared in the nanocomposite, illustrating presence of GO in the nanocomposite, because C=C was a distinct characteristic band of GO. Comparing C1s spectrum in Figures 4.17 and 4.19,

illustrates that due to the presence of GO, height ratio of C-N had a rapid increase from o.31 to o.72, verifying the previous conclusion regarding reasons of doubling of atomic percentage of N based on survey spectrum‘s data [60,61,67,68].

Afterwards, XPS spectrum of O1s core level of CH/GO1 was obtained leading to identification of three peaks at 531.53 eV, 532.22 eV and 532.82 eV and were assigned to O=C, O-C and O-H bands with corresponding height ratios of 0.68, 1 and 0.52 respectively [15,70].

XPS spectrum of N1s core level of CH/GO1 was recorded resulting in identification of three peaks in total, N-C=O, NH_2 and NH_3^+ which were found at 398.97 eV, 398.34 eV and 399.66 eV respectively.(Figure 4.19) By comparing binding energy of identified peaks with that of chitosan, all band have shifted which occurred due to interactions of GO and chitosan. Height ratios of peaks were measured at 1.00, 0.75 and 0.36 for N-C=O, NH_2 and NH_3^+ respectively. Height ratio of NH_2 decreased from 1.00 in chitosan to 0.75 in CH/GO1 in contrast to NH_3^+ which increased from 0.05 in chitosan to 0.36 in CH/GO1, meaning that intensity N of nitrogen atoms interaction in the form of NH_3^+ had significantly increased, once again leading to the conclusion that hydrogen binding of carboxylic and hydroxyl groups of GO with amine group of chitosan plays a very important role in the nanocomposite formation [15,60,61,67,68].

XPS survey spectrum of CH/GO2 was obtained and based on the data, C1s, O1s and N1s peaks appeared at 291.08 eV, 538.08 eV and 405.58 eV respectively.(Figure 4.20) There were noticeable shifts in binding energy of C1s, O1s and N1s peaks compared to peaks which appeared in survey spectrum of CH/GO1(Table 4.11), which were due to increase of GO content. Measured atomic percentages of C, O and N in CH/GO1 were 65.71%, 28.80% and 5.59%.(Table 4.15) Atomic percentages of O and N had increased compared to that of CH/GO1 [41,60,61,68]. Due to increase in the GO content, atomic concentration of oxygen increased and atomic concentration of carbon decreased, but the increase in atomic concentration of N occurred due to increase in the amount of chemical binding to amine group [67,68].

XPS spectrum of C1s core level of CH/GO2 was obtained and five peaks were identified in total, C-N, C=C, C=O, C-C and C-O which were found at 285.54 eV, 283.44 eV, 287.13 eV, 283.9 eV and 284.48 eV respectively. There were slight but noticeable shifts in binding energy of obtained peaks compared to peaks found in C1s deconvolution curve of CH/GO1 which were due to increase of GO content and therefore increase in the amounts of C and O in the material. Height ratio of identified peaks were calculated at 1.00, 0.43, 0.25,0.56 and 0.28 for C-N, C=C, C=O, C-C and C-O bands. There was an obvious increase in the height ratio of C-N band, verifying previous conclusions and demonstrating the increased intensity of chemical bindings with amino group, which it is believed is responsible for increasing flexibility of the membranes through increasing elongation of the sample at break point [79,108,109,111,112,113].

XPS spectrum of O1s core level of CH/GO2 was also obtained and three major peaks were identified appearing at 531.23 eV, 532.42 eV and 531.86 eV and were attributed to O=C, O-H and O-C bands respectively. Slight shifts were detected in all three peaks that were results of increase of GO content. Height ratios of identified peaks were measured at 0.77, 0.64 and 1 accordingly [15,60,61,67,68].

Also, XPS spectrum of N1s core level of CH/GO2 was recorded and deconvolution analysis resulted in identification of three peaks in total, N-C=O, NH_2 and NH_3^+ which were found at 398.7 eV, 398.18 eV and 399.15 eV with height ratios of 0.72, 1.00 and 0.5 respectively. With increase in GO content from 0.1%w/w to 0.2%w/w, height ratio of NH_3^+ increased from 0.36 to 0.5 which was considered significant and in accordance to the increase of atomic percentage of N observed in survey spectrum [15,60,61,67,68]. XPS survey spectrum of CH/GO3 was obtained and based on the data demonstrated in Figure 4.21, C1s, O1s and N1s peaks appeared at 291.08 eV, 537.58 eV and 405.08 eV respectively. There were slight shifts in binding energy of C1s, O1s and N1s peaks compared to peaks appeared in survey spectrum of CH/GO2, which were due to increase of GO content. Atomic percentages were calculated at 66.59% for C, 27.62% for O and 5.79% for N. The atomic concentration of N increased from 5.49 to 5.79 when compared to CH/GO2 [15,60,61,67,68].

High resolution XPS spectrum of C1s core level of CH/GO3 was obtained and five main peaks were identified in total, C-N, C=C, C=O, C-C and C-O which were found at 285.52 eV, 283.49 eV, 287.1 eV, 283.96 eV and 284.54 eV respectively. There were noticeable shifts in binding energy of obtained peaks comparing to peaks detected in C1s deconvolution curve of CH/GO2 which were due to increase of GO content and therefore increase in the amounts of C and O in the material. Height ratios of identified peaks were calculated as follows: 1.00 for C-N band, 0.42 for C=C, 0.25 for C=O, 0.57 for C-C and 0.23 for C-O [15,60,61,67,68].

High resolution XPS spectrum of O1s core level of CH/GO3 was also obtained and three major peaks were identified appearing at 531.26 eV, 532.68 eV and 531.97 eV associated with O=C, O-H and O-C bands respectively. Slight shifts were detected in all three peaks that were results of increase of GO content. Height ratios of identified peaks were measured as follows: 1.00 for O-C band, 0.45 for O=C and 0.19 for O-H band [60,61,67,68].

High resolution XPS spectrum of N1s core level of CH/GO3 was also recorded and deconvolution resulted in finding three peaks at 398.47 eV, 397.93eV and 399.08 eV attributed to N-C=O, NH_2 and NH_3^+ respectively. Slight shifts were detected in binding energy of all three peaks, which were due to increase of GO content. Height ratios of identified peaks were calculated as follows: 1.00 for N-C=O band, 0.47 for NH_2 and 0.45 for NH_3^+ band [60, 61, 67, 68]. Comparing atomic percentages of C and N between chitosan, CH/GO1, CH/GO2 and CH/GO3 revealed essential and fundamental information regarding mechanical behavior of prepared membranes as well as their elemental state and chemical structure. C content of chitosan, CH/GO1, CH/GO2 and CH/GO3 are 81.02%, 72.90%, 65.71% and 66.59%. An interesting trend could be observed in the carbon content, whichwas a perfect fit with tensile strength results. It would seem that decrease in the amount of carbon from 81.02% to 65.71%, weakened the material and decreased its resistance and strength against tension. But as the moment the C content started to increase, an unexpected rapid increase in tensile strength occurred. However, it was found that the sudden increase in tensile strength wasn‘t solely due to high C content. As the trend in N atomic percentage also showed

a constant increase upon addition of GO, N played a crucial role in rapid increase in tensile strength of membrane as well. N content in chitosan, CH/GO1, CH/GO2 and CH/GO3 was calculated at 2.47%, 4.71%, 5.49% and 5.79% accordingly which could mean that number of bonded N based functional groups had also increased leading to more hydrogen bonds involving amino group, which resulted in enhancing the resistant tendency of the material against tension [15, 60, 61, 67, 68].

After extensive chemical analysis of pristine chitosan, pristine GO and all nanocomposites, wettability property of chitosan based membranes were investigated using water contact angle test. By dropping a droplet of DI water on the surface of chitosan based plain and sharkskin mimicked membranes, both effects of surface chemistry as well as surface topography were investigated. Volume of the droplet was approximately 3μl and the angle of the droplet was measured at the 10th second after it settled on the surface. Measured water contact angles for plain membranes were $90° \pm 1.87$ for chitosan and $89.87°\pm4.53$ for CH/GO1, $87.30°\pm4.31$ for CH/GO2 and $84.57°\pm3.69$ for CH/GO3 [35, 62]. Water contact angles for SSM membranes were $102.1°\pm1.98$ for chitosan and $100.63°\pm5.03$ for CH/GO1, $98.6°\pm5.11$ for CH/GO2 and $94.35°\pm5.21$ for CH/GO3 [35, 36, 74].

It was concluded that chitosan plain membranes appeared to be hydrophobic with its water contact angle at $90° \pm 1.87$. Upon addition of GO, due to increase in the number of functional groups with tendency towards interaction with water molecules including carboxylic, NH_3^+ and hydroxyl groups, confirmed by XPS results, contact angle of CH/GO membranes decreased and as the concentration of GO increased from 0.1%w/w to 0.2%w/w followed by 0.3%w/w, water contact angle dropped from $89.87°\pm4.53$ to $87.30°\pm4.31$ and $84.57°\pm3.69$ accordingly which was in agreement with results of XPS analysis [35, 62].

For SSM membranes, water contact angle increased from $90°\pm1.87$ to $102.1°\pm1.98$ for chitosan, from $89.87°\pm4.53$ to $100.63°\pm5.03$ for CH/GO1, from $87.30°\pm4.31$ to $98.6°\pm5.11$ for CH/GO2 and from $84.57°\pm3.69$ to $94.35°\pm5.21$ for CH/GO3. This trend indicated that sharkskin surface topography increased the contact angle of water

due to turning the smooth surface of plain membranes into a highly rough surface. The roughness caused by sharkskin micro-morphology was considered significant since the surface of plain membranes had almost no superficial features therefore no roughness according to morphological characterization results, hence making SSM surfaces to act as very rough surfaces [36, 74].

Final stage of characterizing fabricated chitosan based membranes was swelling ratio, which measured the capacity of water absorption of SSM and plain membranes of all nanocomposites. All samples were placed at 50 °C for 24 hours prior to experimentation and DI water was used as the absorbed liquid. As presented in Figures 4.22 to 4.26 and Tables 4.24 and 4.25, swelling ratio of chitosan plain membranes had a sharp acceleration from T=0.0 min to T=5 min at 113.45%±1.95 which reached it maximum at 118.37% ± 2.80 at T=30 min and then dropped again to 115.44%±1.92 at T=4 hr, meaning that at the beginning, interactions of water molecules with functional groups of CH were occurring at a high rate, but by the 30th minute, the material reached and passed its maximum capacity for water absorption so, internal structure of polymer chains started to resist swelling and prolonging caused by accumulation of water molecules between the chains, resulting in forcing excess water out of polymers structure. At T=4 hr , swelling of CH plain membrane stabilized at 115.44% ± 1.92 [64].

As for SSM chitosan membranes, a considerable accelerating trend was detected. Swelling ratio of SSM membranes started at 116.85% ± 0.80 at T=5 min and rose to 133.01% ± 0.88 at T=4 hr with a linearly accelerating trend. This phenomena suggested that sharkskin surface topography had increased surface area leading to an increase in initial swelling ratio at T=5 min of SSM when compared to that of plain membranes. In addition to increased surface area, sharkskin micro-pattern altered the formation of polymeric chains, giving them more adaptability geometrical changes in micron scale due to swelling, increasing chitosan's capacity for water absorption (Figure 4.22).

In CH/GO1 plain membranes, swelling started at T=5 min at 118.94% ± 1.86

which reached it maximum at 123.27% ± 2.35 at T=60 min and then dropped and stabilized at 121.13% ± 1.49 at T=4 hr. By comparing these data with data of chitosan membrane, the effect of GO in increasing water absorption capacity of chitosan was deduced. It was concluded that just like water contact angle test results suggested, addition of GO increased amount of functional groups with high tendency towards interaction with water molecules, leading to raise in water absorption capacity of the chitosan membranes. Based on the data obtained from swelling test results, increasing GO concentration did not result in an accelerating linear trend. In fact as the content of GO increased from 0.2%w/w to 0.3%w/w, at T=2 hr, a significant decrease in swelling ratio of plain CH/GO3 had occurred resulting in the swelling ratio to be less than that of CH/GO2 [75]. This phenomena was also observed in SSM membranes with a slight difference of time of decrease. In SSM membranes CH/GO3 swelling ratio started at 119.53% ± 1.17 at T=5 min and increased to 129.55% ± 1.64 at T=4 hr whereas for CH/GO2, at T=5 min swelling percentage was 119.90 ± 2.99 which raised to 134.75% ± 2.86 at T=4 hr. These data suggested that despite increasing effect of sharkskin topography, the swelling capacity of CH/GO nanocomposites was more affected and controlled by GO inhibiting effect at high concentrations, in other words chemical factors, rather than physical and geometrical factors. The inhibiting effect of GO at high concentrations was attributed to the increase in amount of interactions specially hydrogen bonds, which increased the strength of the material against physical and geometrical changes such as swelling as discussed in the XPS results earlier.

According to the data presented in Figures 4.23 to 4.26 and Tables 4.24 and 4.25, in pristine chitosan group, the difference between swelling ratio of plain and SSM membranes was considered significant due to increase in surface area caused by sharkskin pattern. Upon addition of GO, that difference started to neglect and as the concentration of GO increased from 0.1%w/w to 0.3%w/w, the sharkskin effect was completely suppressed by GO's positive effect in increasing swelling capacity. This once again verified the superior effect of chemistry to geometry and physical features [64].

To the best of our knowledge, this is the first study on the effects of surface micron-scale topography on chitosan's swelling abilities.

5.4 Cell Culture Studies (MTT Assay)

The effect of GO concentration on the viability of fibroblast cells (L929) was investigated on plain membranes of CH, CH/GO1 and CH/GO2 nanocomposites. Elimination of CH/GO3 plain membrane group was due to the results of morphological characterization according to which, CH/GO3 did not replicate sharkskin micro-structure as well as CH/GO1 and CH/GO2 along with superficial features with no specific shapes found on the surface on plain CH/GO3 membranes which would have acted as an unwanted and uncontrollable variable which could have altered the results of cell culture experiments.

After culturing selected membranes with L929 cells, MTT assay was used to determine the viability of cells at day 7. According to Table 4.26 and Figure 4.27 which present MTT assay results at day 7, TCP which was the control group, showed highest cellular activity whereas cell viability on pristine CH membrane was the lowest due to the high WCA of CH resulting in representation of hydrophobic behavior [57]. Addition of 0.1%w/w GO increased cell viability by 98%. But when the GO content increased from 0.1%w/w to 0.2%w/w, cell viability unexpectedly decreased. It would seem that although addition of GO had a positive effect on cell viability, cells did not respond well to high concentrations of it leading to the conclusion that cells have a threshold for chemical characteristics of the substrate namely swelling ratio. In pristine chitosan membranes, swelling ratio was not as high as CH/GO1 and CH/GO2, which apparently have affected cellular attachment in a negative manner. As GO entered the chemical structure, many chemical characteristics of the membranes changed such as reduction of water contact angle and increase in swelling ratio. Upon comparing water contact angle and swelling ratio data for CH/GO1 and CH/GO2 with MTT results of these groups, it was concluded that the cells did not favor too much swelling capacity and surface wettability. Nevertheless, cell viability in CH/GO2 was still higher than pristine chitosan suggesting the effect of GO on cell culture in an improving manner.

5.5 Future Studies

The possibility of preparation of sharkskin mimicked chitosan based membranes, effect of surface morphology on chemical and morphological characteristics of chitosan based membranes was investigated along with effect of GO on replication, chemical and mechanical properties of chitosan based membranes. Some preliminary studies were conducted in order to obtain information regarding cellular behavior of fibroblast cells on obtained plain membranes with different GO content. Therefore, investigating the effects of sharkskin micro-pattern on cellular response along with investigating antibacterial effects of GO and sharkskin micro-pattern on SSM and plain nanocomposite membranes would be of great importance that could lead to promising outcomes.

REFERENCES

1. Bhushan, B., "Bioinspired structured surfaces," *Langmuir*, Vol. 28, no. 3, pp. 1698–1714, 2012.

2. Chen, H., X. Zhang, L. Ma, D. Che, D. Zhang, and T. S. Sudarshan, "Investigation on large-area fabrication of vivid shark skin with superior surface functions," *Applied Surface Science*, Vol. 316, no. 1, pp. 124–131, 2014.

3. Czeisler, C., A. Short, T. Nelson, P. Gygli, C. Ortiz, F. P. Catacutan, B. Stocker, J. Cronin, J. Lannutti, J. Winter, and J. Javier Otero, "Surface Topography During Neural Stem Cell Differentiation Regulates Cell Migration and Cell Morphology," *Journal of Comparative Neurology*, Vol. 520, no. Sfb 655, pp. 633–655, 2016.

4. Yang, X., Y. Tu, L. Li, S. Shang, and X. M. Tao, "Well-dispersed chitosan/graphene oxide nanocomposites," *ACS Applied Materials and Interfaces*, Vol. 2, no. 6, pp. 1707–1713, 2010.

5. Justin, R., and B. Chen, "Characterisation and drug release performance of biodegradable chitosan-graphene oxide nanocomposites," *Carbohydrate Polymers*, Vol. 103, no. 1, pp. 70–80, 2014.

6. Han, D., L. Yan, W. Chen, and W. Li, "Preparation of chitosan/graphene oxide composite film with enhanced mechanical strength in the wet state," *Carbohydrate Polymers*, Vol. 83, no. 2, pp. 653–658, 2011.

7. Han, D., and L. Yan, "Supramolecular hydrogel of chitosan in the presence of graphene oxide nanosheets as 2D cross-linkers," *ACS Sustainable Chemistry and Engineering*, Vol. 2, no. 2, pp. 296–300, 2014.

8. Eichelman, K., "Biomimetics : Prevention of Invasive Species Using the," *University of Pittsburgh, Swanson School of Engineering*, pp. 1–4, 2012.

9. Bhushan, B., and E. K. Her, "Fabrication of superhydrophobic surfaces with high and low adhesion inspired from rose petal," *Langmuir*, Vol. 26, no. 11, pp. 8207–8217, 2010.

10. Feng, L., Y. Zhang, J. Xi, Y. Zhu, N. Wang, Fan Xia, , and Lei Jiang*, "Petal Effect: A Superhydrophobic State with High Adhesive Force," *Langmuir*, Vol. 24, no. 18, pp. 4114–4119, 2008.

11. Dean, B., and B. Bhushan, "Shark-skin surfaces for fluid-drag reduction in turbulent flow: a review," *Philosophical transactions. Series A, Mathematical, physical, and engineering sciences*, Vol. 368, no. 1929, pp. 4775–4806, 2010.

12. Wegst, U. G. K., H. Bai, E. Saiz, A. P. Tomsia, R. O. Ritchie, C. Ortiz, M. Boyce, U. G. K. Wegst, H. Bai, E. Saiz, A. P. Tomsia, and R. O. Ritchie, "Bioinspired structural materials," *Nature materials*, Vol. 14, no. 1, pp. 23–36, 2014.

13. Han, X., and D. Zhang, "Study on the micro-replication of shark skin," *Science in China, Series E: Technological Sciences*, Vol. 51, no. 7, pp. 890–896, 2008.

14. Han, X., D. Zhang, X. Li, and Y. Li, "Bio-replicated forming of the biomimetic drag-reducing surfaces in large area based on shark skin," *Chinese Science Bulletin*, Vol. 53, no. 10, pp. 1587–1592, 2008.

15. Zhang, D. Y., Y. Y. Li, X. Han, X. A. Li, and H. W. Chen, "High-precision bio-replication of synthetic drag reduction shark skin," *Chinese Science Bulletin*, Vol. 56, no. 9, pp. 938–944, 2011.

16. Motta, P., M. L. Habegger, A. Lang, R. Hueter, and J. Davis, "Scale morphology and flexibility in the shortfin mako Isurus oxyrinchus and the blacktip shark Carcharhinus limbatus," *Journal of Morphology*, Vol. 273, no. 10, pp. 1096–1110, 2012.

17. Wen, L., J. C. Weaver, and G. V. Lauder, "Biomimetic shark skin: design, fabrication and hydrodynamic function.," *The Journal of experimental biology*, Vol. 217, no. Pt 10, pp. 1656–66, 2014.

18. Qin, D., Y. Xia, and G. M. Whitesides, "Soft lithography for micro- and nanoscale patterning.," *Nature protocols*, Vol. 5, no. 3, pp. 491–502, 2010.

19. Caner, C., P. J. Vergano, and J. L. Wiles, "Chitosan Film Mechanical and Permeation Properties as Affected by Acid, Plasticizer, and Storage," *Journal of Food Science*, Vol. 63, no. 6, pp. 1049–1053, 1998.

20. Dean, B., and B. Bhushan, "Shark-skin surfaces for fluid-drag reduction in turbulent flow: a review," *Philosophical transactions. Series A, Mathematical, physical, and engineering sciences*, Vol. 368, no. 1929, pp. 4775–4806, 2010.

21. Mann, E. E., D. Manna, M. R. Mettetal, R. M. May, E. M. Dannemiller, K. K. Chung, A. B. Brennan, and S. T. Reddy, "Surface micropattern limits bacterial contamination.," *Antimicrobial resistance and infection control*, Vol. 3, no. 1, p. 28, 2014.

22. Perreault, F., A. F. de Faria, S. Nejati, and M. Elimelech, "Antimicrobial Properties of Graphene Oxide Nanosheets: Why Size Matters," *ACS Nano*, no. 7, p. 150619235210004, 2015.

23. Wan, W., Z. Zhao, H. Hu, Y. Gogotsi, and J. Qiu, "Highly controllable and green reduction of graphene oxide to flexible graphene film with high strength," *Materials Research Bulletin*, Vol. 48, no. 11, pp. 4797–4803, 2013.

24. Liu, S., T. H. Zeng, M. Hofmann, E. Burcombe, J. Wei, R. Jiang, J. Kong, and Y. Chen, "Antibacterial activity of graphite, graphite oxide, graphene oxide, and reduced graphene oxide: Membrane and oxidative stress," *ACS Nano*, Vol. 5, no. 9, pp. 6971–6980, 2011.

25. Hu, W., C. Peng, W. Luo, M. Lv, X. Li, D. Li, Q. Huang, and C. Fan, "Graphene-based antibacterial paper," *ACS Nano*, Vol. 4, no. 7, pp. 4317–4323, 2010.

26. Mangadlao, J. D., C. M. Santos, M. J. L. Felipe, a. C. C. de Leon, D. F. Rodrigues, and R. C. Advincula, "On the antibacterial mechanism of graphene oxide (GO) Langmuir-Blodgett films.," *Chemical communications (Cambridge, England)*, Vol. 51, no. 14, pp. 2886–9, 2015.

27. Akhavan, O., and E. Ghaderi, "Toxicity of graphene and graphene oxide nanowalls against bacteria," *ACS Nano*, Vol. 4, no. 10, pp. 5731–5736, 2010.

28. Zhang, Y., S. F. Ali, E. Dervishi, Y. Xu, Z. Li, D. Casciano, and A. S. Biris, "Cytotoxicity effects of graphene and single-wall carbon nanotubes in neural phaeochromocytoma-derived pc12 cells," *ACS Nano*, Vol. 4, no. 6, pp. 3181–3186, 2010.

29. Kumar, S., and J. Koh, "Physiochemical and optical properties of chitosan based graphene oxide bionanocomposite," *International Journal of Biological Macromolecules*, Vol. 70, pp. 559–564, 2014.

30. Ruan, J., X. Wang, Z. Yu, Z. Wang, Q. Xie, D. Zhang, Y. Huang, H. Zhou, X. Bi, C. Xiao, P. Gu, and X. Fan, "Enhanced Physiochemical and Mechanical Performance of Chitosan-Grafted Graphene Oxide for Superior Osteoinductivity," *Advanced Functional Materials*, pp. 1085–1097, 2015.

31. Dowling, D. P., I. S. Miller, M. Ardhaoui, and W. M. Gallagher, "Effect of Surface Wettability and Topography on the Adhesion of Osteosarcoma Cells on Plasma-modified Polystyrene.," *Journal of biomaterials applications*, Vol. 26, no. 3, pp. 327–347, 2011.

32. Dowling, D. P., I. S. Miller, M. Ardhaoui, and W. M. Gallagher, "Effect of Surface Wettability and Topography on the Adhesion of Osteosarcoma Cells on Plasma-modified Polystyrene.," *Journal of biomaterials applications*, Vol. 26, no. 3, pp. 327–347, 2011.

33. Krasowska, A., and K. Sigler, "How microorganisms use hydrophobicity and what does this mean for human needs?," *Frontiers in Cellular and Infection Microbiology*, Vol. 4, no. August, pp. 1–7, 2014.

34. Horbett, T. a., J. J. Waldburger, B. D. Ratner, and a. S. Hoffman, "Cell adhesion to a series of hydrophilic-hydrophobic copolymers studied with a spinning disc apparatus.," *Journal of biomedical materials research*, Vol. 22, pp. 383–404, 1988.

35. Farris, S., L. Introzzi, P. Biagioni, T. Holz, A. Schiraldi, and L. Piergiovanni, "Wetting of biopolymer coatings: Contact angle kinetics and image analysis investigation," *Langmuir*, Vol. 27, no. 12, pp. 7563–7574, 2011.

36. Rivero, S., M. a. García, and a. Pinotti, "Physical and Chemical Treatments on Chitosan Matrix to Modify Film Properties and Kinetics of Biodegradation," *Journal of Materials Physics and Chemistry*, Vol. 1, no. 3, pp. 51–57, 2013.

37. Bharathidasan, T., T. N. Narayanan, S. Sathyanaryanan, and S. S. Sreejakumari, "Above 170Â° water contact angle and oleophobicity of fluorinated graphene oxide based transparent polymeric films," *Carbon*, Vol. 84, no. 1, pp. 207–213, 2015.

38. Bégin, A., and M. R. Van Calsteren, "Antimicrobial films produced from chitosan," *International Journal of Biological Macromolecules*, Vol. 26, no. 1, pp. 63–67, 1999.

39. Meng, X., R. Xing, S. Liu, H. Yu, K. Li, Y. Qin, and P. Li, "Molecular weight and pH effects of aminoethyl modified chitosan on antibacterial activity in vitro," *International Journal of Biological Macromolecules*, Vol. 50, no. 4, pp. 918–924, 2012.

40. Croce, M., S. Conti, C. Maake, and G. R. Patzke, "Synthesis and screening of N-acyl thiolated chitosans for antibacterial applications," *Carbohydrate Polymers*, Vol. 151, pp. 1184–1192, 2016.

41. Yan, F., Q. Dang, C. Liu, J. Yan, T. Wang, B. Fan, D. Cha, X. Li, S. Liang, and Z. Zhang, "3,6-O-[N-(2-Aminoethyl)-acetamide-yl]-chitosan exerts antibacterial activity by a membrane damage mechanism," *Carbohydrate Polymers*, Vol. 149, pp. 102–111, 2016.

42. Kingkaew, J., S. Kirdponpattara, N. Sanchavanakit, P. Pavasant, and M. Phisalaphong, "Effect of molecular weight of chitosan on antimicrobial properties and tissue compatibility of chitosan-impregnated bacterial cellulose films," *Biotechnology and Bioprocess Engineering*, Vol. 19, no. 3, pp. 534–544, 2014.

43. Pan, J. F., H. W. Chen, D. Y. Zhang, X. Zhang, L. M. Yuan, and L. Aobo, "Large-scale solvent-swelling-based amplification of microstructured sharkskin," *Journal of Micromechanics and Microengineering*, Vol. 23, no. 7, 2013.

44. Takara, E. A., J. Marchese, and N. A. Ochoa, "Naoh treatment of chitosan films: Impact on macromolecular structure and film properties," *Carbohydrate Polymers*, Vol. 132, pp. 25–30, 2015.

45. Lillehoj, P. B., and C. M. Ho, "A long-term, stable hydrophilic poly(dimethylsiloxane) coating for capillary-based pumping," *Mems 2010: 23rd Ieee International Conference on Micro Electro Mechanical Systems, Technical Digest*, pp. 1063–1066, 2010.

46. Noriega, S. E., and A. Subramanian, "Consequences of Neutralization on the Proliferation and Cytoskeletal Organization of Chondrocytes on Chitosan-Based Matrices," *International Journal of Carbohydrate Chemistry*, Vol. 2011, pp. 1–13, 2011.

47. Lamim, R., R. A. de Freitas, E. I. Rudek, H. M. Wilhelm, O. A. Cavalcanti, and T. M. Bresolin, "Films of chitosan and n-carboxymethylchitosan. part ii: Effect of plasticizers on their physiochernical properties," *Polymer International*, Vol. 55, no. 8, pp. 970–977, 2006.

48. Srinivasa, P. C., M. N. Ramesh, and R. N. Tharanathan, "Effect of plasticizers and fatty acids on mechanical and permeability characteristics of chitosan films," *Food Hydrocolloids*, Vol. 21, no. 7, pp. 1113–1122, 2007.

49. Domjan, A., J. Bajdik, and K. Pintye-Hodi, "Understanding of the plasticizing effects of glycerol and peg 400 on chitosan films using solid-state nmr spectroscopy," *Macromolecules*, Vol. 42, no. 13, pp. 4667–4673, 2009.

50. Stankovich, S., R. D. Piner, S. T. Nguyen, and R. S. Ruoff, "Synthesis and exfoliation of isocyanate-treated graphene oxide nanoplatelets," *Carbon*, Vol. 44, no. 15, pp. 3342–3347, 2006.

51. Zuo, P. P., H. F. Feng, Z. Z. Xu, L. F. Zhang, Y. L. Zhang, W. Xia, and W. Q. Zhang, "Fabrication of biocompatible and mechanically reinforced graphene oxide-chitosan nanocomposite films," *Chemistry Central Journal*, Vol. 7, 2013.

52. Khan, T. A., K. K. Peh, and H. S. Ch'ng, "Mechanical, bioadhesive strength and biological evaluations of chitosan films for wound dressing," *Journal of Pharmacy and Pharmaceutical Sciences*, Vol. 3, no. 3, pp. 303–311, 2000.

53. Zajac, A., J. Hanuza, M. Wandas, and L. Dyminska, "Determination of N-acetylation degree in chitosan using Raman spectroscopy," *Spectrochimica Acta - Part A: Molecular and Biomolecular Spectroscopy*, Vol. 134, pp. 114–120, 2015.

54. Matienzo, L. J., and S. K. Winnacker, "Dry processes for surface modification of a biopolymer: Chitosan," *Macromolecular Materials and Engineering*, Vol. 287, no. 12, pp. 871–880, 2002.

55. Leceta, I., P. Guerrero, and K. De La Caba, "Functional properties of chitosan-based films," *Carbohydrate Polymers*, Vol. 93, no. 1, pp. 339–346, 2013.

56. Kiuchi, H., W. H. Kai, and Y. Inoue, "Preparation and characterization of poly(ethylene glycol) crosslinked chitosan films," *Journal of Applied Polymer Science*, Vol. 107, no. 6, pp. 3823–3830, 2008.

57. Sangsanoh, P., O. Suwantong, A. Neamnark, P. Cheepsunthorn, P. Pavasant, and P. Supaphol, "In vitro biocompatibility of electrospun and solvent-cast chitosan substrata towards schwann, osteoblast, keratinocyte and fibroblast cells," *European Polymer Journal*, Vol. 46, no. 3, pp. 428–440, 2010.

58. Leceta, I., P. Guerrero, and K. de la Caba, "Functional properties of chitosan-based films," *Carbohydrate Polymers*, Vol. 93, no. 1, pp. 339–346, 2013.

59. Talukdar, Y., J. T. Rashkow, G. Lalwani, S. Kanakia, and B. Sitharaman, "The effects of graphene nanostructures on mesenchymal stem cells," *Biomaterials*, Vol. 35, no. 18, pp. 4863–4877, 2014.

60. Maachou, H., M. J. Genet, D. Aliouche, C. C. Dupont-Gillain, and P. G. Rouxhet, "XPS analysis of chitosan-hydroxyapatite biomaterials: From elements to compounds," *Surface and Interface Analysis*, Vol. 45, no. 7, pp. 1088–1097, 2013.

61. Amaral, I. F., P. L. Granja, and M. a. Barbosa, "Chemical modification of chitosan by phosphorylation: an XPS, FT-IR and SEM study.," *Journal of biomaterials science. Polymer edition*, Vol. 16, no. 12, pp. 1575–1593, 2005.

62. Hamilton, V., Y. Yuan, D. a. Rigney, a. D. Puckett, J. L. Ong, Y. Yang, S. H. Elder, and J. D. Bumgardner, "Characterization of chitosan films and effects on fibroblast cell attachment and proliferation," *Journal of Materials Science: Materials in Medicine*, Vol. 17, no. 12, pp. 1373–1381, 2006.

63. Ling, X., Y. Zu-yu, Y. Chao, Z. Hua-yue, and D. Yu-min, "Swelling studies of chitosan-gelatin films cross-linked by sulfate," *Wuhan University Journal of Natural Sciences*, Vol. 9, no. 2, pp. 247–251, 2004.

64. Huang, Y., M. Zeng, Z. Feng, D. Yin, Q. Xu, and L. Fan, "Graphene oxide-based composite hydrogels with self-assembled macroporous structures," *RSC Adv.*, Vol. 6, no. 5, pp. 3561–3570, 2016.

65. Pan, Y., T. Wu, H. Bao, and L. Li, "Green fabrication of chitosan films reinforced with parallel aligned graphene oxide," *Carbohydrate Polymers*, Vol. 83, no. 4, pp. 1908–1915, 2011.

66. Stoller, M. D., S. Park, Z. Yanwu, J. An, and R. S. Ruoff, "Graphene-Based ultracapacitors," *Nano Letters*, Vol. 8, no. 10, pp. 3498–3502, 2008.

67. Yang, D., A. Velamakanni, G. Bozoklu, S. Park, M. Stoller, R. D. Piner, S. Stankovich, I. Jung, D. a. Field, C. a. Ventrice, and R. S. Ruoff, "Chemical analysis of graphene oxide films after heat and chemical treatments by X-ray photoelectron and Micro-Raman spectroscopy," *Carbon*, Vol. 47, no. 1, pp. 145–152, 2009.

68. Bustos-Ramírez, K., A. L. Martínez-Hernández, G. Martínez-Barrera, M. de Icaza, V. M. Castaño, and C. Velasco-Santos, "Covalently bonded chitosan on graphene oxide via redox reaction," *Materials*, Vol. 6, no. 3, pp. 911–926, 2013.

69. Kudin, K. N., B. Ozbas, H. C. Schniepp, R. K. Prud'Homme, I. a. Aksay, and R. Car, "Raman spectra of graphite oxide and functionalized graphene sheets," *Nano letters*, Vol. 8, no. 1, pp. 36–41, 2008.

70. Nawrotek, K., M. Tylman, K. Rudnicka, J. Balcerzak, and K. Kami??ski, "Chitosan-based hydrogel implants enriched with calcium ions intended for peripheral nervous tissue regeneration," *Carbohydrate Polymers*, Vol. 136, pp. 764–771, 2016.

71. Yu, Y.-H., Y.-Y. Lin, C.-H. Lin, C.-C. Chan, and Y.-C. Huang, "High-performance polystyrene/graphene-based nanocomposites with excellent anti-corrosion properties," *Polym. Chem.*, Vol. 5, no. 2, pp. 535–550, 2014.

72. Khan, M., A. H. Al-Marri, M. Khan, M. R. Shaik, N. Mohri, S. F. Adil, M. Kuniyil, H. Z. Alkhathlan, A. Al-Warthan, W. Tremel, M. N. Tahir, and M. R. H. Siddiqui, "Green Approach for the Effective Reduction of Graphene Oxide Using Salvadora persica L. Root (Miswak) Extract.," *Nanoscale research letters*, Vol. 10, no. 1, p. 987, 2015.

73. Yang, Y., J. Cui, M. Zheng, C. Hu, S. Tan, and Y. Xiao, "Supplementary Information One step synthesis amino-functionalized fluorescent carbon nanoparticles by hydrothermal carbonization chitosan 1 . Preparation of the fluorescent carbon nanoparticles (CNPs)," *The Royal Society of Chemistry*, 2011.

74. Zhao, D., Q. Tian, M. Wang, and Y. Jin, "Study on the Hydrophobic Property of Shark-Skin-Inspired Micro-Riblets," *Journal of Bionic Engineering*, Vol. 11, no. 2, pp. 296–302, 2014.

75. Dinescu, S., M. Ionita, A. M. Pandele, B. Galateanu, H. Iovu, A. Ardelean, M. Costache, and A. Hermenean, "In vitro cytocompatibility evaluation of chitosan/graphene oxide 3D scaffold composites designed for bone tissue engineering," *Bio-Medical Materials and Engineering*, Vol. 24, no. 6, pp. 2249–2256, 2014.